UNIVERSITY
OF MICHIGAN
JUL 20 1956
CHEMISTRY
LIBRARY

Journal of Research

of the

National Bureau of Standards

JUNE 1956

VOLUME 56 NUMBER 6

U. S. DEPARTMENT OF COMMERCE
Sinclair Weeks, Secretary
NATIONAL BUREAU OF STANDARDS
A. V. Astin, Director

JUNE • 1956
VOLUME • 56
NUMBER • 6

JOURNAL OF RESEARCH
of the
NATIONAL BUREAU OF STANDARDS

PERIODICALS OF THE NATIONAL BUREAU OF STANDARDS
(Published monthly)

The National Bureau of Standards is engaged in fundamental and applied research in physics, chemistry, mathematics, and engineering. Projects are conducted in fifteen fields: electricity and electronics, optics and metrology, heat and power, atomic and radiation physics, chemistry, mechanics, organic and fibrous materials, metallurgy, mineral products, building technology, applied mathematics, data processing systems, cryogenic engineering, radio propagation, and radio standards. The Bureau has custody of the national standards of measurement and conducts research leading to the improvement of scientific and engineering standards and of techniques and methods of measurement. Testing methods and instruments are developed, physical constants and properties of materials are determined, and technical processes are investigated.

JOURNAL OF RESEARCH

The Journal presents research papers by authorities in the specialized fields of physics, mathematics, chemistry, and engineering. Complete details of the work are presented, including laboratory data, experimental procedures, and theoretical and mathematical analyses. Annual subscription: domestic, $4.00; $1.25 additional for foreign mailing.

TECHNICAL NEWS BULLETIN

Summaries of current research at the National Bureau of Standards are published each month in the Technical News Bulletin. The articles are brief, with emphasis on the results of research, chosen on the basis of their scientific or technologic importance. Lists of all Bureau publications during the preceding month are given, including Research Papers, Handbooks, Applied Mathematics Series, Building Materials and Structures Reports, Miscellaneous Publications, and Circulars. Each issue contains 12 or more two-column pages; illustrated. Annual subscription: domestic, $1.00; 35 cents additional for foreign mailing.

BASIC RADIO PROPAGATION PREDICTIONS

The Predictions provide the information necessary for calculating the best frequencies for communication between any two points in the world at any time during the given month. The data are important to all users of long-range radio communications and navigation, including broadcasting, airline, steamship, and wireless services, as well as to investigators of radio propagation and ionosphere. Each issue, covering a period of one month, is released three months in advance and contains 16 large pages, including pertinent charts, drawings, and tables. Annual subscription: domestic, $1.00; 25 cents additional for foreign mailing.

Order all publications from the Superintendent of Documents
U. S. Government Printing Office, Washington 25, D. C.

The printing of this publication has been approved by the Director of the Bureau of the Budget, May 14, 1956.

Journal of Research of the National Bureau of Standards Vol. 56, No. 6, June 1956 Research Paper 2680

Calcium Hydroxide as a Highly Alkaline *p*H Standard

Roger G. Bates, Vincent E. Bower, and Edgar R. Smith

The National Bureau of Standards conventional activity scale of *p*H is defined by a series of standard buffer solutions prepared from certified materials issued as NBS Standard Samples. The five standards thus far established cover the *p*H range 1.68 to 9.18 at 25° C. In order to increase the accuracy of measurements at high *p*H, a highly alkaline standard is needed.

A solution of calcium hydroxide saturated at 25° C is recommended as the sixth *p*H standard. No weighing is necessary, for the solution is easily prepared by shaking finely granular calcium hydroxide with water. The material must not be contaminated with soluble alkalies, but the presence of insoluble carbonate is of no concern. The filtered solution supersaturates readily and can usually be used from 0° to 60° C without the separation of solid phase.

Electromotive-force measurements of 29 cells containing mixtures of calcium hydroxide and potassium chloride were made in the range 0° to 60° C, and standard *p*H values were assigned to 0.0203-, 0.02-, 0.019-, 0.0175-, and 0.015-*M* solutions of calcium hydroxide without added chloride. The saturated solution is about 0.0203 *M* and has a *p*H of 12.45 at 25° C. The buffer capacity is high (0.09 mole/*p*H). Like most other alkaline solutions, however, this standard has a rather large dilution value (−0.28 *p*H unit) and a large temperature coefficient of *p*H (−0.033 *p*H unit/deg C).

1. Introduction

The National Bureau of Standards standard *p*H scale is defined in terms of several fixed points in much the same manner as the International Temperature Scale. The primary standards are solutions whose *p*H values are only slightly affected by dilution or by accidental contamination of the solution with traces of acid or alkali from the walls of the container or from the atmosphere. The substances from which the standards are prepared are, in turn, stable materials; they are obtainable in the form of certified samples from the Bureau. The five standards thus far established cover the *p*H range 1.68 to 9.18 at 25° C.[1] It is the purpose of this paper to describe the establishment of a sixth standard, a solution of calcium hydroxide saturated at 25° C, which will extend the standard scale to *p*H 12.45 at 25° C.

2. Need for an Alkaline *p*H Standard

In practice, most *p*H values are derived either directly or indirectly from the emf of the cell

$$\text{Pt; } H_2 \text{ (g) (or glass electrode), solution X} \mid \text{3.5 } M \text{ or satd. KCl, } Hg_2Cl_2\text{; Hg.} \quad (1)$$

where the vertical line marks a boundary between two liquid phases. The transfer of positive and negative ions at different rates across this liquid junction gives rise to a potential difference. Inasmuch as the transference numbers of the ions vary through the boundary, as do the concentration gradients, the net charge transferred is rarely zero. Furthermore, the sign of the potential difference may be either positive or negative, and the magnitude can neither be measured exactly nor calculated. If included in the measured emf, this potential would result in erroneous *p*H values.

Fortunately, the concentrated solution of potassium chloride that composes the salt bridge reduces the liquid-junction potential to a small constant value for most solutions of intermediate acidity, *p*H 3 to 11. When solution X contains appreciable amounts of the highly mobile hydrogen and hydroxyl ions (*p*H less than 3 or greater than 11), however, the liquid-junction potentials may differ considerably from the relatively constant values maintained in the region of intermediate *p*H. For accurate *p*H measurements in these regions of high acidity or high alkalinity, therefore, it is particularly important that reference standards of low and high *p*H be available.

This need is readily demonstrated. A *p*H measurement is essentially a determination of the difference between $p\text{H}_X$, the *p*H of the unknown solution, and $p\text{H}_S$, that of the standard. If E_X is the emf of cell 1 and E_S that of the same cell when the standard is substituted for solution X, and E_{jX} and E_{jS} are the corresponding liquid-junction potentials, we have

$$p\text{H}_X = p\text{H}_S + \frac{E_X - E_S}{2.3026RT/F} + \frac{E_{jS} - E_{jX}}{2.3026RT/F}, \quad (2)$$

where R, T, and F are the gas constant, the absolute temperature, and the faraday, respectively.

There is no way to evaluate the last term of eq (2). Hence, for the usual *p*H measurement the experimental conditions are chosen so as to nullify the greater part of the junction potential. The two potentials, E_{jS} and E_{jX}, are then assumed to be nearly equal and to cancel rather completely when the difference is taken (eq (2)). Hence the difference of *p*H is assumed to be proportional to the difference of emf, $E_X - E_S$. Evidently the residual liquid-junction potential will be small when the standard solution and the unknown solution differ but little in *p*H, for the concentrations of the free hydrogen or hydroxyl ions (on which the liquid-junction potential largely depends) will be nearly the same in solution X as in solution S.

[1] The assignment of *p*H values to these standards has been described in earlier Bureau papers: Tetroxalate (*p*H 1.68 at 25° C) [1]; tartrate (*p*H 3.56) [2]; phthalate (*p*H 4.01) [3]; phosphate (*p*H 6.86) [4]; and borax (*p*H 9.18) [5]. Figures in brackets indicate the literature references at the end of this paper.

3. Calcium Hydroxide as a *p*H Standard

The ideal *p*H standard is a stable solution easily and reproducibly prepared from pure materials. The *p*H of the solution should not be markedly affected by changes of temperature. The buffer value [6] should be high and the dilution value [7] low; in other words, the *p*H of the solution should not be altered appreciably by contamination with traces of acidic or basic impurities or by a change in the total concentration of the buffer substances.

The ionization of water is strongly affected by temperature changes, and hence the *p*H of most highly alkaline aqueous solutions is also sensitive to alteration of temperature. The *p*H falls with increasing temperature by as much as 0.033 unit/deg C [8]. This imposes, of course, an unfortunate limitation on the use of an alkaline *p*H standard. It should be noted, however, that a certain degree of temperature control is necessary for *p*H measurements in the highly alkaline region, not only because the *p*H of the standard is sensitive to temperature changes but also because the "unknowns," in general, are similarly affected.

The buffer value, or buffer capacity, of solutions containing appreciable concentrations of hydroxide ion is uniformly larger than that of buffer solutions of comparable concentrations in the *p*H range 3 to 11, but these same solutions usually undergo a larger *p*H change on dilution [8]. A high buffer capacity is particularly important in an alkaline *p*H standard, for contamination with atmospheric carbon dioxide during storage and use can never be completely avoided.

In principle, a solution of a strong or moderately strong base will serve as an alkaline standard. In view of the high buffer capacity of aqueous solutions of even incompletely ionized bases at high *p*H, the addition of a salt of the base is unnecessary. However, it is very difficult, if not impossible, to find a strong base, either inorganic or organic, that is a stable solid. The determination of the concentration of the solution by a titration with standard acid is not only inconvenient and time-consuming but compounds the errors of three separate analytical operations. Buffer solutions of trisodium phosphate are subject to the same objections for, owing to the difficulty of preparing a sample of the phosphate salt of the correct composition, they must be made from the secondary phosphate and standard alkali. A *p*H greater than 11.2 at 25° C cannot readily be obtained with solutions of the alkali carbonates. To be most useful, an alkaline standard should have a *p*H of 12 or above.

Substances that form highly alkaline solutions usually become contaminated gradually with carbonate from exposure to the atmosphere when the container is opened. Many are also hygroscopic, and the moisture they acquire is not easily removed by simple drying procedures. If the carbonate were insoluble in water, however, the contaminant could be easily removed by filtration of the solution, and later contamination would be clearly evident when it occurred. If, in addition, the alkaline material were of moderate solubility, the saturated solution would serve as a standard. Under these conditions, the presence of carbonate would cause no concern; furthermore, no weighings would be necessary.

Because of its ease of preparation, a saturated solution of slaked lime, calcium hydroxide, has often been employed as a reference solution of high alkalinity [9, 10, 11]. Tuddenham and Anderson [11] saturated calcium chloride solutions with calcium hydroxide to achieve *p*H values from 11 to over 12, as desired. The concentration of the saturated solution of calcium hydroxide in pure water is about 0.02 *M* and the *p*H about 12.4 at 25° C. A few measurements made in an earlier study [12], however, suggested that the saturated solution, like that of the more soluble barium hydroxide, might not be sufficiently reproducible to serve as a primary standard. Later work has shown that the solubility of samples of calcium hydroxide free from soluble alkalies and salts is indeed reproducible within 1 percent.

The solubility of calcium hydroxide decreases with rising temperature, being about 4 percent higher at 20° than at 25° C, and 4 percent lower at 30°. Nevertheless, a separation of solid phase does not usually occur at 50° or even at 60° C when a solution saturated at 25° is filtered and subsequently heated to those temperatures [13, 14]. A solution of calcium hydroxide that has been saturated at or near 25° C can accordingly be employed as a *p*H standard over a considerable range of temperature.

The properties of a solution of calcium hydroxide saturated at 25° C are compared with those of the phthalate and borax *p*H standards in the following summary:

	Calcium hydroxide	Potassium hydrogen phthalate	Borax
Molar concentration	0.0203	0.05	0.01
Density (25° C)	.9991	1.0017	-----
Buffer value (β), mole/*p*H unit	*ca.* 09	0.016	.020
Dilution value ($\Delta pH_{1/2}$), *p*H units for 1:1 dilution	*ca* −.28	+.05	+.01
dpH/dt, *p*H units/deg C	−.033	+.0012	−.0082

It is seen that the *p*H change, in absolute measure, on dilution of the calcium hydroxide standard is more than 5 times that on dilution of the phthalate solution of *p*H 4.0,[2] whereas the temperature coefficient is 4 times that of the borax standard (*p*H 9.2). It appears that any highly alkaline standard will be subject to these limitations in much the same degree.

4. Method of Assigning *p*H

The emf method by which standard *p*H values were assigned to solutions of calcium hydroxide has been described [1, 2, 8]. It will be summarized briefly here, but certain novel features of the present treatment will be explained in detail.

[2] At low *p*H, the dilution value attains large positive values. For the 0.05 *M* potassium tetroxalate standard (*p*H 1.7), $\Delta pH_{1/2}$ is +0.19.

The first step consisted in the measurement of the emf of cells with hydrogen and silver–silver-chloride electrodes, containing the calcium hydroxide solutions with added potassium chloride:

$$\mathrm{Pt;\ H_2\ (g),\ Ca(OH)_2\ (}m_1\mathrm{),\ KCl\ (}m_2\mathrm{),\ AgCl;\ Ag.} \quad (3)$$

The symbol m represents molality, or moles per kilogram of water. The molality of a solution does not change with temperature and is therefore favored over volume concentration in measurements of this type. Several different molalities of calcium hydroxide in the range 0.015 to 0.0203 were selected. For each calcium hydroxide concentration, three different molalities of potassium chloride, namely, 0.015 m, 0.01 m, and 0.005 m, were studied.

The second step was to compute values of the quantity $pw\mathrm{H}$, defined by eq (4), for each mixture of calcium hydroxide and potassium chloride and to determine, by extrapolation, the value of $pw\mathrm{H}^\circ$, the limit approached by $pw\mathrm{H}$ in calcium hydroxide solutions as the concentration of potassium chloride was reduced to zero. The value of $pw\mathrm{H}$ is computed directly from the measured emf, E, and the standard potential, E°, of the cell [15] by

$$pw\mathrm{H} \equiv -\log\,(f_{\mathrm{H}} f_{\mathrm{Cl}} m_{\mathrm{H}}) = \frac{E-E^\circ}{2.3026RT/F} + \log\, m_{\mathrm{Cl}}, \quad (4)$$

where f is an activity coefficient on the molal scale, R is the gas constant (8.31439 j deg^{-1} mole^{-1}), F is the faraday (96493.1 coulombs equiv^{-1}), and T is the temperature on the Kelvin scale (deg C+273.16).

The values of $pw\mathrm{H}$ obtained by eq (4) for each of the three concentrations of potassium chloride proved to be a linear function of log m_1, the common logarithm of the molality of calcium hydroxide, in the limited range studied ($0.015 < m_1 < 0.0203$). The constants of the equation

$$pw\mathrm{H} = a + b\,\log\, m_1 \quad (5)$$

were determined by the method of least squares and used to compute $pw\mathrm{H}$ for five selected concentrations of calcium hydroxide (m_1=0.015, 0.0175, 0.019, 0.02, and 0.0203) at each of the three chloride concentrations and at the 13 temperatures included in the study. In agreement with our earlier observations, $pw\mathrm{H}$ for a given value of m_1 was found to vary linearly with m_2, the molality of potassium chloride. The limit, $pw\mathrm{H}^\circ$, in the absence of chloride was then determined by fitting the values of $pw\mathrm{H}$ for the five selected calcium hydroxide solutions to the equation

$$pw\mathrm{H} = pw\mathrm{H}^\circ + cm_2 \quad (6)$$

by the method of least squares.

In the third step, the procedure necessarily departs from thermodynamic rigor, for the $p\mathrm{H}$ lacks exact thermodynamic definition. The formal relationship between $pw\mathrm{H}^\circ$ and $p\mathrm{H_S}$ is

$$p\mathrm{H_S} \equiv -\log f_{\mathrm{H}} m_{\mathrm{H}} = pw\mathrm{H}^\circ + \log f^\circ_{\mathrm{Cl}}, \quad (7)$$

where f°_{Cl} is the activity coefficient of chloride ion in the chloride-free solution of calcium hydroxide.

The NBS standard $p\mathrm{H}$ scale is based on the convention that the last term of eq (7) be expressed by the Debye-Hückel equation

$$-\log f^\circ_{\mathrm{Cl}} = \frac{A\sqrt{\mu}}{1+Ba_i\sqrt{\mu}} \quad (8)$$

with a reasonable choice of the ion-size parameter, a_i. In eq (8), μ is the ionic strength, while A and B are constants for the water medium at a particular temperature [16]. The most probable value of a_i for chloride ion in a mixture of simple electrolytes is regarded to lie between 4 and 6, but values as low as 3 or as high as 8 cannot be termed unreasonable. Inasmuch as the convention adopted does not specify a *single* value of a_i, the $p\mathrm{H_S}$ is not defined exactly through eq (7) and (8). The uncertainty amounts to a few thousandths of a $p\mathrm{H}$ unit at an ionic strength of 0.01 and to slightly more than $\pm$0.01 unit at an ionic strength of 0.1 [8].

Because calcium hydroxide is not completely ionized,[3] the ionic strength of calcium hydroxide solutions is somewhat less than $3m_1$. However, the hydroxide ion molality, m_{OH}, can be evaluated with adequate accuracy from $pw\mathrm{H}^\circ$ and the ion-product constant, K_w, for water at the appropriate temperature: [4]

$$\log\, m_{\mathrm{OH}} = \log\, K_w + pw\mathrm{H}^\circ. \quad (9)$$

The first dissociation step is presumed to be complete and the second incomplete; hence, the molalities of the ions Ca^{++} and $CaOH^+$ are given by

$$m_{\mathrm{Ca}} = m_{\mathrm{OH}} - m_1 \quad (10)$$

and

$$m_{\mathrm{CaOH}} = 2\,m_1 - m_{\mathrm{OH}}, \quad (11)$$

and the ionic strength is

$$\mu = 2\,m_{\mathrm{OH}} - m_1. \quad (12)$$

5. Experimental Procedures and Results

5.1. Solubility of Calcium Hydroxide

There is some disagreement among literature values for the solubility of calcium hydroxide, as well as some indication that the apparent solubility is dependent upon crystal size [18, 19]. Bassett [18]

[3] See, for example, the paper of Bell and Prue [17]. The second dissociation constant is about 0.05.

[4] Eq (9) depends for its validity upon the approximate equality of the activity coefficients (f_{Cl} and f_{OH}) of ions of like charge in solutions of moderate concentration and upon the fact that the activity of water in such solutions does not depart greatly from unity. The formula is consequently more accurate the more dilute the solution.

has made an extensive study of the solubility from 0° to 100° C and lists two values over a considerable range of temperature; his "true solubility" is from 6 to 15 percent lower than the solubility of very small crystals. The true solubility at 25° C, in moles per kilogram of water (molality), was found by Bassett to be 0.02018, in reasonable agreement with 0.0205 found earlier by Moody and Leyson [20], but significantly lower than 0.0209 obtained by interpolation between the data at 10° and 42° as determined by Haslam, Calingaert, and Taylor [21].

For the solubility of large crystals at 25° C, however, Johnston and Grove [13] found a value of 0.01976 *m*, and quite recently Peppler and Wells [19] have concluded that the solubility of large, well-formed crystals is 0.0184 *m* at 30°. Inasmuch as the solubility of calcium hydroxide appears to be only about 4 percent lower at 30° than at 25°, there remains a discrepancy of about 2.5 percent between these two determinations of the solubility of large crystals.

In the present study, the solubility of several samples of calcium hydroxide prepared in various ways was determined by shaking the material vigorously with about 15 times its volume of water in a glass-stoppered bottle. Between periods of shaking, the bottle was maintained at a controlled temperature by immersion in a water thermostat. The excess of solid was removed on a sintered-glass funnel of medium porosity, and the concentration of the filtrate was determined by titration with a standard solution of hydrochloric acid to the endpoint of phenol red. Weight burets were used in the titrations. The solubility determinations were reproducible to ±0.5 percent or better.

In the initial experiments with calcium hydroxide of reagent grade, solubilities as high as 0.0229 *m* at 25° C were obtained, but this figure was lowered somewhat by repeated digestion of the hydroxide under hot water. This behavior could result from the extraction of soluble alkaline impurities or from a gradual stabilization of crystal form during the digestion. Thereafter, the samples of hydroxide were prepared from "CP" low-alkali calcium carbonate and the effect was no longer observed.

The finely granular calcium carbonate was ignited in platinum dishes at 1,000° C for about 45 min, and the resulting lime, after cooling in a desiccator, was added with stirring to water. The mixture was heated to boiling with continual stirring and was then filtered. The calcium hydroxide obtained in this way was dried at 110° C and powdered.

The solubility of five samples of hydroxide prepared in this manner was found to be 0.02037 *m*, with a standard deviation of 0.00011, and this figure was substantially unchanged after seven extractions of the product with water. To test the effect of aging, the calcium hydroxide was stored under water in a polyethylene bottle and samples removed from time to time for solubility tests conducted as described above. After 1 month, the solubility of four samples was found to be 0.02032 *m*, with a standard deviation of 0.00006, and after 6 months had elapsed a figure of 0.02022 *m* was obtained as the mean of two determinations. The average solubility is 0.0203 *m* at 25° C. At 20° C the solubility was found to be 0.0211 *m* and at 30° C, 0.0196 *m*.

These figures are in excellent agreement with the true solubility of Bassett [18], who found 0.0211 *m* at 20°, 0.0202 *m* at 25°, and 0.0195 *m* at 30° C. It appears that they represent satisfactorily reproducible concentrations achieved by shaking granular calcium hydroxide, prepared from low-alkali calcium carbonate, with water at 20°, 25°, or 30° C. However, they do not preclude a solubility lower by perhaps 1 to 3 percent for large well-defined crystals of the material. It should be noted that a change of 1 percent in the concentration of calcium hydroxide corresponds to about 0.004 in the *p*H of the nearly saturated solution.

5.2. Electromotive-Force Measurements

The calcium hydroxide solutions for the emf measurements were prepared by dilution of nearly saturated stock solutions whose concentrations had been established by titration with standard acid. A weighed amount of potassium chloride was then added to each solution flask, or a portion of a 0.3–*M* solution of the salt introduced from a weight buret. The dilution and the addition of chloride in an atmosphere of carbon-dioxide-free nitrogen were accomplished with the aid of an arrangement very similar to that described by Bates and Acree [22]. The potassium chloride was a bromide-free fused sample prepared in the manner described in an earlier publication [23].

The cells were rinsed, flushed, and filled in the usual manner. Solution was admitted from the solution flask, the cell emptied and flushed with pure hydrogen, and the cycle repeated before the final portion of solution was admitted. The preparation of the electrodes has been described elsewhere [8]. Each cell contained two pairs of electrodes, and the duplicate measurements were averaged.

Initial measurements were made at 25° C, those from 0° to 30° C on the second day, and those from 30° to 60° C on the third day. With these highly alkaline solutions, the final measurements at 25° C when they were obtained, did not agree as closely with the initial values as those for solutions of low or intermediate *p*H often do. Differences of 0.3 to 0.5 mv were not uncommon. The emf data were corrected in the usual way to a partial pressure of 1 atm of hydrogen.

6. Determination of *pw*H and *pw*H°

A value of *pw*H was computed from each corrected emf value by eq (4), and the constants a and b of eq (5) were obtained for each of the three molalities of potassium chloride (m_2 equal to 0.015, 0.01, or 0.005 in the cell solutions. The data are summarized in table 1. The third column gives the number of cells studied, and the sixth column lists σ, the standard deviation of a single *pw*H value from the line defined by the constants a and b. The last five columns give

pwH at five selected values of m_1, the molality of calcium hydroxide. These figures were computed by eq (5) with the values of a and b given in the table. For each m_1, the limiting value of pwH, namely, pwH°, as the molality (m_2) approached zero, obtained by eq (6), is entered on the fourth line at each temperature. The standard deviation, σ_i, of this intercept (pwH°) is listed on the fifth line.

TABLE 1. *pwH and pwH° for mixtures of calcium hydroxide ($0.015 < m_1 < 0.0203$) and potassium chloride (m_2) from 0° to 60° C; constants of the equation $pw\mathrm{H} = a + b \log m_1$*

t	m_2	Number of cells	a	b	[a] σ	pwH for m_1 equal to				
						0.0203	0.02	0.019	0.0175	0.015
°C										
0	0.015	11	15.121	0.9450	0.003	13.521	13.515	13.494	13.460	13.397
	.010	10	15.137	.9548	.002	13.521	13.515	13.494	13.459	13.396
	.005	8	15.110	.9432	.004	13.513	13.507	13.485	13.452	13.389
	.000	.....	.....	.....	$pw\mathrm{H}^\circ =$	13.510	13.504	13.482	13.449	13.386
	.....	.....	.....	.....	[b] $\sigma_i =$	0.005	0.004	0.004	0.004	0.003
5	.015	11	14.909	.9480	0.005	13.304	13.298	13.277	13.246	13.180
	.010	10	15.095	1.0578	.004	13.305	13.298	13.274	13.237	13.166
	.005	8	14.901	0.9492	.004	13.294	13.288	13.267	13.233	13.169
	.000	.....	.....	.....	$pw\mathrm{H}^\circ =$	13.291	13.285	13.263	13.226	13.161
	.....	.....	.....	.....	$\sigma_i =$	0.006	0.006	0.002	0.003	0.011
10	.015	11	14.705	.9463	0.004	13.103	13.097	13.076	13.042	12.979
	.010	10	14.838	1.0258	.004	13.102	13.096	13.073	13.036	12.967
	.005	8	14.714	0.9584	.005	13.092	13.086	13.065	13.030	12.966
	.000	.....	.....	.....	$pw\mathrm{H}^\circ =$	13.088	13.082	13.060	13.024	12.958
	.....	.....	.....	.....	$\sigma_i =$	0.006	0.006	0.003	0.000	0.006
15	.015	11	14.495	.9360	0.003	12.911	12.905	12.884	12.851	12.788
	.010	10	14.606	1.0093	.004	12.910	12.904	12.881	12.845	12.778
	.005	8	14.478	0.9334	.004	12.898	12.892	12.872	12.838	12.776
	.000	.....	.....	.....	$pw\mathrm{H}^\circ =$	12.893	12.887	12.867	12.832	12.769
	.....	.....	.....	.....	$\sigma_i =$	0.004	0.004	0.003	0.004	0.007
20	.015	11	14.300	.9281	0.004	12.729	12.723	12.703	12.670	12.607
	.010	10	14.376	.9746	.004	12.727	12.720	12.699	12.664	12.599
	.005	8	14.331	.9533	.006	12.717	12.711	12.690	12.656	12.592
	.000	.....	.....	.....	$pw\mathrm{H}^\circ =$	12.712	12.706	12.684	12.649	12.584
	.....	.....	.....	.....	$\sigma_i =$	0.005	0.004	0.003	0.002	0.002
25	.015	11	14.139	.9312	0.002	12.563	12.557	12.537	12.503	12.441
	.010	10	14.166	.9502	.003	12.558	12.552	12.531	12.497	12.433
	.005	8	14.124	.9325	.007	12.545	12.539	12.519	12.485	12.423
	.000	.....	.....	.....	$pw\mathrm{H}^\circ =$	12.537	12.531	12.511	12.477	12.414
	.....	.....	.....	.....	$\sigma_i =$	0.005	0.005	0.004	0.004	0.002
30	.015	11	13.967	.9268	0.004	12.398	12.392	12.372	12.339	12.277
	.010	9	13.975	.9354	.003	12.392	12.386	12.365	12.332	12.269
	.005	7	14.030	.9707	.004	12.387	12.381	12.359	12.324	12.259
	.000	.....	.....	.....	$pw\mathrm{H}^\circ =$	12.381	12.375	12.352	12.317	12.250
	.....	.....	.....	.....	$\sigma_i =$	0.002	0.002	0.002	0.002	0.002
35	.015	11	13.830	.9387	0.006	12.241	12.235	12.214	12.181	12.118
	.010	9	13.817	.9396	.002	12.232	12.226	12.205	12.172	12.109
	.005	7	13.825	.9441	.003	12.227	12.221	12.200	12.166	12.103
	.000	.....	.....	.....	$pw\mathrm{H}^\circ =$	12.219	12.213	12.192	12.158	12.095
	.....	.....	.....	.....	$\sigma_i =$	0.003	0.003	0.003	0.002	0.003
40	.015	11	13.658	.9276	0.006	12.088	12.082	12.062	12.029	11.966
	.010	9	13.682	.9444	.004	12.083	12.077	12.056	12.022	11.959
	.005	7	13.586	.8924	.005	12.076	12.070	12.050	12.018	11.959
	.000	.....	.....	.....	$pw\mathrm{H}^\circ =$	12.070	12.064	12.044	12.012	11.954
	.....	.....	.....	.....	$\sigma_i =$	0.002	0.002	0.000	0.002	0.005
45	.015	10	13.516	.9287	0.007	11.944	11.938	11.918	11.884	11.822
	.010	7	13.546	.9492	.004	11.939	11.933	11.912	11.878	11.814
	.005	7	13.451	.8978	.007	11.932	11.926	11.906	11.876	11.814
	.000	.....	.....	.....	$pw\mathrm{H}^\circ =$	11.926	11.920	11.900	11.871	11.809
	.....	.....	.....	.....	$\sigma_i =$	0.005	0.002	0.000	0.003	0.005
50	.015	11	13.331	.8965	0.007	11.809	11.803	11.783	11.751	11.691
	.010	9	13.252	.8549	.009	11.807	11.800	11.781	11.750	11.693
	.005	7	13.323	.9016	.008	11.796	11.791	11.771	11.739	11.678
	.000	.....	.....	.....	$pw\mathrm{H}^\circ =$	11.790	11.786	11.766	11.735	11.674
	.....	.....	.....	.....	$\sigma_i =$	0.003	0.004	0.005	0.006	0.011
55	.015	10	13.226	.9150	0.007	11.677	11.672	11.651	11.619	11.557
	.010	7	13.269	.9430	.002	11.673	11.667	11.646	11.612	11.549
	.005	7	13.161	.8832	.010	11.666	11.660	11.641	11.609	11.550
	.000	.....	.....	.....	$pw\mathrm{H}^\circ =$	11.661	11.654	11.636	11.603	11.545
	.....	.....	.....	.....	$\sigma_i =$	0.002	0.002	0.000	0.003	0.006
60	.015	11	13.081	.9024	0.006	11.554	11.548	11.528	11.496	11.435
	.010	9	13.245	1.0001	.005	11.553	11.546	11.524	11.488	11.421
	.005	7	13.058	0.8945	.008	11.544	11.538	11.518	11.486	11.426
	.000	.....	.....	.....	$pw\mathrm{H}^\circ =$	11.540	11.534	11.513	11.480	11.418
	.....	.....	.....	.....	$\sigma_i =$	0.005	0.003	0.002	0.003	0.012

[a] Standard deviation of pwH.

[b] Standard deviation of the intercept, $pw\mathrm{H}^\circ$.

7. *p*H of Calcium Hydroxide Solutions

The ionic strengths of the five solutions of calcium hydroxide at 0°, 25°, and 60° C, computed by eq (9) and (12), are as follows:

m_1	μ at—		
	0° C	25° C	60° C
0.0203	0.054	0.049	0.047
.02	.053	.049	.046
.019	.050	.047	.044
.0175	.047	.043	.041
.015	.040	.037	.035

The values of pH_s given in table 2 and plotted as a function of the molality of calcium hydroxide in figure 1 were calculated by eq (7) and (8) with the use of these ionic strengths. Each pH_s value is the mean between that obtained with $a_1=4$ and $a_1=6$; these two different estimates of pH_s differed by 0.009 unit for the solution saturated at 25° (0.0203 *m*) and by 0.007 for the 0.015-*m* solution. In the light of the statistical probable error in $pwH°$ and the partially arbitrary selection of a_1, the pH_s is assigned an uncertainty of ± 0.01 unit. The effect of a_1 on the calculated pH_s is shown in figure 2. The solid line passes through the values listed in table 2, and the dotted lines indicate the displacement resulting from a choice of $a_1=3$ and $a_1=8$.

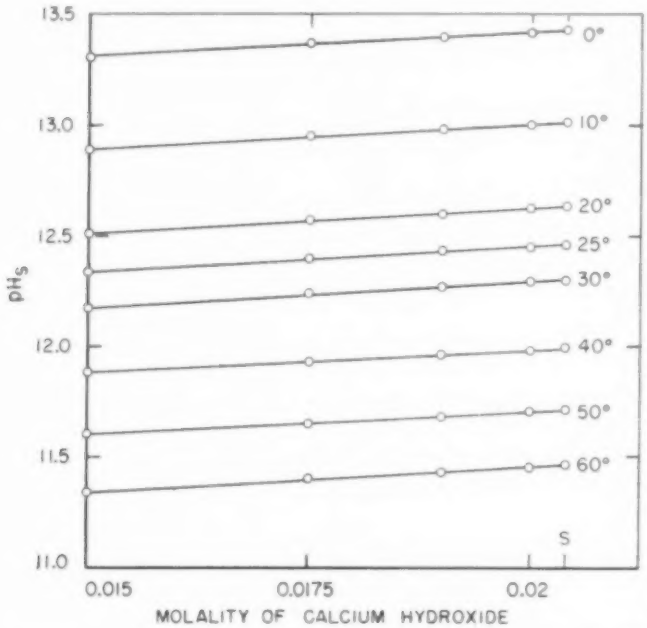

FIGURE 1. *pH_s of solutions of calcium hydroxide from 0° to 60° C, as a function of molality.*

The molality of a solution saturated at 25° C is indicated by *S*.

TABLE 2. *pH_s of five solutions of calcium hydroxide from 0° to 60° C*

t	*0.0203 *m*	0.02 *m*	0.019 *m*	0.0175 *m*	0.015 *m*
° C					
0	13.428	13.422	13.401	13.371	13.311
5	13.208	13.202	13.182	13.147	13.086
10	13.004	12.999	12.978	12.947	12.883
15	12.809	12.805	12.786	12.754	12.694
20	12.629	12.623	12.602	12.570	12.508
25	12.454	12.449	12.429	12.398	12.338
30	12.286	12.291	12.270	12.237	12.174
35	12.135	12.129	12.110	12.078	12.019
40	11.985	11.980	11.961	11.931	11.877
45	11.841	11.836	11.816	11.789	11.731
50	11.704	11.701	11.683	11.653	11.596
55	11.575	11.568	11.552	11.521	11.466
60	11.454	11.448	11.428	11.398	11.340

* Saturated at 25° C.

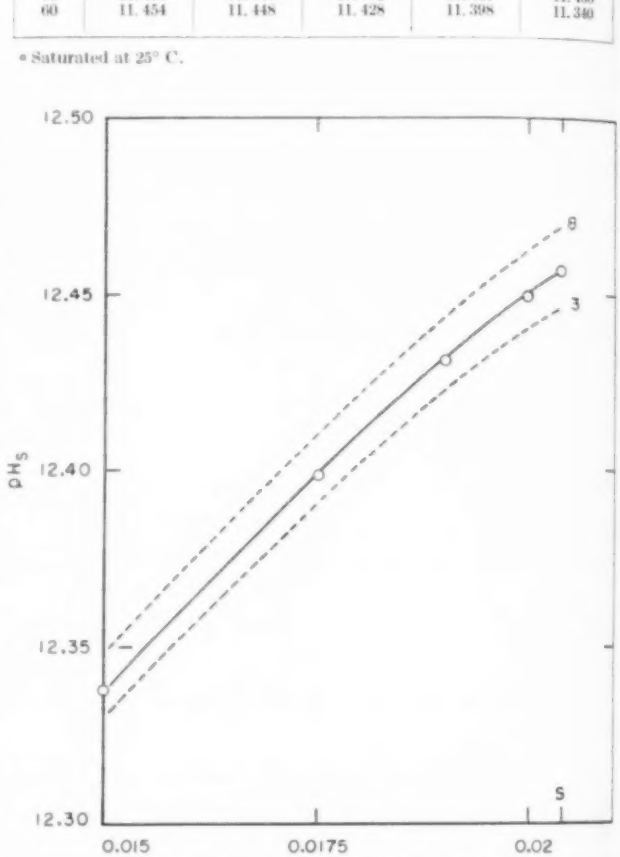

FIGURE 2. *Effect of choice of a_1 (eq 8) on the pH_s values for calcium hydroxide solutions.*

Solid line represents the mean values of pH_s obtained with $a_1=4$ and $a_1=6$; dotted lines show the displacement resulting from choice of $a_1=3$ (lower line) and $a_1=8$ (upper line).

8. Standardization in the Range *p*H 9 to 12.5

As has been pointed out earlier in this paper, a plot of the emf of cell 1 as a function of *p*H is a straight line of slope $2.3026RT/F$ when the *p*H is neither too low nor too high. At high alkalinities a voltage departure or change in slope is to be expected. There will be an accompanying aberration of the practical *p*H scale near its upper end, operating to yield *p*H values that are too low. It is appropriate to consider next the probable magnitude of the error and means of minimizing or eliminating it by proper standardization of the *p*H assembly.

The error has its origin in an experimental defect of the *p*H method, namely the changing liquid-junction potential with alteration of the concentration of highly mobile hydroxide ions. It is often not noticeable below *p*H 11, but earlier work with carbonate buffer solutions [12] has indicated that it may be detectable at *p*H 10. This earlier study suggested further that the magnitude of the discrepancy at 25° C is about 0.01 unit at *p*H 10, 0.02 unit at *p*H 11.1, and about 0.05 unit at *p*H 12.6. The error thus appears to increase in a fairly regular manner with the *p*H of the test solution.

It is of some importance, therefore, to determine whether this apparent regularity extends to solutions of calcium hydroxide. The difference of potential between one hydrogen electrode dipping in a solution saturated with calcium hydroxide at 25° C and another dipping in the standard 0.025 *M* phosphate buffer ($pH_S = 6.86_0$ at 25° C) was therefore determined. A cell consisting of two hydrogen-electrode compartments [12] was used. Contact between the solutions was established through a saturated solution of potassium chloride. The observed difference of potential was 0.3288 v at 25°, corresponding to a *p*H of 12.42_9 for the solution of calcium hydroxide. This solution was assigned a pH_S of 12.454 from measurements of cells without a liquid junction (compare table 2). The discrepancy of 0.03_4 unit at *p*H 12.45 is reasonably consistent with a linear progression of the error from *p*H 9.18 (the pH of the borax standard), which lies in the upper end of the error-free region of the practical *p*H scale [12], to *p*H 12.88, where an error of about 0.05 unit has been found [24].

As a consequence, a *p*H meter standardized at pH 9.18 will yield a slightly low reading between pH 9.18 and 12.45, and a meter standardized at *p*H 12.45 will yield a slightly high reading in the same region of the scale. The error evidently will be $(0.034/3.27)(pH_X - pH_S)$ unit. Hence, we have from eq (2)

$$pH_X = pH_S + \frac{1.0105(E_X - E_S)}{2.3026RT/F} \quad \text{(at 25° C)} \quad (13)$$

$$pH_X = pH_S + 17.08(E_X - E_S) \quad \text{(at 25° C)} \quad (14)$$

Inasmuch as the liquid-junction potential is somewhat dependent upon the structure of the liquid-liquid boundary, it is advisable to determine the error for the particular assembly that is being used. Freshly prepared borax and calcium hydroxide solutions should be used for this purpose. If the error differs much from 0.03 or 0.04 unit, the numerical coefficients of eq (13) and (14) should be adjusted accordingly. The difference as indicated by a *p*H meter may be influenced somewhat by errors in scale length and in the temperature compensator, if these have not been calibrated.

Because the *p*H meter reads *p*H units directly, it may be convenient to apply a correction to the indicated *p*H, rather than to compute the correct figure by eq (13) or (14) from a measurement of the emf. The temperature compensator of the meter is, however, designed to permit the selection of different values of the slope *p*H/emf, corresponding to the value of $F/(2.3026RT)$ at different temperatures. Hence, this device permits *p*H to be read directly from the scale of the instrument, even though the functional relationship between the emf of the cell and the *p*H value varies rather widely, as it may do when the temperature of the cell changes.

When the temperature compensator indicates 25° C, the instrument converts emf differences into *p*H differences according to the relationship $\Delta pH = 16.90\Delta E$; at 20° C, the conversion is made according to $\Delta pH = 17.19\Delta E$. It is evidently possible, then, to compensate the liquid-junction error at the high end of the scale, permitting correct values at 25° C to be read directly from the meter, if the temperature compensator is set at 22° C, for at this temperature $F/(2.3026RT)$ is not far from 17.08 (compare eq (14)). The values of this quantity at other temperatures are:

°C	
10	17.80
15	17.49
20	17.19
25	16.90
30	16.63

The alkaline error of the glass electrode made from Corning 015 glass is very much lower in solutions of calcium salts than in solutions of lithium or sodium salts [25]. However, in a saturated solution of calcium hydroxide, this source of error may be of concern at temperatures from 40° to 60° C. Many of the newer commercial electrode glasses contain no calcium, and hence the voltage departures in calcium solutions are probably negligible.

9. A Standard Solution of Calcium Hydroxide

A solution of calcium hydroxide saturated at room temperature is recommended as a *p*H standard for the highly alkaline range. A considerable excess of pure, finely granular hydroxide is shaken vigorously in a stoppered bottle with water at room temperature. The gross excess of solid is allowed to settle,

the temperature recorded to the nearest degree Celsius, and the suspended material removed by filtration with suction on a sintered-glass funnel of medium porosity.

It has been recommended that a slurry containing excess calcium hydroxide be used for standardization purposes [11]. However, large errors are sometimes incurred in pH measurements of suspensions [26], and it seems best to rule out this uncertainty by removal of the solid phase.

For the saturation, a polyethylene bottle is very satisfactory; in fact, it may be found convenient to keep the solid continuously under water in a well-stoppered polyethylene bottle ready for final saturation and filtration when a fresh solution is needed. Contamination of the solution with atmospheric carbon dioxide prior to filtration is obviously of little concern. Contamination of the filtered standard solution renders it turbid and is a cause for replacement.

The temperature coefficient of solubility is negative, but the solution supersaturates readily and no precipitation of solid is ordinarily observed at 60° C. Unfortunately, however, the change of solubility with temperature is sufficiently large to require that the saturation temperature be noted and the $p\mathrm{H_s}$ values (column 2, table 2) adjusted by the appropriate amount. These values for saturation temperatures of 20°, 25°, and 30° C are:

Saturation temperature	Solubility (m)	$p\mathrm{H_s}$ at (° C)—			Correction to column 2, table 2
		20	25	30	
°C					
20	0.0211	12.64	12.47	12.31	+0.015
25	.0203	12.63	12.45	12.30	0
30	.0195	12.61	12.44	12.28	−.016

The calcium hydroxide should be prepared from well-washed calcium carbonate of low-alkali grade. The carbonate is heated slowly to 1,000° C and ignited for at least 45 min at that temperature. After cooling, the calcium oxide is added slowly to water with stirring and the suspension heated to boiling, cooled, and filtered on a sintered-glass funnel of medium porosity. The solid is dried in an oven and crushed to a uniform finely granular state for use.

It is advisable to determine the concentration of a saturated solution of one portion of calcium hydroxide prepared from each particular lot of calcium carbonate, as described earlier in this paper. The molality (m) and molarity (M) of the saturated solution are practically identical, differing by only 0.3 percent. If the concentration of the solution saturated at 25° C appears to exceed 0.0206 M, the presence of soluble alkalies is indicated. If calcium carbonate of a higher grade cannot readily be obtained, the impurity in the available carbonate or hydroxide should be extracted by careful washing with water.

10. References

[1] V. E. Bower, R. G. Bates, and E. R. Smith, J. Research NBS **51,** 189 (1953) RP2450.
[2] R. G. Bates, V. E. Bower, R. G. Miller, and E. R. Smith, J. Research NBS **47,** 433 (1951) RP2268.
[3] W. J. Hamer, G. D. Pinching, and S. F. Acree, J. Research NBS **36,** 47 (1946) RP1690.
[4] R. G. Bates and S. F. Acree, J. Research NBS **34,** 373 (1945) RP1648.
[5] G. G. Manov, N. J. DeLollis, P. W. Lindvall, and S. F. Acree, J. Research NBS **36,** 543 (1946) RP1721.
[6] D. D. Van Slyke, J. Biol. Chem. **52,** 525 (1922).
[7] R. G. Bates, Anal. Chem. **26,** 871 (1954).
[8] R. G. Bates, Electrometric pH determinations, chapters 4, 5, and 7 (John Wiley & Sons, Inc., New York, N. Y., 1954).
[9] E. P. Flint and L. S. Wells, BS J. Research **11,** 167 (1933) RP584.
[10] G. G. Manov, N. J. DeLollis, and S. F. Acree, J. Research NBS **34,** 115 (1945) RP1632.
[11] W. M. Tuddenham and D. H. Anderson, Anal. Chem. **22,** 1146 (1950).
[12] R. G. Bates, G. D. Pinching, and E. R. Smith, J. Research NBS **45,** 418 (1950) RP2153.
[13] J. Johnston and C. Grove, J. Am. Chem. Soc. **53,** 3976 (1931).
[14] T. Noda and A. Miyoshi, J. Soc. Chem. Ind., Japan **35,** 3173 (1932).
[15] H. S. Harned and R. W. Ehlers, J. Am. Chem. Soc. **55,** 1350, 2179 (1933); R. G. Bates and V. E. Bower, J. Research NBS **53,** 283 (1954) RP2546.
[16] G. A. Manov, R. G. Bates, W. J. Hamer, and S. F. Acree, J. Am. Chem. Soc. **65,** 1765 (1943).
[17] R. P. Bell and J. E. Prue, J. Chem. Soc., 362 (1949).
[18] H. Bassett, J. Chem. Soc., 1270 (1934).
[19] R. B. Peppler and L. S. Wells, J. Research NBS **52,** 75 (1954) RP2476.
[20] G. T. Moody and L. T. Leyson, J. Chem. Soc. **93,** 1767 (1908).
[21] R. T. Haslam, G. Calingaert, and C. M. Taylor, J. Am. Chem. Soc. **46,** 308 (1924).
[22] R. G. Bates and S. F. Acree, J. Research NBS **30,** 129 (1943) RP1524.
[23] G. D. Pinching and R. G. Bates, J. Research NBS **37,** 311 (1946) RP1749.
[24] R. G. Bates and V. E. Bower, Anal. Chem. (publication pending).
[25] M. Dole, The glass electrode, ch. 7 (John Wiley & Sons, Inc., New York, N. Y., 1941).
[26] H. Jenny, T. R. Nielsen, N. T. Coleman, and D. P. Williams, Science **112,** 164 (1950).

WASHINGTON, February 6, 1956.

Journal of Research of the National Bureau of Standards Vol. 56, No. 6, June 1956 Research Paper 2681

Heats of Formation of Hexacalcium Dialumino Ferrite and Dicalcium Ferrite

E. S. Newman and Roald Hoffman

Measurements were made of the heat of solution of $6CaO{\cdot}2Al_2O_3{\cdot}Fe_2O_3$ and $2CaO{\cdot}Fe_2O_3$ in HCl, $26.61H_2O$ (2.000 normal at 25° C). From these data, together with appropriate heat-of-dilution measurements and data taken from the literature, the heats of formation of the two compounds were calculated.

1. Introduction

The major part of the iron in portland cement clinker is found in combination with lime and alumina in the form of solid solutions between the compounds $6CaO{\cdot}2Al_2O_3{\cdot}Fe_2O_3$ and $2CaO{\cdot}Fe_2O_3$[1].[1] One such solution, brownmillerite, had been recognized earlier as an important constituent of portland cement [2]. Thorvaldsen, Edwards, and Bailey [3] determined the heat of formation of this material, and Lerch and Bogue [4] measured its heat of hydration. A general investigation of the thermochemistry of the compounds occurring in hydraulic cements is being conducted at the National Bureau of Standards. The heats of solution of solid solutions of $6CaO{\cdot}2Al_2O_3{\cdot}Fe_2O_3$ and $2CaO{\cdot}Fe_2O_3$, measured in a mixture of nitric and hydrofluoric acids, were given in a previous paper [5]. The present paper gives the heats of solution of these two compounds in hydrochloric acid and the heats of formation calculated therefrom.

2. Experimental Procedure and Results

2.1. Thermochemical Equations

Heats of formation are usually obtained by the addition of a considerable number of thermochemical equations. The equations must be written with the proper coefficients to agree with the stoichiometry of the reactions they describe and to fit the experimental conditions chosen. After a few experimental conditions have been arbitrarily selected, others in subsequent experiments will be fixed by the relationships among the equations. To find these conditions, the entire series of thermochemical equations must be written in detail. For this reason, the thermochemical equations for the determination of the heats of formation of $6CaO{\cdot}2Al_2O_3{\cdot}Fe_2O_3$ and $2CaO{\cdot}Fe_2O_3$ are given here. For completeness, the heats of reaction are also given, although some of the values were obtained as the experimental results of the work described hereafter. The arbitrarily selected experimental conditions were based on the volume of the heat-of-solution calorimeter and the solubilities of the substances involved. The conditions chosen were such that a sample weight of 1 g of powdered sample would be dissolved in 600.0 g of 2.000 N HCl (HCl, $26{\cdot}61_4H_2O$ at 25° C). Upon this basis the following thermochemical equations were written. The reasons for their use will be apparent or will be discussed later. Unless otherwise noted, the equations are written for isothermal reactions at 25° C.

a. Heat of Formation of $6CaO{\cdot}2Al_2O_3{\cdot}Fe_2O_3$

The heat of formation of $6CaO{\cdot}2Al_2O_3{\cdot}Fe_2O_3$ from the oxides may be obtained by summing the equations

$$(784.1HCl,\ 6CaCl_2,\ 4AlCl_3,\ 2FeCl_3,\ 2168OH_2O)(soln) \rightarrow 6CaO{\cdot}2Al_2O_3{\cdot}Fe_2O_3(c) + 814.1(HCl,\ 26.61H_2O)\ (soln),\quad \Delta H_1 = 402.41\ \text{kcal}. \tag{1}$$

$$6CaO(c) + 12(HCl,\ 26.61H_2O)(soln) \rightarrow 6(CaCl_2,\ 53.23H_2O)(soln) + 6H_2O(l),\quad \Delta H_2 = -280.58\ \text{kcal}. \tag{2}$$

[1] Figures in brackets indicate the literature references at the end of this paper.

$$6H_2O(l)+6(CaCl_2,\ 53.23H_2O)(soln)\rightarrow 6(CaCl_2{\cdot}54.23H_2O)(soln),\quad \Delta H_3=-0.06\ \text{kcal.} \tag{3}$$

$$Fe_2O_3(c,\ 20^\circ\ C)+6(HCl,\ 200H_2O)(soln,\ 20^\circ\ C)\rightarrow 2(FeCl_3,\ 601.5H_2O)(soln,\ 20^\circ\ C),\quad \Delta H_4=-24.74\ \text{kcal.} \tag{4}$$

$$Fe_2O_3(c,\ 25^\circ\ C)\rightarrow Fe_2O_3(c,\ 20^\circ\ C),\quad \Delta H_5=-0.124\ \text{kcal.} \tag{5}$$

$$6(HCl,\ 200H_2O)(soln,\ 25^\circ\ C)\rightarrow 6(HCl,\ 200H_2O)(soln,\ 20^\circ\ C),\quad \Delta H_6=-107.13\ \text{kcal.} \tag{6}$$

$$2(FeCl_3,\ 601.5H_2O)(soln,\ 20^\circ\ C)\rightarrow 2(FeCl_3,\ 601.5H_2O)(soln,\ 25^\circ\ C)\quad \Delta H_7=107.79\ \text{kcal.} \tag{7}$$

$$2(FeCl_3,\ 601.5H_2O)(soln)\rightarrow 2(FeCl_3,\ 81.34H_2O)(soln)+1040H_2O,\quad \Delta H_8=4.028\ \text{kcal.} \tag{8}$$

$$6(HCl,\ 26.61H_2O)(soln)+1040H_2O\rightarrow 6(HCl,\ 200H_2O)(soln),\quad \Delta H_9=-2.568\ \text{kcal.} \tag{9}$$

$$2Al_2O_3(c,\alpha)+12(HCl,\ 26.61H_2O)(soln)\rightarrow 4(AlCl_3,\ 81.34H_2O)(soln),\quad \Delta H_{10}=-119.44\ \text{kcal.} \tag{10}$$

$$6(CaCl_2,\ 54.23H_2O)(soln)+784.1(HCl,\ 26.61H_2O)(soln)\rightarrow(784.1HCl,\ 6CaCl_2,\ 21190H_2O)(soln),\quad \Delta H_{11}=0.29\ \text{kcal.} \tag{11}$$

$$4(AlCl_3,\ 81.34H_2O)(soln)+(784.1HCl,\ 6CaCl_2,\ 21190H_2O)(soln)\rightarrow(784.1HCl,\ 6CaCl_2,\ 4AlCl_3,\ 21520H_2O)(soln),\quad \Delta H_{12}=0.48\ \text{kcal.} \tag{12}$$

$$2(FeCl_3,\ 81.34H_2O)+(784.1HCl,\ 6CaCl_2,\ 4AlCl\ 21520H_2O)(soln)\rightarrow(784.1HCl,\ 6CaCl_2,\ 4AlCl_3,\ 2FeCl_3,\ 21680H_2O)(soln),\quad \Delta H_{13}=1.35\ \text{kcal.} \tag{13}$$

The sum of eq (2) and (3) is

$$6CaO(c)+12(HCl,\ 26.61H_2O)(soln)\rightarrow 6(CaCl_2,\ 54.23H_2O)(soln),\quad \Delta H_{14}=-280.64\ \text{kcal.} \tag{14}$$

The sum of eq (4) to (9), inclusive, is

$$Fe_2O_3(c)+6(HCl,\ 26.61H_2O)(soln)\rightarrow 2(FeCl_3,\ 81.34H_2O)(soln),\ \Delta H_{15}=-22.74\ \text{kcal.} \tag{15}$$

These two equations (14 and 15) represent the solution of two of the oxide constituents of $6CaO{\cdot}2Al_2O_3{\cdot}Fe_2O_3$ in HCl, $26.61H_2O$.

The sum of eq (1) to (13), inclusive, represents the formation of $6CaO{\cdot}2Al_2O_3{\cdot}Fe_2O_3$ from the oxides,

$$6CaO(c)+2Al_2O_3(c,\alpha)+Fe_2O_3(c)\rightarrow 6CaO{\cdot}2Al_2O_3{\cdot}Fe_2O_3(c),\quad \Delta H_{16}=-18.29\ \text{kcal.} \tag{16}$$

b. Heat of Formation of $2CaO{\cdot}Fe_2O_3$

In a similar manner, the heat of formation of $2CaO{\cdot}Fe_2O_3$ from the oxides was obtained from the equations

$$(306.2HCl,\ 2CaCl_2,\ 2FeCl_3,\ 8419H_2O)(soln)\rightarrow 2CaO{\cdot}Fe_2O_3(c)+316.2(HCl,\ 26.61H_2O)(soln),\quad \Delta H_{17}=107.40\ \text{kcal.} \tag{17}$$

$$2CaO(c)+4(HCl,\ 26.61H_2O)(soln)\rightarrow 2(CaCl_2,\ 54.23H_2O)(soln),\ \Delta H_{18}=-93.55\ \text{kcal.} \tag{18}$$

$$Fe_2O_3(c)+6(HCl,\ 26.61H_2O)(soln)\rightarrow 2(FeCl_3,\ 81.34H_2O)(soln),\quad \Delta H_{15}=-22.74\ \text{kcal.} \tag{15}$$

$$2(CaCl_2,\ 54.23H_2O)(soln)+306.2\,(HCl,\ 26.61H_2O)(soln)\rightarrow(306.2HCl,\ 2CaCl_2,\ 8256H_2O)(soln),\quad \Delta H_{19}=0.11\ \text{kcal.} \tag{19}$$

$$2(FeCl_3,\ 81.34H_2O)(soln)+(306.2HCl,\ 2CaCl_2,\ 8256H_2O)(soln)\rightarrow(306.2HCl,\ 2CaCl_2,\ 2FeCl_3,\ 8419H_2O)(soln),\quad \Delta H_{20}=1.34\ \text{kcal.} \tag{20}$$

The sum of the above five equations represents the formation of $2CaO{\cdot}Fe_2O_3$ from the oxides,

$$2CaO(c)+Fe_2O_3(c)\rightarrow 2CaO{\cdot}Fe_2O_3(c),\quad \Delta H_{21}=-7.44\ \text{kcal.} \tag{21}$$

2.2. Preparation of the Samples

The samples of dicalcium ferrite and hexacalcium dialumino ferrite used in this investigation were the same ones used in the previous work [5], and their preparation has been described. Because in 8 years of storage the ignition losses had become about 0.2 percent, the samples were sintered overnight at 1,200° C and reground for 2 hr in a power-driven mortar just before the beginning of the present heat-of-solution measurements. The heat-of-dilution experiments were performed with solutions of calcium chloride, aluminum chloride, and ferric chloride prepared from analytical reagents. The manufacturers' lot analyses were assumed correct, because the heat effects to be measured were small and minor errors in the concentrations of the solutions would have a negligible effect on the measured values.

2.3. Apparatus and Procedure

a. Heats of Solution

All experiments were performed in an air-conditioned room controlled at 25 ± 0.8° C and a maximum relative humidity of 50 percent. The heats of solution were determined using 1-g samples in an isothermal-jacket calorimeter [6] containing 600.0 g of HCl, 26.61_4H_2O. The temperature changes were measured with a 25.5-ohm platinum resistance thermometer, Mueller bridge, and a galvanometer with an 8-m optical lever. The sensitivity of the measuring system was such that a scale deflection of 1 mm corresponded to a temperature change of about 0.000073 deg C. The corrected temperature rises were calculated according to the method described by White [7, p. 42]. Time-temperature data were taken with the aid of a chronograph during the rapid-rise portion of the experimental period, and the area under the time-temperature curve was obtained by using the trapezoidal rule. The 1-g samples dissolved in 30 to 40 min. The powdered samples were kept in the balance case, the temperature of which was recorded, and appropriate corrections were made for the sensible heat introduced into the calorimeter with the samples, using 0.2 cal/g for their specific heat. The final calorimeter temperature was always within a few hundredths of a degree of 25.00° C, and no further corrections were made to bring the measured isothermal heats of solution to that reference temperature. The thermochemical calorie of 4.1840 absolute joules was used. The calorimeter containing the solvent acid was calibrated electrically [14, p. 217] over approximately the temperature range covered by the heat-of-solution measurements. The standard cell and standard resistors used in measuring the electric energy were calibrated by the Electricity and Electronics Division of the Bureau, and the input was timed using a chronograph and the standard seconds signals originating in the Mechanics Division. The resistance thermometer was used in the customary manner without converting resistance changes to degrees Celsius. Hence the energy equivalent was obtained in calories per ohm, and is approximately equal to calories per 9.901 deg C.

b. Heats of Dilution

The heats of dilution were determined in a calorimeter consisting of a 1-pt wide-mouthed vacuum flask partially submerged in a constant-temperature water bath. The cork and upper end of the flask were protected from room-temperature variations by a double-walled copper cap dipping into the water, as suggested by White [7, p. 152]. The liquid sample was held in a thin-walled glass bulb with a long stem. The bulb was placed beneath the surface of the calorimeter acid with the stem held in a clamp above the copper cap. A thin glass rod was placed so as to rest in the bulb with the upper end protruding slightly above the stem, and a 40-cm glass tube of larger diameter was attached to the stem with a short piece of rubber tubing. An 8-g weight was held at the top of the tube, to which was connected a 100-ml reservoir containing air at a gage pressure of about 0.3 lb/in^2. To introduce the sample, the weight was allowed to fall, and the impact drove the lower end of the rod through the bulb. A small quantity of air passed through the tube until the pressure in the reservoir fell to about 0.1 lb/in^2. The pressure was then released to allow the stem of the bulb to fill to

the liquid level in the calorimeter. This somewhat elaborate system was used to insure complete and prompt introduction of the sample. The arrangement of the calorimeter required that the bulb be placed off center, and the stem frequently broke if the bulb was simply pushed against the hemispherical bottom of the vacuum flask. On the other hand, the rod frequently punched only a small hole through the bottom of the bulb, and the air pressure was necessary to make certain that the sample passed into the calorimeter acid.

Three-hundred-seventy-gram quantities of HCl, $26.61H_2O$ or of distilled water were used in the calorimeter. The heat-of-dilution experiments were performed by using proportions of acid or of water to solution such that the final concentrations should be identical with those in the heat-of-solution determinations. The concentrations and quantities to be used in each experiment were calculated from the appropriate thermochemical equation listed in section 2.1. The calorimeter was calibrated electrically, using the same procedure and equipment described in the preceding section. The heat capacities of the solutions contained in the sample bulbs were estimated from the apparent molal heat capacities of the solutes, and the energy equivalent of the vacuum flask calorimeter and its contents was increased correspondingly. Here again the heat effects to be measured were small, and small errors in the heat capacity did not affect the final results significantly. The final temperature of the calorimeter was always close to 25.00° C, and, as in the heat-of-solution measurements, no further corrections were made to obtain the heats of dilution at the reference temperature. Using the platinum resistance thermometer described in section 2.3.a, the bridge current was reversed each time the calorimeter temperature was recorded. This reversal, by doubling the observed deflection, doubled the sensitivity of the measurements. The very small corrected temperature changes during the experimental period were calculated by graphical or analytical extrapolation of the time-temperature data observed during the initial and final rating periods [14, p. 232].

The heat effect of breaking the sample bulbs was determined by performing heat-of-dilution experiments in which the solution in the bulb was the same as that in the calorimeter. Under these conditions, no dilution effects would occur. The average value of this blank determination was subtracted from each heat-of-dilution measurement.

2.4. Experimental Results

In table 1 are given the results of the calibration experiments for the heat-of-solution calorimeter, and of the heat-of-solution and heat-of-dilution measurements. The measured heat effects of breaking a number of sample bulbs such as were used in the heat-of-dilution

TABLE I. *Calorimetric results*

Energy equivalent of heat-of-solution calorimeter	$6CaO{\cdot}2Al_2O_3{\cdot}Fe_2O_3$				$2CaO{\cdot}Fe_2O_3$			Blank[a]
	Heat of solution	Heat of mixing of solutions			Heat of solution	Heat of mixing of solutions		
		$CaCl_2$, $54.23H_2O$ (eq 11)	$AlCl_3$, $81.34H_2O$ (eq 12)	$FeCl_3$, $81.34H_2O$ (eq 13)		$CaCl_2$, $54.34H_2O$ (eq 19)	$FeCl_3$, $81.34H_2O$ (eq 20)	
cal/ohm[b]	*cal/g*	*cal/g*[c]	*cal/g*[c]	*cal/g*[c]	*cal/g*	*cal/g*[c]	*cal/g*[c]	*cal*
5813.25	575.77	−0.38	−0.75	−1.96	394.91	−0.48	−4.98	0.04
5815.06	570.13	−.43	−.65	−1.94	395.88	−.39	−4.82	.02
5813.57	578.48	−.42	−.70	−1.83	394.55	−.44	−5.00	.02
5821.04	573.80	−.44	−.64	−1.97	394.32	−.34	−4.90	.06
5820.62	575.88	−.38	.....	−1.94	394.32	.....	.....	.....
.....	575.17	.....	.....	.....	395.02	.....	.....	.05
.....	574.25	.....	.....	.....	396.43	.....	.....	.....
.....	575.08	.....	.....	.....	.....	.....	.....	.....
Avg 5816.70	574.82	−0.410	−0.685	−1.928	395.06	−0.412	−4.925	.048
S. D.[d] 1.71	0.83	.015	.025	0.025	0.25	.030	0.041	.012

[a] Heat effect of breaking the bulb containing the solution.
[b] $\triangle R/\triangle T$ is approximately 0.1010 ohm/deg at 25° C. Therefore, 5816.70 cal/ohm is approximately 587.5 cal/°C.
[c] Calories per gram of ferrite comound. These quantities have been corrected for the average energy of breaking the bulbs.
[d] Standard deviation of the average, $\sqrt{[\Sigma x^2-(\Sigma x)^2/n]/n(n-1)}$.

experiments are also given. The observed heats of dilution were corrected for the average observed energy of breaking the sample bulb before being calculated to the basis of 1 g of powdered sample as given in table 1.

2.5. Heats of Formation

The procedure for calculating the heats of formation of the two ferrites from the oxides has been outlined by the equations in section 2.1. The experiments and calculations represented by the equations will now be discussed.

a. Heat of Formation of $6CaO{\cdot}2Al_2O_3{\cdot}Fe_2O_3$

Equation (1) represents the experimental determination of the heat of solution of $6CaO{\cdot}2Al_2O_3{\cdot}Fe_2O_3$, converted to a molar basis. The equation is written in reverse for addition, the sign of the heat effect being changed. The experimental results in table 1 give the value 402.41 $\pm$0.58 kcal/mole for the heat of solution. (The standard deviation of the average is given here and elsewhere in this paper.)

Equations (2) and (3) together represent the measurement of the heat of solution of 6 moles of calcium oxide in an equivalent amount of hydrochloric acid. The heat of reaction ΔH_2 was calculated from heat-of-formation data taken from Circular 500 of the National Bureau of Standards [13]. Revised values [11] were used for the heat of formation of HCl, aq. The data for $CaCl_2$ solutions [13] were plotted and ΔH_3 was calculated as the slope of the curve of the heat of formation versus n, at $n=54$ moles of water per mole of $CaCl_2$.

The heat of solution of Fe_2O_3 in HCl, $26.61H_2O$ cannot be determined directly, because Fe_2O_3 will not dissolve. Thorvaldsen, Edwards, and Bailey [3] determined the heat of solution in HCl, 200 at 20° C by an indirect method. Equations (5) to (9) represent the recalculation of their result, given as eq (4), to the appropriate conditions for the present investigation, i. e., the heat of solution at 25° C in HCl, $26.61H_2O$. Equations (5), (6), and (7) represent the heat effect of changing the temperature of the reaction to 25° C. The heat capacity value of 24.7 cal/deg-mole used in calculating ΔH_5 was taken from Kelley's compilation of low-temperature heat capacities [9]. Revised values [11] for the apparent heat capacity of HCl, aq. were used in estimating the value -29.3 cal/deg-mole for the apparent heat capacity of HCl, $200H_2O$ over the range 20° to 25° C. This value was used in calculating ΔH_6. The apparent heat capacity of $FeCl_3$, $601.5H_2O$, used in calculating ΔH_7, was determined by a plot of heat capacity versus the square root of the molality, calculated from the data of Kangro and Flugge [10]. The value -51.4 cal/deg-mole at 20° C was obtained. It was estimated [11] that the apparent heat capacity would become about 1 cal/deg-mole more positive for each degree rise in temperature, and the average value -48.9 cal/deg-mole was used for the change from 20° to 25° C represented by eq (7).

To obtain the value of ΔH_8, the dilution experiment represented by eq (8) (written in reverse) was performed. Ferric chloride solutions are subject to hydrolysis and the formation of complexes, and relatively few heat-of-dilution data are available [10]. A few drops of HCl were added to the ferric chloride solution to stabilize it. The heat effect possibly caused by the presence of this small amount of acid was ignored, as Thorvaldsen and his coworkers [3] found that the heat of mixing of ($FeCl_3$, $600H_2O$+HCl, $200H_2O$) with HCl, $200H_2O$ was negligible. The heat-of-dilution value -2.014 ± 0.014 kcal/mole was found as the average of five determinations. Equation (9) represents the dilution of HCl, 26.61 H_2O to HCl, $200H_2O$. The heat effect of this reaction was calculated from the revised values of the heat of formation of HCl, aq. The sum of eq (4) to (9) gives

$$Fe_2O_3(c)+6(HCl,\ 26.61H_2O)\ (soln)\rightarrow 2(FeCl_3,\ 81.34H_2O)\ (soln),\quad \Delta H_{15}-22{\cdot}74\ \text{kcal}. \quad (15)$$

Aluminum oxide, like ferric oxide, cannot be dissolved in HCl, 26.61 H_2O. Its heat of solution was calculated in an earlier paper [12]. The calculation was repeated by using the revised heats of formation of hydrochloric acid solutions, and ΔH_{10} was obtained.

Equations (11), (12), and (13) represent a dilution experiment in which solutions of $CaCl_2$, $AlCl_3$, and $FeCl_3$ were added in succession to a single calorimeter charge of HCl, $26.61H_2O$. The proportions and concentrations to be used were calculated from the equations, and the experiment was performed a number of times. The detailed results are given in table 1. The average values obtained were calculated to the basis of 1 mole of $6CaO{\cdot}2Al_2O_3{\cdot}Fe_2O_3$, and are given as 0.29, 0.48, and 1.35 kcal for ΔH_{11}, ΔH_{12}, and ΔH_{13} respectively. The corresponding standard deviations are ± 0.010, ± 0.017, and ± 0.017 kcal, respectively.

The summation of eq (1) to (13), inclusive, gives eq (16), representing the formation of $6CaO{\cdot}2Al_2O_3{\cdot}Fe_2O_3$ from the oxides,

$$6CaO(c)+2Al_2O_3(c,\ \alpha)+Fe_2O_3(c)\rightarrow 6CaO{\cdot}2Al_2O_3{\cdot}Fe_2O_3(c),\ \Delta H-18.29\ \text{kcal}. \qquad (16)$$

The standard deviation of the heat of formation, estimated from the sum of the variances of the heats of reaction entering into its calculation, is about ± 0.6 kcal/mole.

b. Heat of Formation of $2CaO{\cdot}Fe_2O_3$

The heat of formation of dicalcium ferrite was calculated in a manner analogous to that of $6CaO{\cdot}2Al_2O_3{\cdot}Fe_2O_3$. Equation (14) represents the heat of solution of $2CaO{\cdot}Fe_2O_3$ written in reverse. The heat of solution, calculated from the data in table 1, was 107.40 ± 0.068 kcal/mole. Equation (18), which is one-third of eq (14), represents the heat of solution of 2 moles of CaO in HCl, $26.61H_2O$, with a heat effect of -93.55 kcal. Equation (15) has been discussed. The last two equations, (19) and (20), represent the appropriate heat-of-dilution measurements in which first $CaCl_2$ and then $FeCl_3$ solution was added to a single calorimeter acid charge. The experiment was performed, in proportions of solution to acid calculated from the equations, and the values 0.11 and 1.34 kcal per mole of $2CaO{\cdot}Fe_2O_3$ obtained for ΔH_{19} and ΔH_{20}, respectively. The corresponding standard deviations are ± 0.008 and ± 0.011 kcal, respectively. The summation of the equations indicated in section 2.1.b gives eq (21), representing the formation of $2CaO{\cdot}Fe_2O_3$ from the oxides.

$$2CaO(c)+Fe_2O_3(c)\rightarrow 2CaO{\cdot}Fe_2O_3(c),\quad \Delta H_{21}=-7.44\ \text{kcal}. \qquad (21)$$

The standard deviation of the heat of formation, estimated in a similar manner to that of $6CaO{\cdot}2Al_2O_3{\cdot}Fe_2O_3$, is about 0.1 kcal/mole.

3. Summary

Measurements were made of the heat of solution of $6CaO{\cdot}2Al_2O_3{\cdot}Fe_2O_3$ and $2CaO{\cdot}Fe_2O_3$ in HCl, $26.61H_2O$ (2.00 N at 25° C). Heats of dilution of aqueous $CaCl_2$, $AlCl_3$, and $FeCl_3$ in the same acid were also determined. From these measurements and from data in the literature, the heats of formation of the two compounds from the oxides were calculated to be -18.3 and -7.4 kcal/mole, respectively.

4. References

[1] M. A. Swayze, Am. J. Science **244,** 1–30 (1946).
[2] R. H. Bogue, Ind. Eng. Chem. Anal. Ed. **1,** 192 (1929).
[3] T. Thorvaldsen, R. R. Edwards, and E. C. Bailey, Z. anorg. u. allgem. Chem. **236,** 310 (1938).
[4] W. Lerch and R. H. Bogue, BS J. Research **12,** 645 (1934) RP 684.
[5] E. S. Newman, J. Research NBS **38,** 661 (1947) RP 1805.
[6] E. S. Newman, J. Research NBS **54,** 347 (1955) RP 2597.
[7] W. P. White, The modern calorimeter (The Chemical Catalog Co., New York, N. Y., 1928).
[8] E. S. Newman and L. S. Wells, J. Research NBS **20,** 825 (1938) RP 1107.
[9] K. K. Kelley, U. S. Bureau of Mines Bulletin 477 (1950).
[10] W. Kangro and R. Flugge, Z. phys. Chem. **175,** 187 (1935).
[11] W. H. Evans (private communication).
[12] R. B. Peppler and E. S. Newman, J. Research NBS **47,** 439 (1951) RP2269.
[13] F. D. Rossini, D. D. Wagman, W. H. Evans, S. Levine, and I. Jaffe, NBS Circ. 500 (1952).
[14] H. C. Dickenson, Bul. BS **11,** 189 (1915) S230.

Washington, January 4, 1956.

Journal of Research of the National Bureau of Standards Vol. 56, No. 6, June 1956 Research Paper 2682

Response of a Sodium-Iodide Scintillation Spectrometer to 10- to 20-Million-Electron-Volt Electrons and X-Rays[1]

H. W. Koch and J. M. Wyckoff

The response of a large-crystal sodium-iodide spectrometer was studied for individual monoenergetic electrons extracted from a 50-million-electron-volt betatron operated between 1 and 20 Mev. The energy resolution with crystals 5 inches in diameter by 4 inches in length and 5 inches in diameter by 9 inches in length reaches its optimum value for electrons of 6 Mev, where the total width of the pulse-height distribution at half maximum is 4 percent. Syntheses of pulse-height distributions for 11- and 19-Mev monoenergetic X-ray photons are made by using the experimental electron pulse-height distributions. The computed results compare favorably with the measured pulse-height distributions for 11.6- and 17.6-Mev gamma rays. Syntheses provide one of the few procedures for predicting spectrometer response functions in this X-ray energy range.

1. Introduction

The pulse-height distributions produced in total-absorption spectrometers by monoenergetic X-rays show a narrow peak with small tail at low pulse heights [1].[2] These spectrometers are therefore suitable for the accurate study of continuous distributions of X-rays and for analyses of the shape of the continuum. However, an analysis of the spectrometer output in terms of the number of X-ray photons at each photon energy requires detailed information about the response function of the spectrometer to monoenergetic X-rays or gamma rays in the energy range of interest.

For energies below 3 Mev, gamma rays from long-lived radioactive sources are available at sufficiently small energy intervals to permit the accurate evaluation of the spectrometer response.

At energies above 3 Mev, the available nuclear gamma rays are few, weak in intensity, and generally unsuitable for the determination of response functions. For example, the relatively monoenergetic $Li^7(p,\gamma)Be^8$ gamma rays are a 17.6-Mev gamma ray accompanied by a broad line at 14.8 Mev. The lower energy line is sufficiently broad as to obscure somewhat the interpretation of the shape of the 17.6-Mev pulse-height distribution. Similarly, the $B^{11}(p,\gamma)C^{12}$ and the $Be^9(\alpha,n\gamma)C^{12}$ reactions provide 11.6- and 4.43-Mev gamma rays, respectively, that are weak in intensity, and experiments with them are consequently troubled by large relative backgrounds.

The response function can also be obtained by a Monte Carlo calculation [2]. However, these calculations are tedious and very time-consuming even when performed with the aid of automatic computers. The difficulty arises from the multiple interactions that must be followed in some detail at energies above 1 Mev.

In order to provide some detailed data on the response of a large-crystal spectrometer for 10- to 20-Mev monoenergetic X-rays, the response to monoenergetic electrons was examined [3] as described in this report, and then the pulse-height distributions for two X-ray energies were synthesized from these data. Specific X-ray energy values of 11 and 19 Mev were chosen for the synthesis on the basis of a planned matrix covering the 10- to 20-Mev region. These values are also reasonably near experimentally measured monoenergetic gamma-ray peaks of 11.6 and 17.6 Mev, and so the calculations lend themselves to a comparison with the experimental results.

The sodium-iodide crystals in the scintillation spectrometer used in the electron part of the experiment were 5-in. diameter by 4 in. long, 5 in. diameter by 5 in. long, and 5 in. diameter by 9 in. long. Pulse-height distributions were obtained for electrons with energies between 1 and 20 Mev. The results gave the shapes of the distributions, the variation of the relative resolution (full-width at half maximum divided by the pulse height at the maximum) with electron energy, and the linearity of the pulse height of the peak of the pulse-height distribution versus electron energy.

The pulse-height distributions for monoenergetic X-rays were synthesized for a 5-in.-diameter by 9-in.-long-crystal spectrometer from the electron results. This work, which is also described in this report, was motivated by the fact that good predictions of pulse-height distributions produced by X-rays are difficult to obtain. By using the experimentally determined pulse-height distributions for electrons with energies above 6 Mev, one removes the necessity for following the electron through its detailed interactions, as would ordinarily have to be done in a complete calculation.

2. Response of the Spectrometer to Electrons

The electron beam was removed from a 50-Mev betatron by a pulsed electromagnetic extractor [4]. Individual electrons with fixed energies in the range 1 to 20 Mev were directed against the center of the flat surface of the sodium-iodide crystal, as shown in figure 1.

Electrons were available from the extractor during a time interval of approximately 0.2 μ sec every 5,500 μsec. The electrons from the betatron should be monoenergetic to at least 0.1 percent over periods

[1] This research was supported by the United States Air Force, through the Office of Scientific Research of the Air Research and Development Command.
[2] Figures in brackets indicate the literature references at the end of this paper.

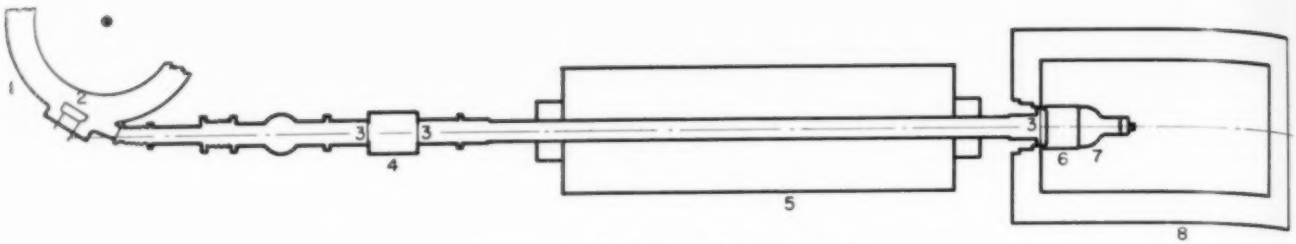

FIGURE 1. *Experimental arrangement.*

The electrons from the betatron accelerating tube (1) are extracted by an electron beam extractor (2) into a vacuum tube. The electrons proceed through foils at (3), a low pressure ionization chamber at (4), and a focusing magnet at (5) into the crystal at (6). The photomultiplier (7) and crystal are located within a 4-in.-thick lead shield (8).

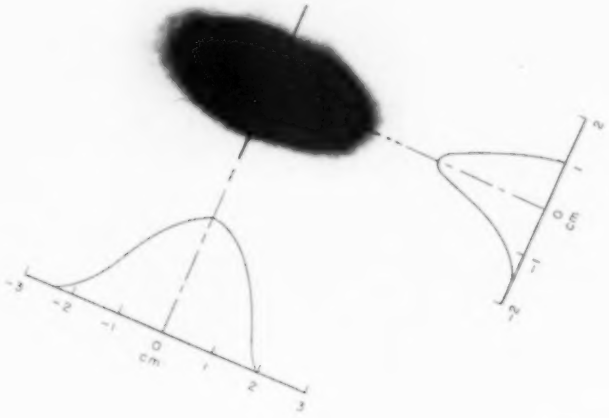

FIGURE 2. *The electron beam at the exit of the vacuum tube.*

The intensity curves shown were taken from a film with a densitometer. The electron beam current for this picture was of the order of 10^{-10} amperes.

FIGURE 3. *Pulse-height distributions produced by electrons from a betatron in a 5-in.-diameter by 5-in.-long sodium-iodide spectrometer.*

The electron energies given on each curve were determined from an energy comparison of the peak pulse heights with those obtained with 1.12- or 4.6-Mev gamma rays.

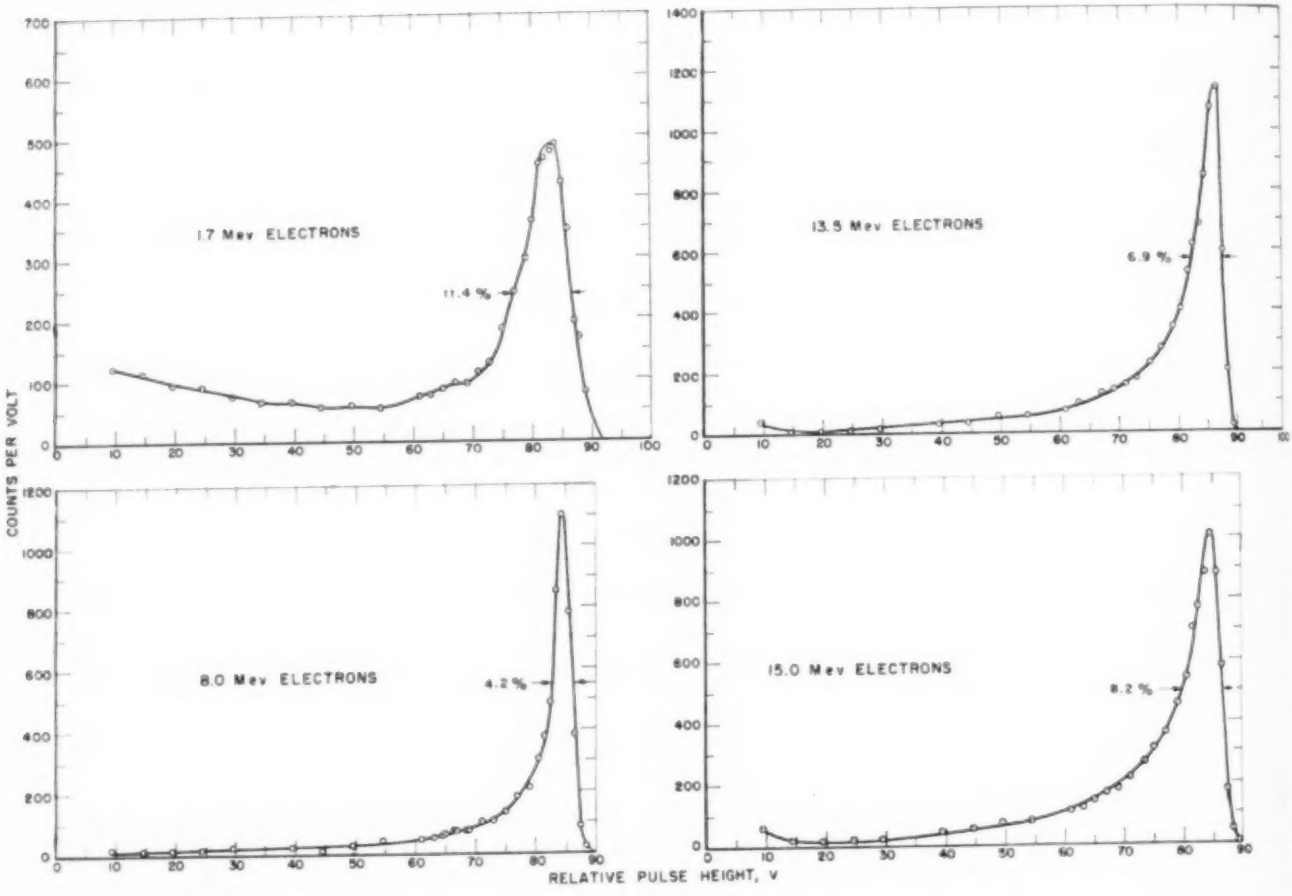

of time of the order of minutes [5]. Energy straggling of the electrons produces the largest uncertainty in the energy in the present experiment because of the three 0.0014-in. aluminum vacuum windows and the aluminum-magnesium-oxide entrance window of the crystal container. The most probable energy loss is 300 kev [5], and the energy uncertainty is less than 100 kev.

Adjustments on a beam of 10^9 electrons/sec were made to direct the electrons down the collimator hole and to set the focusing magnet current without the spectrometer. The electron-beam intensity was then adjusted so that the counting rate with the spectrometer was limited to five electrons detected per second. Since 180 bursts of electrons come from the betatron in 1 sec, the coincidence detection of electrons during any one betatron burst was limited to about 3 percent of all electrons detected. A picture of the electron-beam size at the crystal position is shown in figure 2.

The individual light pulses in the sodium-iodide crystals were detected by the photomultiplier-amplifier arrangements previously described [1]. The output pulses from the linear amplifier were sent into a gain-of-two amplifier and into a 30-channel differential analyzer. Two separate runs at each electron energy were made in order to check, first, the over-all shape of the pulse-height distribution, and, second, the detailed shape of the peak. The two runs were separated and followed by calibration runs with a mercury-relay precision sliding pulser and a radioactive gamma-ray source. The 4.43-Mev gamma rays from a RaD(α,Be) source or the 1.12-Mev gamma rays from Zn^{65} were used as calibration sources.

The betatron energy control developed by Saunders [6] in conjunction with the beam extractor arrangement was used to produce electrons with energies of 1.22, 1.96, 4.04, 5.12, 6.18, 8.30, 12.2, 13.8, 15.3, 17.15, and 17.9 Mev, respectively. The energy of the electrons entering the crystal was assumed to be 300 kev less than these values.

Typical pulse-height distributions for 1.7-, 8.0-, 13.5-, and 15-Mev electrons entering the 5-in.-diameter by 5-in.-long sodium-iodide crystal are shown in figure 3.

Results of the percentage resolution as a function of the incident electron energy are given in figure 4.

The resolution for electrons of energy less than 6 Mev deviates markedly from that expected on the basis of the statistical fluctuations in the number of photons detected by the photomultipliers [1]. This was due to the scattering and straggling in the crystal entry window, which are important at low energies. At about 6 or 7 Mev the resolution values are those one would expect from the statistical fluctuations. Because the synthesis of pulse-height distributions for X-rays that follows depends on pulse height distributions obtained for electrons liberated on the crystal axis and within the crystal, the energy resolution values used for electron energies less than 6 Mev were those assumed to be determined by statistical fluctuations with a Gaussian half-width inferred from previous work with a similar spectrometer [1]. For electron energies above 6 Mev, the experimental distributions similar to those in figure 3 were used.

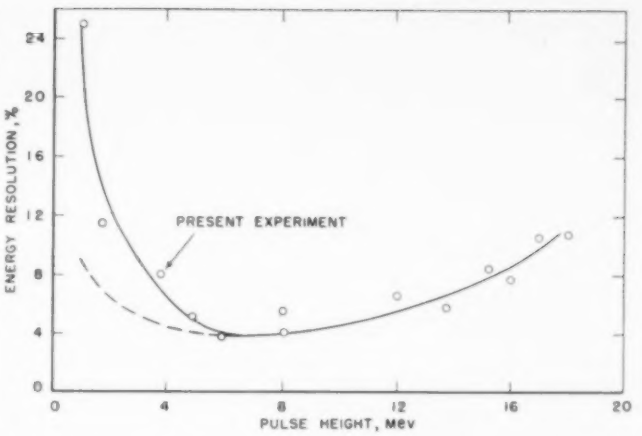

FIGURE 4. *Percent energy resolution inferred from curves of the type shown in figure 3.*

The lower curve from 1 to 6 Mev was derived from earlier data [1] with gamma rays.

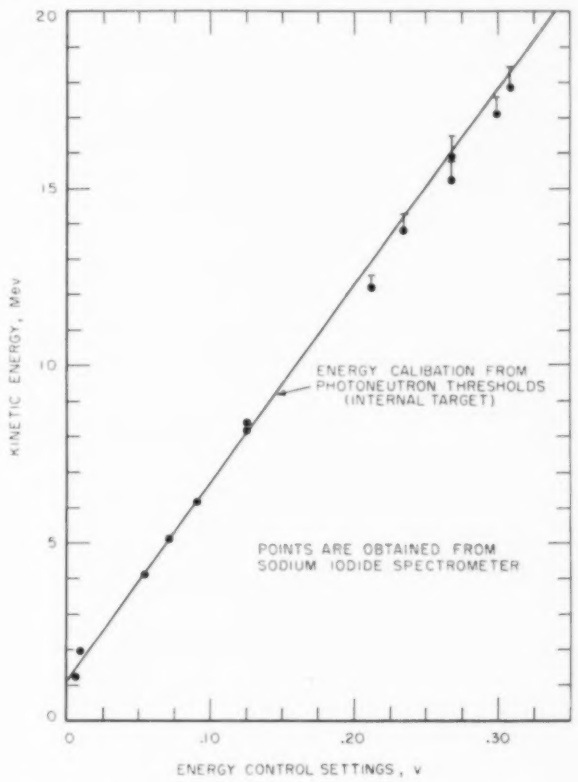

FIGURE 5. *Energy calibration of the betatron with the spectrometer data.*

The points are located at energies determined by gamma-ray energy calibrations plus a most probable energy loss correction due to foils between the betatron and the spectrometer crystal. The vertical lines above the experimental points indicate the possible error due to an assignment of energy by a comparison of the peak pulse-height positron in the electron distributions and the low-energy gamma-ray distributions.

Figure 5 provides a crude test of the linearity of the spectrometer response to electron energy. The ordinate is the kinetic energy of the electrons. The

abscissa scale is the potentiometer setting in volts on the betatron energy control [6] to which the electron energy has been shown to be related by a linear function. The experimental points are the energy values assigned to the pulse heights of the peaks in figure 4 plus 300 kev. This assignment was made by a comparison with a known gamma-ray energy of 4.43 or 1.12 Mev.

Tests were also made with a 5-in.-diameter by 4-in.-long crystal and a 5-in.-diameter by 9-in.-long crystal. No significant departures in distribution shapes or resolution values were found for the different sized crystals. It was found that only 10 percent of the 15.6-Mev electrons produced a contribution in the last 4 in. of the 9-in.-long crystal arrangement. This contribution consisted of very small pulse heights. It was inferred from these tests that the energy loss from the three sizes of crystal used in this experiment is predominantly due to energy escaping from the crystal sides.

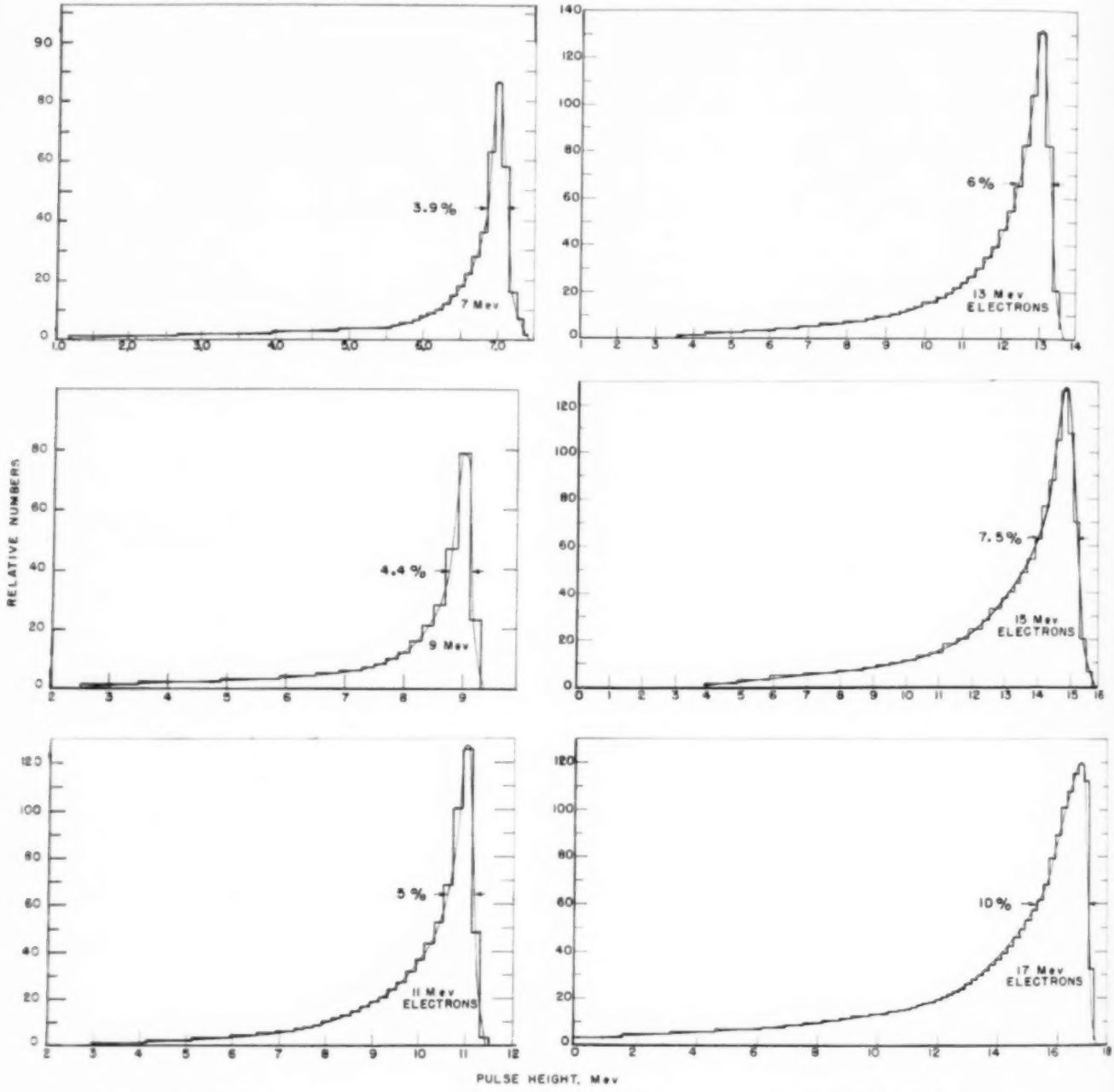

FIGURE 6. *Histograms representing the pulse-height distributions for 7-, 9-, 11-, 13-, and 17-Mev electrons.*

The 5-Mev histogram is not shown. It was a Gaussian with a small tail at small pulse heights. The 1- and 3-Mev distributions were assumed to be Gaussian with a percent half-width inferred from the lower curve of figure 4.

3. Synthesis of X-Ray Pulse-Height Distributions

3.1. Pair Electron Contributions

The most important contribution to the pulse-height distribution of X-rays above 10 Mev results from the energy loss in the crystal produced by the pair electrons. Specifically, at 11 Mev, 68 percent and at 19 Mev, 84 percent of the initial interactions will be by the pair production process.

The origin of the electron pairs produced in the 5-in. by 9-in. crystal will be distributed along the axis of the crystal if the X-rays are assumed apertured into a narrow beam that is directed along the axis. If it is further assumed that the electrons and positrons behave sufficiently identically in their scattering and energy-loss characteristics, except for the production of annihilation radiation by the positrons, the resulting pulse-height distributions can be predicted by folding together the measured distributions described in the last section for those electron energies that could combine to form a pair. The combined electron energy would be the incoming X-ray energy minus twice the electron rest-mass energy.

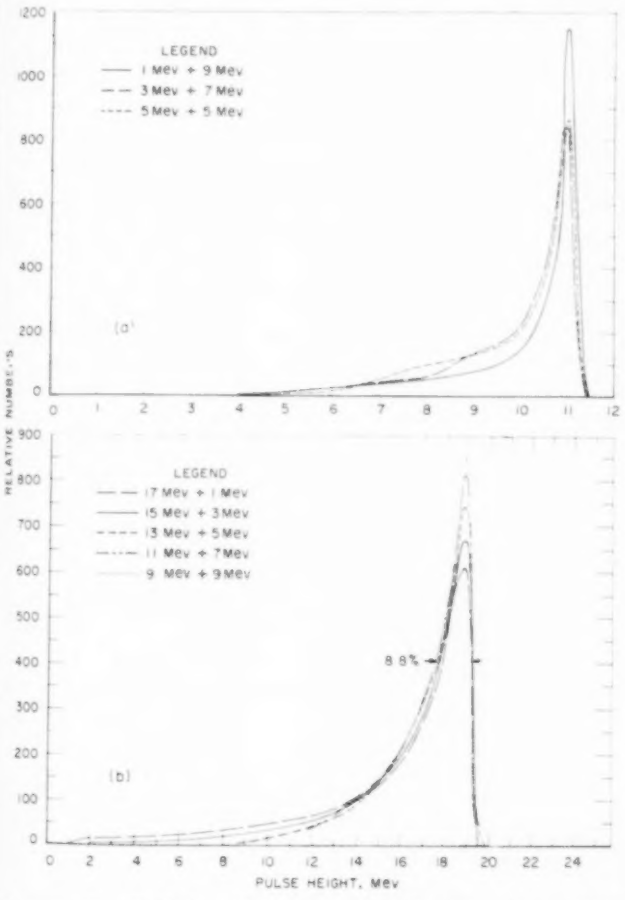

FIGURE 7. *Folded pulse-height distributions for various combinations of pair electron energies.*

The structure at small pulse heights is not significant and resulted from the detailed, assumed shapes of the histograms of figure 6.
(a) Total energy of the two electrons was assumed to be 11 Mev.
(b) Total energy of the two electrons was assumed to be 19 Mev.

There are obvious differences between the test electrons from the betatron and the pair electrons produced by an absorption of an X-ray photon. One difference is the angular orientation of the electrons with respect to the crystal axis. If either of the two electrons of a pair has an energy less than 6 Mev, the probability that it will lose energy by bremsstrahlung is small. Therefore, the knowledge of the angles into which the electrons are emitted is unimportant, because the electrons will lose energy by collision loss and produce a Gaussian-type pulse-height distribution (see fig. 4 and its discussion above). On the other hand, if the electron energies are greater than 6 Mev, the electrons will be projected into angles less than 10° [7]. For the present purposes, these angles are small enough to allow one to assume production of all pair electrons parallel to the crystal axis.

Another difference between test and pair electrons is the crystal depth to the point of initial interaction. The test electrons interact as soon as they enter the crystal, whereas the pair electrons interact after the depth of X-ray absorption. However, for the 5-in.-diameter by 9-in.-long crystal, 85 percent of the photons interact in the first 5 in. of the crystal. Also very little effect of length from 4 to 9 in. was detectable in the electron experiment described above. Therefore, there should be little difference in the actual available interaction distance for test and pair electrons.

With the above assumptions, the pulse-height distributions produced by pair electrons were obtained by folding together the pulse-height distributions for electrons whose combined total energy equaled the X-ray energy of interest minus 1 Mev. The individual distributions were inferred from the experimental data such as shown in figure 4, and are drawn as histograms in figure 6. The results of folding together distributions of electrons with kinetic energies of 1 and 9 Mev, 3 and 7 Mev, and 5 and 5 Mev are given in figure 7, a. Similarly, distributions of electrons of 1 and 17, 3 and 15, 5 and 13, 7 and 11, and 9 and 9 Mev are given in figure 7, b. As all pair electron distributions are equally probable [8], these curves are simply added together, with double weight being given to the 5 plus 5 Mev and the 9 plus 9 Mev curves, respectively. The annihilation radiation contributions are not shown in these curves but are treated separately in part 3.4. These contributions to the final syntheses of the X-ray pulse-height distributions will be shown in figures 9 and 10.

3.2. Compton Electron Distributions

The incoming X-rays with energies between 10 and 20 Mev can enter the crystal and undergo Compton scattering as well as produce pairs. In order to include these contributions in the X-ray pulse-height distribution, it has been assumed that the distribution of electron energies for the initial Compton interaction of high-energy photons represents the distribution of the sum of the electron energies after multiple Compton interactions of the same initial photons.

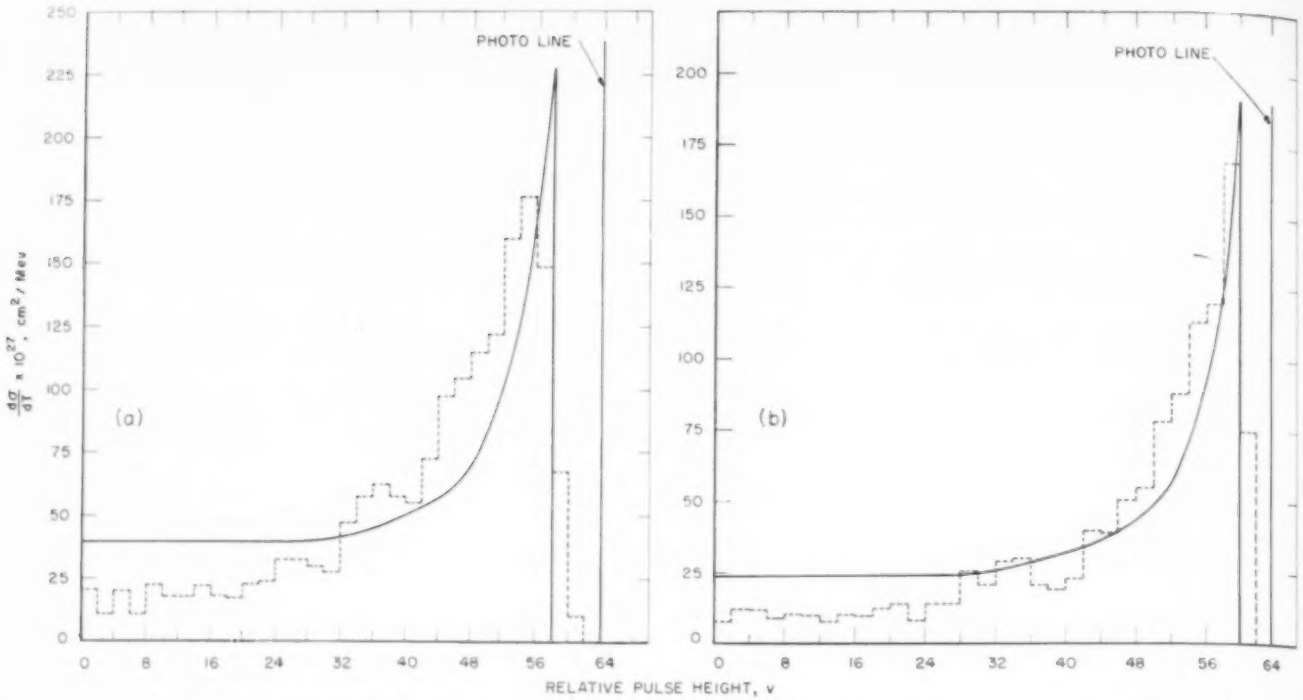

FIGURE 8. *Comparison between Monte Carlo predictions (histograms) and a single-interaction calculation (solid curve) for the Compton electron distributions.*

The predictions apply to a 5-in.-diameter by 9-in.-long crystal.
(a) Incident photon energy was 2.62 Mev.
(b) Incident photon energy was 4.45 Mev.

The justification for this assumption comes from a consideration of the Monte Carlo predictions of Berger and Doggett [2]. One of their results [9] was the predicted distribution of electron energies resulting from multiple interactions of an X-ray photon. The histograms in figures 8, a and 8, b are their data, before a Gaussian distribution has been added, for an X-ray energy of 2.6 and 4.4 Mev, respectively. Also drawn on these same figures are the Compton electron distributions for a single interaction [10] for the same X-ray energies. The similarity between the single- and multiple-interaction distributions is striking. As the X-ray energy increases, these distributions will become more peaked and more similar.

Because the Monte Carlo calculation and the single-interaction distribution are similar, the theoretical distribution [10] was used to represent the electron energy distribution resulting from the Compton scattering of X-rays in the range from 10 to 20 Mev. This should be a valid assumption especially because the Compton process is a correction and does not predominate in the determination of the shape of the pulse-height distribution for X-rays.

3.3. Compton Scattering Electron Contribution to the Photoline Energy

Those Compton scattering events for which the scattered X-ray interacts several times within the crystal, can lead to total absorption of the primary X-ray energy. These events have been included as a Gaussian-shaped contribution at the photoline energy. (The photopeak itself, arising from photons that have lost all their energy by the photoelectric process, is negligibly small at these energies.) In the 10- to 20-Mev energy range, the area of this Gaussian was related to the Compton electron distribution by the following extrapolation from lower energies.

The photofraction, p^*, has been defined [2] as the ratio of the area under the photopeak of the pulse-height distribution, which is represented by a Gaussian, to the area under the entire pulse-height distribution. Two constants characteristic of a particular geometry and energy enter the expression for this ratio. The constant a is that fraction of the total pair production events for which both annihilation quanta are absorbed in the crystal. The constant b is that fraction of the Compton scattered photons that are multiply scattered and totally absorbed in the crystal. In terms of the photoelectric (τ), pair (π), Compton (σ), and total (μ) absorption cross sections, p^* is defined as equal to $(\tau+a\pi+b\sigma)/\mu$.

In order to extrapolate values of b to an energy of 19 Mev, b was calculated up to 5 Mev from the data for a and p^* from reference 2. These calculations are shown in table 1 for a 5-in. diameter by 9-in.-long sodium-iodide crystal. As will be observed from the sixth column, b varies slowly and should continue to vary slowly up to 19 Mev for a 5-in. by 9-in. crystal. As the Compton cross section (σ) is small and thus the product $b\sigma$ is small, errors due

TABLE 1. *Calculation* [a] *of photofraction, p^*, where $p^*=(\tau+a\pi+b\sigma)/\mu$; $a=0.633$ [2]; and the sodium-iodide crystal is 5 in. in diameter by 9 in. long*

E	μ	τ	π	σ	b	p^*
Mev	*cm²/g*	*cm²/g*	*cm²/g*	*cm²/g*		
2	0.0411	0.0011	0.0022	0.0378	0.681	0.685
3	.0361	.0006	.0059	.0296	.632	.640
4	.0347	.0004	.0096	.0247	.615	.625
5	.0345	.0003	.0129	.0213	.600	.617

[a] The values of the absorption coefficients μ, τ, π, and σ for sodium iodide were taken from G. White of the Bureau (private communication).

TABLE 2. *Calculation* [a] *of modified photofractions, P^*, where $P^*=(\tau+A\pi+b\sigma)/\mu$; $A=0.633$ [2], and the sodium-iodide crystal is 5-in. in diameter by 9 in. long*

E	μ	τ	π	σ	b	P^*
Mev	*cm²/g*	*cm²/g*	*cm²/g*	*cm²/g*		
6	0.0347	0.0003	0.0156	0.0188	0.590	0.614
8	.0357	.0002	.0201	.0154	.580	.613
10	.0371	.0002	.0238	.0131	.570	.617
11	.0375	.0001	.0255	.0120	.570	.619
19	.0435	.0001	.0355	.0080	.550	.623

[a] The values of the absorption coefficients μ, τ, π, and σ for sodium iodide were taken from G. White of the Bureau (private communication).

to the extrapolation of b in the evaluation of the 19-Mev photofraction values should be small.

The extrapolated values of b are given in table 2 together with the modified photofraction, P^*, from 6 to 19 Mev, and the absorption coefficient data corresponding to those in table 1. P^* is differentiated from the low energy p^* because the latter values for energies above 5 Mev cannot be compared directly with experimental values. P^* contains a component $A\pi$, contrasted to $a\pi$ of p^*, which includes the total area under the pair electron contribution and not just the pair electron area under a Gaussian curve at the photoline position.

In synthesizing the X-ray pulse-height distribution, the Compton scattering events that result in contributions at the photoline energy were included as a Gaussian with an area b and a half-width of $0.09\sqrt{E}$ [1,2]. The area under the Compton electron distribution was, likewise, taken as $(1-b)\sigma$.

3.4. Contributions Due to the Escape of Annihilation Radiation

The only remaining influence on the broadening of the distribution due to X-rays will result from the escape of one or two annihilation photons from the positron of the electron pair originally produced by the incoming X-ray. Berger and Doggett [2] have calculated the escape of annihilation photons from a 5-in.-diameter by 9-in.-long crystal and found that 63.3 percent of the photons will be completely captured, and 21.5 percent of the events have exactly one annihilation photon escape with no interaction. The remaining 15.2 percent of the events have some interaction of the one or two annihilation photons before some of their energy escapes from the crystal. For the present purposes it is sufficiently accurate to assume that 36.7 percent of the events have exactly one annihilation escape and, therefore, that percentage of the folded electron-pair pulse-height distribution will be displaced downward in energy by 0.51 Mev.

3.5. Synthesis of the X-Ray Pulse-Height Distributions

The four contributions discussed above have been used to synthesize the pulse-height distribution for 11- and 19-Mev X-ray photons. The areas of these contributions were all referred to the area under the folded electron-pair distribution. The relative contributions are given in table 3.

The component distributions are given in figure 9,a for 11 Mev X-rays and in figure 10,a for 19 Mev X-rays. The sum of these distributions and the final result of the predictions are given as the solid lines in the b curves of these figures.

TABLE 3. *Relative areas of the four contributions to the X-ray pulse-height distribution*

Contribution	Fraction (F)	[a] 11-Mev value (F_{11})	[a] 19-Mev value (F_{19})
Compton events to photoline	$b\sigma/a\pi$	0.423	0.195
Compton distribution	$(1-b)\sigma/a\pi$	.319	.160
Folded electron pair distribution	$a\pi/a\pi$	1	1
Secondary annihilation distribution	$(1-a)\pi/a\pi$	0.580	0.580

[a] Values in table 3 were calculated with data from tables 1 and 2.

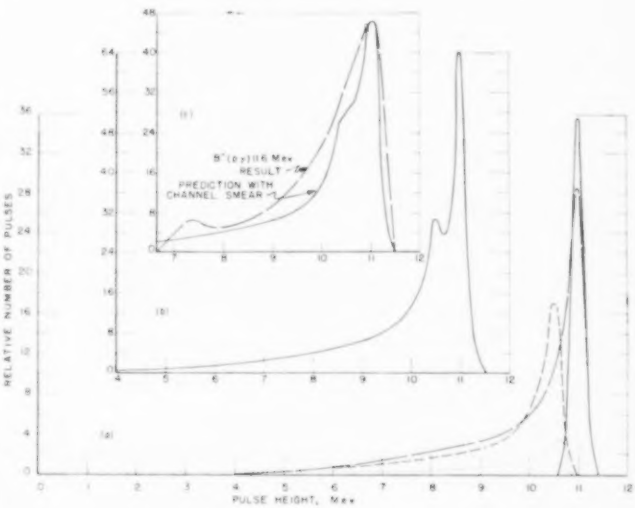

FIGURE 9. *Synthesis of the pulse-height distribution produced by 11-Mev X-rays in a 5-in.-diameter by 9-in.-long sodium iodide crystal spectrometer.*

(a) Four contributions to the synthesized distribution: (1) Compton electron distribution (dotted curve); (2) multiple Compton interactions that contribute to the photoline energy (solid curve); (3) folded electron-pair distribution (long dashed curve); (4) secondary distribution due to loss of annihilation radiation (short dashed curve).

(b) Addition of the four curves of (a) to obtain the predicted pulse height distribution.

(c) Comparison of the 11-Mev distribution of (b) with the experimental 11.6 Mev distribution. The distribution of (b) has been smoothed by the channel widths used in obtaining the experimental distribution. The abscissa and ordinate scales of the experimental distribution were normalized to the predicted distribution.

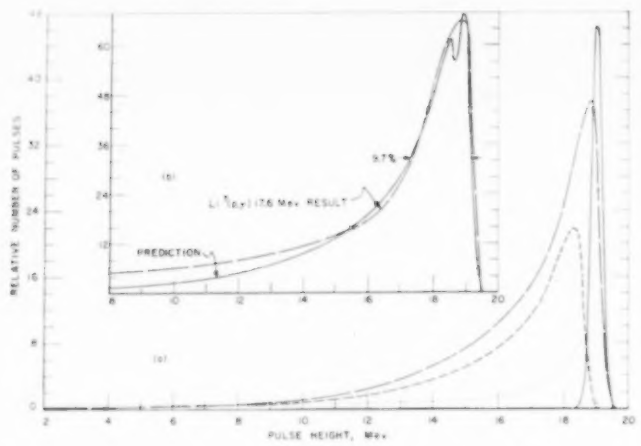

FIGURE 10. *Synthesis of the pulse-height distribution produced by 19-Mev X-rays in a 5-in.-diameter by 9-in.-long sodium-iodide crystal spectrometer.*

(a) Four contributions to the synthesized distribution: (1) Compton electron distribution (dotted curve); (2) multiple Compton interactions that contribute to the photoline energy (solid curve); (3) folded electron-pair distribution (long dashed curve); (4) secondary distribution due to loss of annihilation radiation (short dashed curve).

(b) Composite distribution (solid curve) obtained by adding the curves in (a). Comparison is made with the experimental 17.6-Mev distribution. In this case the experimental spectrum was taken with small channel widths so that the smearing thus introduced was negligible (dashed curve). The abscissa and ordinate scales of the experimental distribution were normalized to the predicted distribution.

4. Discussion

The synthesized pulse-height distributions for 11-Mev and 19-Mev X-rays were compared with experimental distributions obtained previously with 11.6- and 17.6-Mev gamma rays [1].

Figure 9,c, shows the experimental distribution for the $B^{11}(p,\gamma)$ gamma-rays [1]. Because the intensity of this source was small, the channel window size on the differential pulse-height analyzer had to be made large. The curve of figure 9,b, has been smeared with the channel window used in the experiment in order to arrive at the prediction shown as the solid curve of figure 9,c. The experimental and predicted curves have been normalized at the peak. The experimental curve is higher than the predicted one, at pulse heights smaller than the one at which the peak occurs, for practically all pulse heights. However, the differences can be attributed to the Compton scattered gamma rays from the thick copper target assembly, and to the collimator wall effects used in the work described in reference [1]. The wall of the $\frac{3}{8}$-in.-diameter collimator hole subtended a relatively large solid angle for the gamma rays from the target. Hence gamma rays could interact and lose energy in the wall and then penetrate into the large-diameter crystal. Both effects of target and collimator would result in degraded-energy gamma rays entering the crystal. Similar comments can be made regarding the comparison in figure 10,b, of the 19-Mev prediction with that obtained with the 17.6-Mev gamma rays from the $Li^7(p,\gamma)$ reaction [1].

No detailed calculation to correct the experimental curves has been made because the experimental data [1], particularly that of the 11.6-Mev line, were too poor to warrant extensive interpretations. Nevertheless, the comparison between prediction and experiment is considered to be good.

The method of synthesizing pulse-height distributions due to X-rays, which has been outlined, is the best procedure known to the present authors in the X-ray range from 10 to 20 Mev. Because of the general success and the expected validity of the predictions, it is planned to apply a similar procedure for energies from 5 to 19 Mev in 2-Mev increments. These results, combined with the work of Berger and Doggett [2], will allow an interpretation of experimental pulse-height distributions in the range from 100 kev to 20 Mev, when a total absorption spectrometer with a 5-in. diameter and a 9-in.-long crystal are used.

The work of B. Petree and E. G. Fuller in obtaining a well-controlled electron beam for the present experiment is gratefully acknowledged. Discussions with M. Berger and N. Starfelt were very helpful.

5. References

[1] R. S. Foote and H. W. Koch, Rev. Sci. Instr. **25,** 746 (1954).
[2] M. J. Berger and J. Doggett, J. Research NBS **56,** 355 (1956) RP2686.
[3] H. W. Koch, J. Wyckoff, and B. Petree, Phys. Rev. **99,** 663 (1955).
[4] R. S. Foote and Ben Petree, Rev. Sci. Instr. **25,** 694 (1954).
[5] E. L. Goldwasser, F. E. Mills, and A. O. Hanson, Phys. Rev. **88,** 1137 (1952).
[6] E. Saunders (private communication).
[7] H. W. Koch and R. E. Carter, Phys. Rev. **77,** 165 (1950).
[8] W. Heitler, The quantum theory of radiation, 2d ed. (Oxford Univ. Press, Oxford, England, 1949).
[9] M. Berger and J. Doggett (private communication).
[10] Ann Nelms, NBS Circular 542 (1953).

WASHINGTON, December 5, 1955.

Journal of Research of the National Bureau of Standards Vol. 56, No. 6, June 1956 Research Paper 2683

Hydrogarnet Formation in the System Lime-Alumina-Silica-Water

Elmer T. Carlson

Glasses of the composition of grossularite and similar glasses poorer in silica were treated hydrothermally, and the composition of the resulting hydrogarnets was estimated from the unit cell size as calculated from X-ray powder patterns. The silica content of the hydrogarnets increased continuously with the temperature of formation, approximating that of grossularite at 800° C. When mixtures of lime, alumina, and silica, either as such or in various states of combination, were treated in the same manner as the glasses, equilibrium was not attained even after several weeks. At times as many as three distinct hydrogarnet compositions were found to coexist. The equilibrium temperature for the hydrothermal decomposition of $3CaO{\cdot}Al_2O_3{\cdot}6H_2O$ to $4CaO{\cdot}3Al_2O_3{\cdot}3H_2O$ plus $Ca(OH)_2$ was found to be between 220° and 226° C. Hydrogarnets containing increasing amounts of silica underwent the same type of decomposition at progressively higher temperatures.

1. Introduction

The relationship between the isometric tricalcium aluminate hexahydrate and grossularite garnet was pointed out by Flint, McMurdie, and Wells [1,2].[1] It was shown that these two compounds are the end members of a series of solid solutions, of garnet-like crystalline structure, which were termed "hydrogarnets." The general formula may be written, $3CaO{\cdot}Al_2O_3{\cdot}mSiO_2{\cdot}(6-2m)H_2O$, where m may vary from 0 to 3. The present work is an extension of these earlier studies, undertaken for the purpose of answering certain questions not previously covered completely.

The first of these questions to be considered is the relation between temperature and pressure and the composition of the hydrogarnet in equilibrium with the fluid phase. Flint and Wells prepared their hydrogarnets from mixtures of various raw materials in the desired lime-alumina-silica ratios, selecting by trial-and-error methods the optimum temperature for each preparation. In general, the results obtained at other temperatures were not reported. It has been pointed out by Yoder [3] that theoretically the composition of the solid-solution phase at equilibrium should be a function of temperature and pressure. This was supported by his data, on the basis of which he constructed a pressure-temperature diagram showing the variation in refractive index of the hydrogarnet phase. With the exception of one point, all his data were obtained at 500° C. or higher. It was considered desirable to obtain some data at lower temperatures.

Another objective of the present study is to determine how the course of the reaction is affected by the choice of raw materials. In theory, the composition of the product at a given temperature and pressure should be independent of the previous state of the reactants; nevertheless, it was found by Flint and Wells that different results were obtained with different starting materials. It must be assumed that this was due to nonequilibrium conditions. Such conditions are likely to exist in actual practical processes involving formation of hydrogarnet; hence a study of these variations should be of some interest.

Finally, there is the question of the upper limit of stability of the hydrogarnets under hydrothermal conditions. Flint, and McMurdie, and Wells [1] stated that a sample of tricalcium aluminate hexahydrate containing a small amount of silica was stable up to 300° C, at which point it decomposed to calcium hydroxide and gibbsite. However, it was later shown by Johnson and Thorvaldson [4] that pure tricalcium aluminate hexahydrate under these conditions breaks down to form a less basic aluminate, $4CaO{\cdot}3Al_2O_3{\cdot}3H_2O$, plus calcium hydroxide. This was confirmed by Peppler and Wells [5], who placed the decomposition temperature at about 215° C. A study of the effect of silica on this reaction appeared desirable.

The work of Flint, McMurdie, and Wells included also a series of quinary compositions, the fifth component being ferric oxide. This is omitted from consideration in the present paper.

2. Materials, Apparatus, and Procedures

2.1. Materials

The alumina used was a commercial preparation of gibbsite ($Al_2O_3{\cdot}3H_2O$) containing about 0.30 percent of Na_2O, other impurities being negligible in amount. All other raw materials, except as otherwise noted, were reagent grade chemicals. Ordinary distilled water was used without further purification.

2.2. Apparatus

Most of the reactions were carried out in stainless-steel pressure bombs of the Morey type. The bombs were heated in vertical tube furnaces, and the temperature was automatically controlled and recorded by conventional apparatus using iron-constantan thermocouples. The temperature gradient in each furnace was carefully explored, and the bombs were positioned so that a thermocouple in the normal recording position and another at the bottom of the

[1] Figures in brackets indicate the literature references at the end of this paper.

bomb chamber gave readings agreeing within 1 deg. This minimized an error that might otherwise have been as great as 10 deg, judging from preliminary tests.

No provision was made for independent pressure control, hence the pressure developed in the bomb was a function of temperature and of the degree of filling of the bomb. For temperatures below the critical point, excess liquid water was present, and the pressure was estimated from steam tables. For higher temperatures the pressure-volume-temperature data of Kennedy [6] were used.

A cold-seal hydrothermal apparatus of the type designed by Tuttle [7] was also used, permitting extension of the study to higher temperatures. In this apparatus, both pressure and temperature were controlled manually. A pressure of 15,000 psi was used, except for a few experiments on the effect of varying pressure.

2.3. Procedures

The solid reactants, lime, alumina, and silica, may be introduced in a variety of forms or states of combination. The separate oxides, or hydrates, for example, may be mixed. When this procedure was used, the lime was usually present as the oxide (freshly prepared by calcining the carbonate), the alumina as gibbsite, and the silica as gel ("silicic acid").

Alternatively, two or more of the components may be chemically combined. For example, tricalcium aluminate was prepared by heating a mixture of calcium carbonate and alumina; likewise, tricalcium silicate from calcium carbonate and silica. Tricalcium aluminate hexahydrate was prepared (a) by hydration of tricalcium aluminate at 150° to 200° C, and (b) by the reaction between lime and freshly precipitated alumina at boiling temperature. The latter method was also modified by the coprecipitation of small amounts of silica with the alumina. Three hydrogarnet preparations were obtained by this method, containing 0.10, 0.26, and 0.58 mole of SiO_2 per mole of Al_2O_3, respectively. However, as is shown later, in the last of these not all the silica was present in the hydrogarnet. In lieu of a synthetic aluminum silicate, Georgia kaolin, activated by heating at 750° C, was used for a few experiments.

Finally, there is the possibility of using ternary glasses in which the three components are present in the desired proportions. Glasses were prepared by heating mixtures of calcium carbonate, gibbsite, and silica gel in a Globar-type furnace. The lime:alumina ratio was kept at 3 to 1, whereas the silica:alumina ratio ranged from 0.4 to 3.0. Mixtures that did not fuse at the highest temperature of the furnace (about 1,450° C) or that devitrified on cooling were given further treatment. Fragments were held in an oxygen-gas blast until fused to a clear glass, and the molten drops were quenched in water. The glass was ground to pass a No. 200 sieve before hydrothermal treatment.

The starting materials, totaling a few tenths of a gram, usually were mixed with water to a paste or slurry in a small platinum crucible, which was then placed in the bomb with the desired quantity of water and kept in a furnace at constant temperature (±3 deg C) for several days. When the cold-seal apparatus was used, the weight of solids averaged about 0.05 g, and the amount of water was generally between 0.02 and 0.05 g. The mixture was enclosed in a small platinum capsule, which was then placed in the bomb; the bomb was connected to the pressure line, the pressure raised, and the heat applied. The warmup period averaged about 30 min. After a heating period ranging from a few hours to 3 days, the bomb was cooled in air (usually requiring about 15 min) and opened.

As a general procedure, the solid reaction products were filtered off and dried by washing with alcohol and ether. Frequently, when the Morey bombs were opened, the reaction products were almost dry; in such cases the drying was completed in an oven at about 100° C, without intervening filtration.

The dried products were first examined under the polarizing microscope, after which X-ray powder diffraction patterns usually were obtained. The patterns were made with a recording X-ray diffractometer, using copper Kα radiation. The X-ray patterns served not only for identification of crystalline phases, but also as a means of estimating the composition of the hydrogarnet solid solution. It was shown by Flint, McMurdie, and Wells [1] that the hydrogarnets crystallize in the isometric system, and that the unit cell size is a function of composition. In the solid solution series $3CaO{\cdot}Al_2O_3{\cdot}3SiO_2$–$3CaO{\cdot}Al_2O_3{\cdot}6H_2O$, the cell constant was found to range from 11.84 to 12.56 A. On the basis of data from several sources, Yoder [3] presents a diagram showing the relation between composition and cell constant in this series. The relation is shown to be nearly, but not quite, linear. Thus if the cell constant is known, the composition can be estimated with fair precision.

The cell constant may be readily calculated from the interplanar spacings, which in turn are derived from the X-ray diffraction angles. For accurate measurement of the angles it is necessary to have a sharp, distinct pattern, also to have a standard present for comparison. In many of the reaction products discussed in the following sections, calcium hydroxide was present, serving as a reliable internal standard. The calculated unit cell sizes are believed to be accurate to ±0.01 A for the determinations in which an internal standard was present, and ±0.03 A otherwise.

In numerous cases, as is discussed later, there was clear evidence of the presence of two, or occasionally three, separate hydrogarnet compositions in the same reaction product. It seems evident that, in such cases, equilibrium had not been attained. Although the condition usually could not be detected microscopically, it was disclosed by the X-ray patterns, in which many of the prominent lines appeared either as doublets or as pairs (occasionally triads) of lines, depending on the relative compositions. When this occurred, only the low- and medium-angle reflections could be relied on, as there was considerable overlapping at the higher angles.

3. Results and Discussion

3.1. Relation Between Temperature and Composition

The phase equilibrium relationships involved in this study are complex, because the system is quaternary, the temperature range extends beyond the critical point for water, and the phase of primary interest is a solid solution. A discussion of the theoretical aspects is beyond the scope of this paper. However, it may be mentioned that there can be as many as four solid phases (five, above the critical temperature) existing together at equilibrium, hence the presence of other solid phases along with the hydrogarnet is not evidence of failure to reach equilibrium. On the other hand, the coexistence of two solid phases that are members of the same solid solution series would indicate lack of attainment of equilibrium. This condition was observed in a number of instances reported in the tables. The converse, that a single hydrogarnet phase indicates equilibrium, is not necessarily valid. Nevertheless, in the absence of any better criterion, the observation of a single well-defined hydrogarnet phase, independent of the duration of treatment within the limits of the experimental conditions, is herein taken to indicate the attainment of equilibrium.

After numerous experiments with various starting materials it was concluded that the glasses yielded equilibrium products more readily than did any of the other combinations. The data in table 1, therefore, were obtained entirely from experiments with glasses.

The crystals formed were always very small, often barely visible under the microscope, so that it was usually difficult to determine the refractive index even approximately. In some cases, particularly with the low-silica glasses, hydration and crystallization appeared to take place without altering the shape of the glass fragments.

Table 1 presents the results of two series of experiments: (A) those in which the Morey-type bombs

TABLE 1. *Hydrothermal reactions of glasses of composition* C_3AS_m

Experiment	SiO_2	Temperature	Pressure	Duration[a]	Unit cell edge of hydrogarnet formed	Remarks
			A. EXPERIMENTS IN MOREY BOMBS			
	Mole	*°C*	*atm*		*A*	
1	0.4	116	2	34 d.	12.52	Small amount of unidentified phase.
2	.4	250	40	14 d.	12.48	Trace of $C_4A_3H_3$.[b]
3	.4	356	175	14 d.	.....	Decomposed to $Ca(OH)_2$ and $C_4A_3H_3$.
4	.7	246	35	7 d.	12.48	Also 12.35 and 12.25 A (nonequilibrium).
5	.7	251	40	9 d.	12.44	Also 12.20 A (nonequilibrium).
6	.7	280	65	14 d.	12.40	Trace of $C_4A_3H_3$.
7	1.2	150	4	34 d.	12.50	Also 12.24 A; lines broad (nonequilibrium).
8	1.2	300	85	18 d.	12.41	Also 12.13 A; lines broad (nonequilibrium).
9	1.2	350	165	13 d.	12.42	Also 12.30 A (nonequilibrium).
10	1.2	371	210	18 d.	12.30	Also 12.16 A; $Ca(OH)_2$ and $C_4A_3H_3$ present.
11	2.0	250	40	15 d.	12.11	
12	2.0	354	170	15 d.	12.07	
13	2.0	400	280	19 d.	12.06	$C_4A_3H_3$ also present.
14	2.7	354	170	34 d.	11.98	
15	3.0	200	15	8 d.	.....	Mostly unaltered glass.
16	3.0	278	65	8 d.	12.05	Weak pattern; CSH (B) present.
17	3.0	334	135	14 d.	11.99	Few unidentified weak lines.
18	3.0	400	280	14 d.	11.96	Nuclei of lower refractive index.
19	3.0	488	485	14 d.	11.89	Do.
20	3.0	510	610	7 d.	11.91	
			B. EXPERIMENTS IN COLD-SEAL APPARATUS			
21	0.4	160	1,020	1 d.	12.48	Possibly a second hydrogarnet pattern.
22	.4	185	1,020	1 d.	12.50	
23	.7	145	1,020	1 d.	12.47	Also a second, weak hydrogarnet pattern.
24	.7	200	1,020	1 d.	12.47	Also 12.27 (nonequilibrium).
25	1.2	155	1,020	2 d.	12.47	Also 12.23 (nonequilibrium).
26	1.2	180	1,020	2 d.	12.47	Also 12.25 (nonequilibrium).
27	2.0	135	1,020	1 d.	.....	Lines too broad and faint for determination of a.
28	2.0	200	1,020	5 hr.	12.20	Very weak pattern.
29	2.0	245	1,020	1 d.	12.14	Lines slightly broadened.
30	3.0	195	1,020	2 d.	.....	Glass only superficially altered.
31	3.0	240	1,020	2 d.	12.15	Also a CSH (B) pattern of medium intensity.
32	3.0	300	1,020	7 hr.	.....	Very weak pattern; CSH (B) present.
33	3.0	310	340	3 d.	12.03	CHS (B) present.
34	3.0	355	1,020	7 hr.	11.99	
35	3.0	385	375	7 hr.	11.99	Also a few weak unidentified lines.
36	3.0	395	1,020	5 hr.	11.97	Also a weak CSH (B) pattern.
37	3.0	440	1,020	5 hr.	11.94	
38	3.0	495	1,020	5 hr.	11.93	
39	3.0	570	1,020	6 hr.	11.90	
40	3.0	680	1,020	7 hr.	11.85	
41	3.0	800	1,020	6 hr.	11.85	Spacings corrected by use of internal standard.

[a] d=days; hr, hours. [b] C=CaO; A=Al_2O_3; S=SiO_2; H=H_2O; see footnote 2 of text.

were used, and (B) those in which the cold-seal apparatus was used. Within each series the arrangement is in order of increasing silica content and increasing temperature.

Figure 1 is based on the data in table 1, with the omission of those experiments in which there is evidence that equilibrium was not reached. Here the unit cell size (a function of composition) is plotted against temperature of formation. The relation between composition and unit cell size is probably not quite linear. The composition lines adjacent to the vertical scale of figure 1 are based on Yoder's diagram [3], to which reference was made earlier.

Attainment of equilibrium was slow. For example, in experiment 9, after 13 days at 350° C, the X-ray pattern indicated the presence of two distinct hydrogarnet compositions, with cell constants 12.42 and 12.30 A, respectively. This is evidence of nonequilibrium conditions. With the higher pressures attainable in the cold-seal apparatus, equilibrium was reached more quickly, but even here there was evidence of variable composition, in that the crystals often contained nuclei of lower refractive index than that of the surrounding shell. This indicates a relative deficiency in silica in the nuclei of the crystals, from which it is assumed that these may have formed at lower temperatures, during the warmup period. In most cases the amount was insufficient to affect the X-ray diffraction pattern, but it was often enough to interfere with a precise determination of index of refraction. For this reason, and also because an extraneous siliceous phase usually was present as a product of the reaction, little success was achieved in correlating the index of refraction with the composition derived from the X-ray pattern.

Considering first the data for the glass with 3 moles of silica (that is, having the composition of grossularite), it is seen that at the two highest temperatures a product was obtained having a unit cell edge of 11.85 A. The corresponding figure reported for grossularite is 11.84 A [1], or 11.85 [3]. The pattern for experiment 41 was prepared with the inclusion of an internal standard (tungsten), hence the lattice constant given for this product is probably

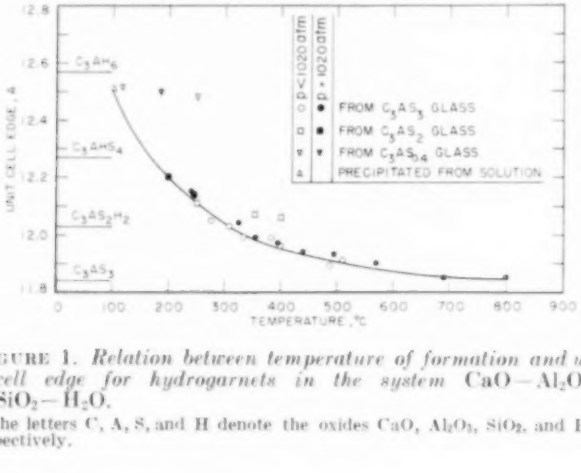

FIGURE 1. *Relation between temperature of formation and unit cell edge for hydrogarnets in the system* $CaO-Al_2O_3-SiO_2-H_2O$.

The letters C, A, S, and H denote the oxides CaO, Al_2O_3, SiO_2, and H_2O, respectively.

correct to ±0.01 A. Because of the extreme fineness of the material it was impossible to make a satisfactory determination of refractive index. The loss on ignition was zero, within the limits of analytical error. This fact, considered with the X-ray data, makes it evident that the product was very close to the composition of grossularite.

At lower temperatures of formation the cell constant is progressively larger, indicating that the composition is poorer in silica and richer in water. Here the X-ray patterns are weaker, the lines often broader, and lines of other crystalline phases appear together with those of the hydrogarnet. This is understandable, as the silica content of the hydrogarnet is now less than that of the glass. The excess silica reacts with part of the lime, thus reducing the amount of the latter available for hydrogarnet formation. Some alumina is thereby left unaccounted for, but the form in which it is present is not known. The identity of the calcium silicate may be considered established in at least a few cases. The product of experiment 31 gave an X-ray pattern of moderate intensity, which, after subtraction of the hydrogarnet lines, agrees rather well with that given by Heller and Taylor [8], for CSH I[2] (CSH(B) according to Bogue's classification [9]). With this as a standard for comparison, the presence of much smaller amounts of the same phase was detected in several other preparations. In a few cases, however, the extraneous lines did not fit this pattern.

At lower temperatures the reaction becomes progressively slower. Thus after 2 days at 195° C (experiment 30) there was little evidence of alteration of the glass. Glasses poorer in silica were found to react more readily, and were therefore used in the experiments at the lower temperatures. The silica content of the hydrogarnet appeared to be independent of that of the parent glass (compare, for example, experiments 29 and 31), except that the hydrogarnet was never richer in silica than the glass. This limitation accounts for the points in figure 1 that fall significantly above the curve. Such a departure should not occur if the mixtures have reached equilibrium (assuming that the curve is a true equilibrium line). Probably the explanation will have to await a more complete study of the quaternary system.

Even with the low-silica glasses, the results at the lowest temperatures were rather unsatisfactory. The point plotted in figure 1 for 100° C represents a hydrogarnet prepared not from a glass but from a boiling mixture of lime water, alumina, and sodium silicate, with the silica in moderate excess.

The use of the low-silica glasses at the higher temperatures is also limited by the breakdown of the hydrogarnet phase to $4CaO{\cdot}3Al_2O_3{\cdot}3H_2O$ (see experiments 2, 3, 6, 10, and 13).

To determine the effect of varying pressure on the composition of the hydrogarnet, experiments 33 and 35 were conducted at lower pressures than the other

[2] In the interest of brevity, the convention of using the letters C, A, S, and H to represent CaO, Al_2O_3, SiO_2, and H_2O, respectively, is followed throughout this paper.

members of this series. The pressures in the Morey bombs (experiments 1 to 20) were likewise lower. In figure 1, the experiments at 1,020 atm are represented by filled symbols; those at lower pressures by open symbols. The fact that a single curve approximates both sets of points indicates that pressure is of relatively little effect within the range covered. A similar conclusion was reached by Yoder on the basis of results at higher temperatures [3].

3.2. Hydrothermal Reactions of Heterogeneous Lime-Alumina-Silica Mixtures

In the experiments described below, the solid components were present initially not as a homogeneous glass but as mixtures of various compounds. In most cases the results departed more or less from those of the comparable experiments with glasses, as described above. This is ascribed to lack of attainment of equilibrium in the heterogeneous mixtures. The results obtained, nevertheless, may be of interest, as the experimental conditions are more closely related to those that may exist in actual practical processes.

The data presented in tables 2 to 5 are representative of a considerably larger number of experiments. The data given were selected not only to illustrate general trends but to point out anomalies as well.

a. Mixtures of Tricalcium Aluminate and Tricalcium Silicate

The hydration of tricalcium aluminate in the presence of tricalcium silicate is of some interest because it represents, in greatly simplified form, the reactions of the aluminate phase of cement clinker during hydration. In the series of experiments recorded in table 2, the ratio of C_3S to C_3A ranged from 0.7 to 3.0. The ratio is well below that existing in normal portland cements, but the present study is concerned primarily with the hydrogarnet phase, in which the ratio of silica to alumina does not exceed 3.0.

Several facts may be noted. Perhaps the most obvious is that in most cases equilibrium was not attained even after 35 days (experiments 4, 11). This is evidenced by the coexistence of two or more hydrogarnet phases. Furthermore, a comparison of experiments Nos. 3 and 4 indicates no progress toward equilibrium between 1 and 35 days. In all the experiments below 170° C, and in some as high as 182° C (experiments 15, 21) there was evidence of only one hydrogarnet phase and this had the unit cell size (12.57 A) of tricalcium aluminate hexahydrate. It must be borne in mind that the presence or absence of the second hydrogarnet phase was determined by examination of the X-ray patterns, and as a result the presence of such a phase in small amounts would fail to be observed. Nevertheless, it appears that the aluminate and silicate phases have hydrated separately at the lower temperatures. On the other hand, above 225° C, and in some cases as low as 201° C, $3CaO{\cdot}Al_2O_3{\cdot}6H_2O$ is absent, and only the siliceous hydrogarnet is observed. This may occur even after only 1 day (experiment 17).

The unit cell size of the siliceous hydrogarnet varies little with the quantity of silica in the reaction mixture, and apparently not at all with temperature, except for a few random inconsistencies. On the basis of Yoder's diagram, previously cited, the 12.40 A unit cell would indicate about 0.5 mole of SiO_2 per mole of $3CaO{\cdot}Al_2O_3$, and 12.32 A would correspond to about 0.8 mole of SiO_2. In no case would this account for all the silica present; hence part of the silica must be present in another phase. In two instances (experiments 9 and 22) there is evidence of a small amount of hydrogarnet with somewhat higher silica, but these appear to be exceptions. Experiment 8 also fails to conform to the general pattern.

TABLE 2. *Hydrothermal reactions of mixtures of tricalcium aluminate and tricalcium silicate*

Experiment	Molar ratio, C_3S/C_3A	Temperature	Pressure	Duration	Phases present in product [1]			
					$Ca(OH)_2$	Hydrogarnets		Other phases [2]
						C_3AH_6	Siliceous (cell constant)	
		°C	atm	Days			A	
1	0.7	143	3	1	+	+	—	a
2	.7	179	10	7	+	+	—	b
3	.7	218	20	1	+	+	[3] 12.40	b
4	.7	220	25	35	+	+	[3] 12.40	b
5	.7	261	45	9	+	—	12.39	b, c
6	.7	300	85	9	+	—	12.39	b, c
7	1.0	170	8	7	+	+	[3] 12.37	.....
8	1.0	173	8	7	+	+	[3] 12.44	.....
9	1.0	181	10	7	+	+	[3] 12.37, 12.23	.....
10	1.0	225	25	7	+	+	[3] 12.39	.....
11	1.0	221	25	35	+	—	[3] 12.52 (trace), 12.39	.....
12	1.0	300	85	15	+	—	12.38	.....
13	1.3	142	3	7	+	+	—	a
14	1.3	172	8	7	+	+	—	b
15	1.3	180	10	7	+	+	—	a
16	1.3	201	15	7	+	—	12.35	.....
17	1.3	219	25	1	+	—	12.36	b
18	1.3	221	25	35	+	—	12.36	b
19	1.3	338	140	16	+	—	12.36	b
20	2.0	146	4	7	+	+	—	a
21	2.0	182	10	7	+	+	—	b
22	2.0	202	15	7	+	+	[3] 12.36 to 12.25 (diffuse).	b
23	2.0	224	25	7	+	—	12.35	b
24	2.0	361	185	17	+	—	12.35	b
25	3.0	225	25	7	+	?	12.32	b

[1] + indicates present; —, absent.
[2] "a" is believed to be CSH (CSH(A), according to Bogue's classification); "b" is probably C_2S γ-hydrate ($C_2SH(C)$, according to Bogue's classification); "c" is unidentified.
[3] From coexistence of hydrogarnet phases it is concluded that equilibrium was not attained.

All the reaction products contained free calcium hydroxide, as would be expected. In most cases the X-ray patterns showed a few weak or medium lines that could not be attributed either to a hydrogarnet or to $Ca(OH)_2$. Unaccountably, such lines were conspicuously absent from the patterns of experiments 7 to 12, in which equimolar amounts of the aluminate and silicate were initially present, although with both higher and lower proportions of silica the lines were observed. Interpretation of the patterns is highly speculative, because most of the lines were very weak, and undoubtedly many still weaker lines were masked by the patterns of the predominant

phases. It is reasonable to assume that they represent one or more hydrated calcium silicates. Most of the extraneous patterns were of two types, here designated "a" and "b." The former bears some resemblance to that of the $CaO{\cdot}SiO_2{\cdot}H_2O$ described by McMurdie and Flint [10], designated CSH (A) by Bogue [9], although the fit is imperfect. The "b" pattern resembles that of the so-called C_2S γ-hydrate, which Bogue calls C_2SH (C). Here again the fit is not perfect, but better than in the previous case. The possibility remains, of course, that these patterns are indicative of one or more quaternary compounds or solid solutions of unknown composition.

Although the identity of the calcium silicate hydrates formed in these reactions cannot be considered well established, it is significant that there is no evidence of the presence of either xonotlite or hillebrandite, which Peppler [11] has shown to be the stable phases in the $CaO{\cdot}SiO_2{\cdot}H_2O$ system under equivalent conditions of temperature and pressure.

b. Mixtures of 3 $CaO{\cdot}Al_2O_3{\cdot}6H_2O$ with Silica or Calcium Silicate Hydrate

It is of interest to ascertain how tricalcium aluminate hexahydrate, prepared in the absence of silica, reacts on subsequent treatment in the presence of silica. The data presented in table 3 are typical of the results of a considerable number of experiments of this nature. In experiments 1 to 10 the silica was present as silica gel. As previously noted by Flint and Wells [2], the aluminate takes up silica under these conditions, forming silica-bearing hydrogarnets. Flint and Wells relied on refractive index measurements in estimating the amount of silica taken up. The X-ray diffraction method employed in the present work provides a somewhat more precise indication of the silica content. It is clear that experiments 3, 5, and 6 failed to reach equilibrium, because a new hydrogarnet phase is seen to exist together with part of the original $3CaO{\cdot}Al_2O_3{\cdot}6H_2O$. By the use of higher temperatures and pressures, equilibrium apparently was obtained. The product of experiment 10 was of almost the same composition as that obtained by treatment of the ternary glass under similar conditions. As in the experiments with the glasses, several of the reaction products formed at the lower temperatures contained hydrated calcium silicate CSH(B). In a few instances the extraneous lines in the X-ray patterns could not be positively identified.

In experiments 11 to 13 the silica was initially present as a synthetic gel of approximate composition CSH, whereas for Nos. 14 to 16 a synthetic C_2SH(B) containing about 10 percent of xonotlite was used. These preparations reacted readily with the aluminate, forming $Ca(OH)_2$ and a siliceous hydrogarnet. No consistent relation is observed between composition of the hydrogarnet and temperature of formation; also there is evidence of failure to reach equilibrium.

c. Mixtures of Calcium Hydroxide and Dehydrated Kaolin

Among the possible practical aspects of hydrogarnet formation is the reaction between lime and pozzolanic materials, particularly if conducted at elevated temperatures. Pozzolans usually contain both silica and alumina in active form. A sample of Georgia kaolin, activated by heating at 700° C, was used as a representative material of this type. Table 4 gives the results of a few experiments with mixtures of lime with the activated kaolin. The ratio of reactants was such as to give an over-all composition of $3CaO{:}Al_2O_3{:}2SiO_2$.

Like the other mixtures described above, the lime-kaolin mixtures failed to reach equilibrium during the

TABLE 3. *Hydrothermal reactions between* $3CaO{\cdot}Al_2O_3{\cdot}6H_2O$ *and silica present as gel or hydrosilicate*

Experiment	Siliceous compound	Molar ratio, $S{:}C_3A$	Temperature	Pressure	Duration [a]	Phases present in product [b]			
						$Ca(OH)_2$	Hydrogarnets		Other phases
							C_3AH_6	Siliceous (cell constant)	
			°C	atm				Å	
1	SiO_2 gel	1.0	210	20	7 d	−	+	.....	CSH(B)
2	do	1.0	225	25	2 d	−	+	.....	CSH(B)
3	do	1.0	265	50	7 d	−	+	[c] 12.07	.....
4	do	1.5	236	30	8 d	−	+	−	CSH(B)
5	do	1.5	253	40	7 d	−	+	[c] 12.05	CSH(B)
6	do	1.5	344	150	7 d	−	+	[c] 11.99	$C_4A_3H_3$(?)
7	do	3.0	140	1,020	1 d	−	+	[c] −	+
8	do	3.0	355	1,020	6 hr	−	−	12.00 (tr)	CSH(B)
9	do	3.0	395	1,020	1 d	−	−	11.97	+
10	do	3.0	715	1,020	6 hr	−	−	11.87	.....
11	CSH	1.0	249	40	7 d	+	+	[c] 12.23	.....
12	do	1.0	350	160	7 d	+	+	[c] 12.19	.....
13	do	1.5	350	160	7 d	+	tr.	[c] 12.23	.....
14	C_2SH(B)	1.0	250	40	7 d	+	−	12.43	C_2SH(B)
15	do	1.0	350	160	7 d	+	tr.	[c] 12.19	.....
16	do	2.0	250	40	7 d	+	−	12.28	C_2SH(B)

[a] d = days; hr, hours.
[b] + indicates present; −, absent; tr., trace.
[c] From coexistence of hydrogarnet phases it is concluded that equilibrium was not attained.

reaction period with the possible exception of experiment 7. If in the product of each of the last four members of this series only the phase highest in silica (smallest in unit cell dimensions) be considered, the agreement with the equilibrium curve in figure 1 is good. It should be noted that the unit cell size in experiment 7 indicates nearly 3 moles of silica in the hydrogarnet, which value is higher than the proportion originally present. The excess lime and alumina are accounted for by the $Ca(OH)_2$ and $4CaO{\cdot}3Al_2O_3{\cdot}3H_2O$ present.

TABLE 4. *Hydrothermal reactions of mixtures of lime and activated kaolin*

Experiment	Molar ratio, S:C_3A	Temperature	Pressure	Duration	Phases present in product [a]			
						Hydrogarnets		Other phases
					$Ca(OH)_2$	C_3AH_6	Siliceous (cell constant)	
		°C	atm	Days			Å	
1	2.0	180	10	10	—	—	[b] 12.50, 12.24	+
2	2.0	224	25	10	—	—	[b] 12.51, 12.32, 12.24	CSH(B)
3	2.0	261	45	10	—	—	[b] 12.47, 12.26	CSH(B)
4	2.0	302	85	7	—	—	[b] 12.46, 12.23, 12.01	+
5	2.0	349	160	7	+	—	[b] 12.45, 12.24, 11.95	+
6	2.0	396	265	7	+	—	[b] 12.24, 11.91	$C_4A_3H_3$
7	2.0	445	385	7	+	—	11.89	$C_4A_3H_3$

[a] + indicates present; —, absent.
[b] From coexistence of hydrogarnet phases it is concluded that equilibrium was not attained.

d. Mixtures of the Hydrated Oxides

In another short series of experiments, the reactants were present as hydrated oxides; the lime as hydroxide, the alumina as gibbsite, and the silica as gel. The ratio of lime to alumina was kept at 3 to 1, as in the foregoing, but the silica was varied. The results are presented in table 5. Lack of attainment of equilibrium during the reaction period is again observed in certain cases. The occurrence of $4CaO{\cdot}3Al_2O_3{\cdot}3H_2O$ in experiments 1 and 3 deserves comment. It will be shown later that this phase would be expected to appear only at somewhat higher temperatures in the presence of silica in the amounts indicated in table 5. This may be taken as further evidence of lack of equilibrium.

TABLE 5. *Hydrothermal reactions of mixtures of lime, alumina, and silica*

Experiment	Molar ratio, S:C_3A	Temperature	Pressure	Duration	Phases present in product [a]			
						Hydrogarnets		Other phases
					$Ca(OH)_2$	C_3AH_6	Siliceous (cell constant)	
		°C	atm	Days			Å	
1	0.2	235	30	5	+	+	—	$C_4A_3H_3$
2	.2	285	65	5	+	+	[b] 12.45	$C_4A_3H_3$
3	.5	243	35	4	+	—	12.49	$C_4A_3H_3$
4	.5	275	60	4	+	—	12.44	$C_4A_3H_3$
5	1.0	212	20	9	tr.	+	[b] 12.47, 12.16	+
6	1.0	301	85	9	—	—	[b] 12.48, 12.27, 11.97	—

[a] + indicates present; —, absent; tr., trace.
[b] From coexistence of hydrogarnet phases it is concluded that equilibrium was not attained.

3.3. Hydrothermal Decomposition of the Hydrogarnets

As noted in the introduction, tricalcium aluminate hexahydrate decomposes under hydrothermal conditions at about 215° C, yielding calcium hydroxide and a less basic aluminate. The equation may be written

$$3(3CaO{\cdot}Al_2O_3{\cdot}6H_2O) \rightleftarrows 4CaO{\cdot}3Al_2O_3{\cdot}3H_2O + 5Ca(OH)_2 + 10H_2O.$$

Data obtained in the present work (experiments 1 and 2 in table 6) indicate that the equilibrium temperature is between 220° and 226° C. If a hydrogarnet of composition $3CaO{\cdot}Al_2O_3{\cdot}mSiO_2{\cdot}(6-2m)H_2O$ breaks down in the same manner the silica liberated may be expected to combine with part of the lime.

Table 6 presents data obtained on hydrogarnets and glass compositions covering a wide range of silica content. The hydrogarnets (experiments 3 to 11) were prepared from boiling solutions as described in section 2.3. The silica content indicated was determined by analysis of the product, but it is probable that not all the silica was actually in the hydrogarnet phase, especially in the case of the most highly siliceous preparations (experiments 9 to 11).

All the preparations, with silica ranging up to 2 moles per mole of C_3A, when treated hydrothermally at sufficiently high temperatures yielded decomposition products in which $4CaO{\cdot}3Al_2O_3{\cdot}3H_2O$ could be

TABLE 6. *Effect of silica on the decomposition temperature of lime-alumina-silica hydrogarnets under hydrothermal conditions*

Experiment	Original material	Molar ratio, S:C_3A	Temperature	Duration	Phases present in product [a]		
					Hydrogarnet	$C_4A_3H_3$	$Ca(OH)_2$
			°C	Days			
1	C_3AH_6	0	220	7	+	—	—
2	do	0	226	7	—	+	+
3	Hydrogarnet	0.1	231	17	+	—	—
4	do	.1	258	7	+	+	+
5	do	.1	261	7	—	+	+
6	do	.3	276	7	+	—	—
7	do	.3	287	7	+	+	+
8	do	.3	307	7	—	+	+
9	do	.6	301	7	+	—	—
10	do	.6	313	7	+	+	+
11	do	.6	350	7	—	+	+
12	Glass	.2	210	14	+	—	—
13	do	.2	244	7	+	+	+
14	do	.4	240	18	+	—	—
15	do	.4	250	14	+	+	+
16	do	.4	356	14	—	+	+
17	do	.5	246	14	+	—	—
18	do	.5	263	14	+	+	+
19	do	.5	360	7	—	+	+
20	do	.7	251	9	+	—	—
21	do	.7	269	19	+	+	+
22	do	.7	372	33	—	+	+
23	do	1.2	300	18	+	tr.	—
24	do	1.2	371	18	+	+	+
25	do	2.0	372	7	+	—	—
26	do	2.0	400	19	+	+	—

[a] + indicates present; —, absent; tr., trace.

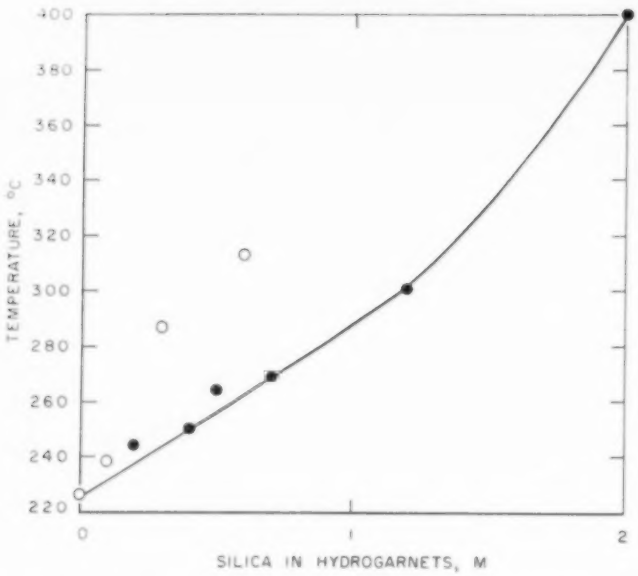

FIGURE 2. *Lowest temperature of formation of* $4CaO{\cdot}3Al_2O_3{\cdot}3H_2O$ *by hydrothermal decomposition of hydrogarnets in the system* $CaO-Al_2O_3-SiO_2-H_2O$.

○, experiments on hydrogarnets as starting materials; ● those on glasses.

identified. Calcium hydroxide was also observed except in the most silica-rich preparation, where presumably the lime had all combined with the silica. One or more other phases, usually ill-defined, were also present in the siliceous preparations. These presumably were calcium silicate hydrates, but in most cases they could not be definitely identified.

The minimum temperature of formation of $4CaO{\cdot}3Al_2O_3{\cdot}3H_2O$ is shown as a function of silica content in figure 2. The filled circles, representing data for the glass compositions, fall close to a smooth curve; nevertheless, the diagram should be interpreted with caution, because complete decomposition was not obtained except at considerably higher temperatures. Furthermore, the open circles representing the data for hydrogarnet starting materials are considerably above the curve, whereas under equilibrium conditions they should coincide. As a possible explanation for the discrepancy, it is suggested that the hydrogarnet phase formed from the glass during the warmup period might have been poorer in silica than that formed at the equilibrium temperature, and therefore subject to decomposition at a lower temperature. If this supposition is correct, the open circles more closely represent the true equilibrium curve.

3.4. Experiments With Cements

In view of the possible relation between these reactions and the setting of hydraulic cements, a few tests were made on two cements of domestic manufacture, one aluminous and one portland, to see whether the hydrated aluminate phases could be identified. The anhydrous cement was mixed with water and hydrothermally treated for 1 day.

After treatment at 185° C the aluminous cement gave an X-ray pattern in which the lines of a hydrogarnet with unit cell about 12.55 A could be distinguished. Within the limits of measurement, this could be interpreted as indicating pure tricalcium aluminate hexahydrate or a hydrogarnet containing a very small amount of silica. The other lines of the pattern fit the published patterns of afwillite fairly well, but were too weak for positive identification. A companion sample treated at 250° C showed a weaker hydrogarnet pattern plus a number of lines due to $4CaO{\cdot}3Al_2O_3{\cdot}3H_2O$. The latter phase was also observed under the microscope. The X-ray lines attributed tentatively to afwillite remained the same.

It is evident that the hydration of the aluminous cement at 185° C produces a hydrogarnet containing little or no silica, despite the presence of sufficient silica in the cement to form a hydrated silicate. It may be noted that similar results were obtained from the mixtures of tricalcium aluminate and tricalcium silicate at comparable temperatures (see, for example, experiments 15 and 21 in table 2). The similarity, however, seems to have disappeared at 150° C.

The sample of portland cement treated hydrothermally at 185° C gave a product showing a very weak hydrogarnet pattern with unit cell 12.41 A, indicating the presence of silica in the hydrogarnet phase. Calcium hydroxide was present in larger amount, and the rest of the lines resembled the published patterns for $3CaO{\cdot}SiO_2{\cdot}2H_2O$. The sample held at 250° C gave a similar pattern, with no indication of formation of $4CaO{\cdot}3Al_2O_3{\cdot}3H_2O$. Thus the portland cement differs from the aluminous cement in respect to hydrothermal hydration of its aluminate constituent. It does not necessarily follow that all portland cements would behave in similar manner. The cement used contained 7.1 percent of Al_2O_3, which is higher than average. With lower alumina content it might prove impossible to identify any hydrated aluminate by X-ray means.

The results obtained with both cements should be interpreted with caution because of the undetermined effect of the iron, alkalies, and other components present in the cement. Substitution of Fe_2O_3 for Al_2O_3 would increase the unit cell size [1] and thus might compensate for the effect of higher silica content.

4. Summary

Hydrothermal treatment of lime-alumina-silica glasses of the composition of grossularite produced hydrogarnets increasing in silica content with the temperature of formation and approximating the composition of grossularite at 800° C. The curve was extended at the lower temperature end through the use of glasses poorer in silica.

Mixtures of lime, alumina, and silica as such or in various states of combination, on hydrothermal treatment, usually failed to reach the equilibrium state attained with the glasses. At times as many

as three distinct hydrogarnet compositions were found to coexist after reaction periods of several days.

The equilibrium temperature for the decomposition of $3CaO{\cdot}Al_2O_3{\cdot}6H_2O$ under hydrothermal conditions was found to be between 220 and 226° C, the products being $4CaO{\cdot}3Al_2O_3{\cdot}3H_2O$ and $Ca(OH)_2$. Hydrogarnets containing increasing amounts of silica underwent the same type of decomposition at progressively higher temperatures.

Compounds of the hydrogarnet series were also formed by hydrothermal treatment of aluminous and portland cements. The product of the aluminous cement contained little or no silica, whereas that of the portland cement contained an appreciable amount.

5. References

[1] E. P. Flint, H. F. McMurdie, and L. S. Wells, J. Research NBS **26,** 13 (1941) RP1355.
[2] E. P. Flint and L. S. Wells, J. Research NBS **27,** 171 (1941) RP1411.
[3] H. S. Yoder, Jr., J. Geology **58,** 221 (1950).
[4] H. Johnson and T. Thorvaldson, Can. J. Research **21,** 236 (1943).
[5] R. B. Peppler and L. S. Wells, J. Research NBS **52,** 75 (1954) RP2476.
[6] G. C. Kennedy, Am. J. Sci. **248,** 540 (1950).
[7] O. F. Tuttle, Geol. Soc. Am. Bull. **60,** 1727 (1949).
[8] L. Heller and H. F. W. Taylor, J. Chem. Soc. **1952,** 1018.
[9] R. H. Bogue, Portland Cement Assn. Fellowship Paper No. 69 (Sept. 1954).
[10] H. F. McMurdie and E. P. Flint, J. Research NBS **31,** 225 (1943) RP1560.
[11] R. B. Peppler, J. Research NBS **54,** 205 (1955) RP2582.

Washington, March 2, 1956.

Journal of Research of the National Bureau of Standards Vol. 56, No. 6, June 1956 Research Paper 2684

Infrared Absorption Spectrum of Trimethylborane

James E. Stewart

The infrared absorption spectrum of gaseous trimethylborane, $B(CH_3)_3$, has been observed in the 2- to 40-micron spectral region. Vibrational assignments have been made for infrared bands, as well as for the Raman lines reported by other investigators. The perfect gas entropy was calculated for a temperature of 199.92° K and compared with the experimental value. Barriers to internal rotation of methyl groups of about 750 or 1,640 calories per mole are calculated for structures with or without a threefold axis of symmetry.

1. Introduction

This study of the infrared spectrum of gaseous trimethylborane was undertaken as part of a program of the National Bureau of Standards for the investigation of chemical and physical properties of boron compounds.

The infrared and Raman spectra of trimethylborane were first reported by Goubeau and Becher [1].[1] Their data were used by Siebert [2] in a normal coordinate treatment. The infrared spectrum of Goubeau and Becher does not extend beyond about 600 cm^{-1}, and it contains impurity bands not observed in the present study. Accordingly, it seemed desirable to repeat and extend the measurements. Very recently Levy [3] measured the very near infrared spectrum of trimethylborane and other boron compounds.

2. Experimental Procedure

The samples of trimethylborane were prepared by A. R. Glasgow, Jr., and G. S. Ross, Sr., of the Bureau's Pure Substances Section by reaction of hydrogen chloride with the ammonia adduct $B(CH_3)_3{:}NH_3$. After subsequent purification [4], purities of two lots were determined calorimetrically by G. T. Furukawa of the Thermodynamics Section and found to be 99.7 ± 0.1 and 99.9 ± 0.1 percent. These lots were indistinguishable spectroscopically.

The material was stored as liquid at reduced temperature in stainless-steel cylinders and was distilled into an auxiliary glass bulb immediately before admission into the absorption cell. Purification procedures were monitored by obtaining spectra after successive operations on samples from both the liquid and gas phases in the cylinder. This procedure was of value in the identification of impurity bands. Pressures were measured with a mercury manometer.

Spectra were obtained with a Perkin-Elmer model 21 double-beam spectrophotometer equipped with prisms of sodium chloride and cesium bromide for the 2- to 15-μ and 15- to 40-μ regions, respectively. Stray radiation encountered when using the cesium bromide prism was limited to 2 percent or less for wavelengths less than 38 μ by means of reststrahlen filters of lithium fluoride and calcium fluoride. A Perkin-Elmer model 12B spectrometer with a lithium fluoride prism was also used for the near infrared region. A potassium bromide prism was not required because no bands were observed between 15 and 25 μ. Standard Perkin-Elmer gas-cell bodies of nickel-plated brass were used. Potassium bromide and cesium bromide windows were mounted with silicone rubber gaskets coated with silicone grease, with polychlorotrifluoroethylene wax, or with a beeswax-rosin mixture.

3. Results

Trimethylborane is very reactive with oxygen and ignites spontaneously in air. Very slow decomposition of the sample in the cell was observed, probably due to slight air leakage at the window seals. No spectral evidence was found for the formation of methane, ethane, ethylene, or carbon dioxide during this reaction. The appearance of a band near 1,370 cm^{-1} is very likely associated with the formation of B—O—C bonds [5], suggesting that boron methoxides are produced by slow oxidation. Additional bands appeared at 1,479, 1,220, 1,062-1,055-1,048 (PQR-like structure), 950, 787, and 590 cm^{-1}. When purified material was stored for several weeks at reduced temperature and reexamined, none of the above bands was seen except 787 cm^{-1}. An additional band was found at 730 cm^{-1}.

Goubeau and Becher reported medium to strong bands at 620, 635, 648, 667, 720, and 800 cm^{-1}, which were not observed in the present study even at higher pressures. Furthermore, several bands were not resolved in their spectrum because sufficiently low pressure was not used.

The sodium chloride and cesium bromide spectra are shown in figure 1, and the complete spectrum is tabulated in table 1, along with the Raman spectrum of Goubeau and Becher.

[1] Figures in brackets indicates the literature references at the end of this paper.

TABLE 1. *Vibrational frequencies and assignments for trimethylborane*

(w, weak; m, medium; s, strong; v, very; b, broad; sh, shoulder)

Raman (liquid)	Infrared (gas)	C_s symmetry	Assignment	C_{3h} symmetry
cm^{-1}	cm^{-1}			
320 4b	320 m	$\nu_{17}(a')$, $\nu_{31}(a'')$	C_3B bending	$\nu_{18}(e')$
	336 m	$\nu_{16}(a')$	C_3B out-of-plane	$\nu_{10}(a'')$
	345 sh	$\nu_{31}(a'')$?, $\nu_{16}(a')B^{10}$	C_3B^{10} out-of-plane	$\nu_{10}(a'')B^{10}$
394 0			?	
486 2			?	
675 6		$\nu_{15}(a')$	$\nu B-C$	$\nu_6(a')$
755 0			?	
864 2b	855 m	$\nu_{14}(a')$	ρCH_3	$\nu_{21}(e'')$
906 $\frac{1}{2}$		$\nu_{13}(a')$	ρCH_3	$\nu_5(a')$
	951 w, sh	ν_{30} P branch	$968+\nu_4-\nu_1$	ν_9 P branch
970 $\frac{1}{2}$	968 s	$\nu_{30}(a'')$	ρCH_3	$\nu_9(a'')$
	983 m	$\nu_{29}(a'')$ ρCH_3		$675+320=995$
1060 $\frac{1}{2}$			Impurity?	
1145 6b	1149 vs	$\nu_{12}(a')$	ρCH_3	$\nu_{17}(e')$
	1162 vs	$\nu_{28}(a'')$ ρCH_3		$855+320=1175$
1195 0	1189 m		$855+336=1191$	
	1300 sh		$983+320=1303$, $968+336=1304$	
1295 1b	1309 vs	$\nu_{11}(a')$, $\nu_{27}(a'')$	νBC	$\nu_{16}(e')$
1440 2b		$\nu_9(a')$, $\nu_{10}(a')$, $\nu_{26}(a'')$	δCH_3	$\nu_3(a')$, $\nu_4(a')$, $\nu_{20}(e'')$
	1459 m	$\nu_8(a')$, $\nu_7(a')$, $\nu_6(a')$, $\nu_{25}(a'')$, $\nu_{24}(a'')$, $\nu_{23}(a'')$	δCH_3	$\nu_8(a'')$, $\nu_{14}(e')$, $\nu_{15}(e')$
	1721 vw		$2\times855=1710$	
	1828 vw		$1149+675=1824$	
	1976 w		$1309+675=1984$	
	2167 w		$1309+855=2164$	
	2255 vw		$2921-675=2246$	
	2444 w		$1459+983=2442$	
	2456 w		$1309+1149=2458$	
	2472 vw		$1162+1309=2471$	
	2591 vw		$1149+1440=2589$	
2875 8b		$\nu_4(a')$, $\nu_3(a')$	νCH	$\nu_2(a')$
	2921 s	$\nu_{22}(a'')$	νCH	$\nu_{13}(e')$
2975 4b		$\nu_1(a')$, $\nu_2(a')$, $\nu_3(a')$	νCH	$\nu_1(a')$, $\nu_{19}(e'')$
	2986 s	$\nu_{19}(a'')$, $\nu_{20}(a'')$, $\nu_{21}(a'')$	νCH	$\nu_7(a'')$, $\nu_{12}(e')$
	3300 w		$2975+320=3295$	
	3522 w		$2875+2\times320=3515$	
	3575 w		$2921+2\times320=3561$	
	3729 w, sh		$855+2875=3730$	
	3853 w		$968+2875=3843$	
	4060 w		$1149+2921=4070$	
	4144 w		$2986+1149=4135$, $2975+1162=4137$	
	4362 w		$2921+1440=4361$	
	5798 w		$2921+2875=5796$	

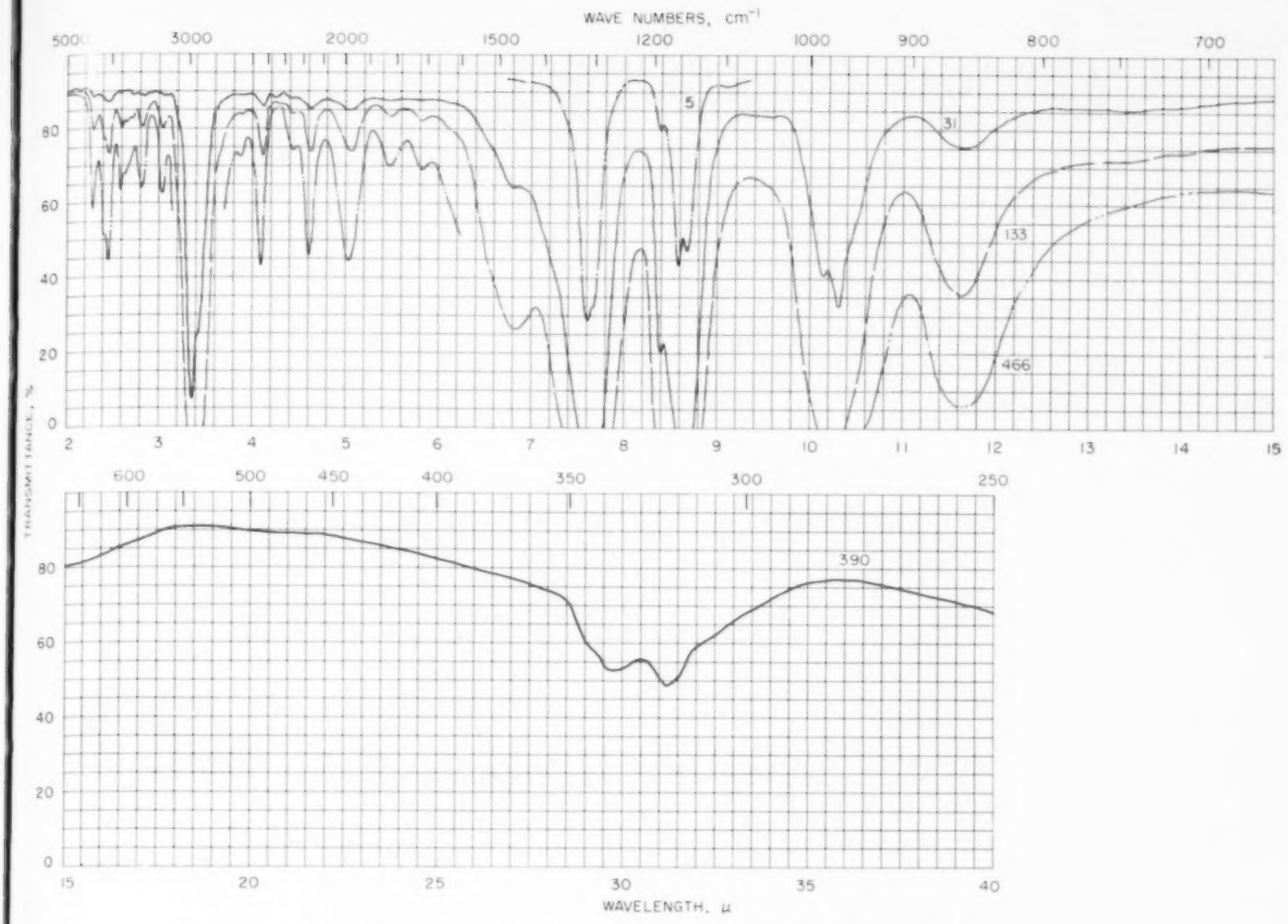

FIGURE 1. *Infrared spectrum of gaseous trimethylborane*, $B(CH_3)_3$.

99.7 mole percent pure, 10-cm cell, pressures in millimeters of mercury.

4. Structure, Vibrational Assignment, and Discussion

Electron diffraction studies [6] have shown trimethylborane to have a planar C_3B skeleton of symmetry D_{3h}. The configuration of the hydrogen atoms is not known. Barring completely free methyl group rotation, the molecule can be in one of the following symmetry classes: C_{3v} with one hydrogen from each methyl on one side of the C_3B plane and the remaining hydrogens on the other side; C_{3h} with one hydrogen from each methyl in the C_3B plane; C_3 with the methyls rotated by an equal amount about their axes; C_s with a plane of symmetry containing the C_3 axis of the C_3B skeleton; or C_1 with no symmetry at all. The study of molecular models shows that the C_{3v} structure can probably be ruled out, whereas the C_{3h} structure is most attractive from steric considerations. The number of vibrations observed in the Raman effect but not in the infrared, and vice versa, is evidence against C_1, C_3, and C_s symmetry, in which all transitions are both Raman and infrared active. On the other hand, the abundance of vibrations observed in the 850 to 1,200 cm^{-1} region makes the nondegenerate C_1 or C_s symmetry more reasonable than the degenerate structures. In view of these considerations, both the C_s and the C_{3h} structures are treated, with the reservation that in the case of C_s symmetry the C_3B skeletal modes may behave as though they were in a molecule of D_{3h} symmetry because of weakness of methyl-skeleton interactions.

There are no assignments available for other boron-alkyl compounds to be used as a guide in the analysis of the trimethylborane spectrum. Sheppard and Simpson [7] have considered the effect of substituting fluorine for methyl groups in several paraffins and found good correlation between skeletal vibrations with usually little frequency shift for the unsymmetric vibrations and a moderate shift to higher frequencies for the symmetric vibrations of the fluorine analogs. This suggests that the vibrational assignment for BF_3 can be used as an aid in assigning the skeletal modes of trimethylborane

In order to demonstrate the extent of the reliability of this procedure, data for five pairs of compounds resembling BF_3 and $B(CH_3)_3$, and not discussed by Sheppard and Simpson, are tabulated in table 2. The skeletal modes for acetone are assigned from the frequencies given by Price. All other assignments are those given by the original author. With the exception of the asymmetric stretching modes of NF_3, all vibrations are shifted to higher frequencies upon substitution of fluorine, some by quite large amounts. Of the two possible choices for the asymmetric stretching vibration for trimethylborane at 1,309 and 1,149 cm^{-1}, 1,309 cm^{-1} seems to be more probable by analogy with boron trifluoride. This is in disagreement with Siebert's choice of 1,149 cm^{-1}.

The infrared spectra of a series of seven trialkyl boranes have been measured by Pickard, Dulaney, and Polly [8]. In addition, the infrared [2] and Raman [9] spectra of triethylborane have been measured at the Bureau. From these curves it is possible to select a satisfactory sequence of frequencies converging on 1,309 cm^{-1} for trimethylborane for assignment to asymmetric skeletal stretching vibrations.

Intensity considerations supply further evidence concerning the assignment of the asymmetric stretching vibration. The band at 1,309 cm^{-1} must include some contribution from the symmetric CH_3 deformation modes. But it seems much too intense relative to the asymmetric CH_3 deformation at 1,459 cm^{-1} to be entirely due to CH_3 vibrations. Hence another vibration must be superposed. Furthermore the great intensity of 1,145 cm^{-1} in the Raman effect argues against its assignment to a nontotally symmetric mode. The corresponding vibration in the Raman spectrum of BF_3 is not observed even though it is not a forbidden transition. On the other hand, no band is available in the neighborhood of 1,309 cm^{-1} for assignment to the B^{10} isotopic molecule, whereas, 1,149 cm^{-1} has such a neighbor of proper intensity at 1,189 cm^{-1}.

Siebert's assignment of 486 cm^{-1} to the BC_3 out-of-plane bending vibration is satisfactory by analogy with the corresponding frequency in BF_3, but this vibration is Raman inactive and infrared active under the D_{3h} selection rules of BF_3 (and also under C_{3h}), whereas just the reverse activity is observed for the 486 cm^{-1} band. Therefore, 336 cm^{-1} is assigned to this vibration. The assignment of 320 cm^{-1} to the in-plane deformation mode is natural and agrees with Siebert.

A choice must be made between the vibrations at 675 and 864 cm^{-1} for assignment to the symmetric B—C stretching mode. 864 cm^{-1} is perhaps in better agreement with the BF_3 analogy, but its use would leave 675 cm^{-1} unexplained, whereas 864 cm^{-1} can be reasonably assigned to a methyl rocking mode. Furthermore, 675 cm^{-1} is reported to be sharp and very strong in the Raman effect and is unobserved in the infrared, whereas 864 cm^{-1} is broad in the Raman effect and of medium intensity in the infrared spectrum. The assignment of 675 cm^{-1} to the symmetric stretch is therefore preferred, in agreement with Siebert.

[2] Unpublished curve obtained by the author.

TABLE 2. *Skeletal vibration frequencies of fluoro and methyl compounds*

Compound reference		Asymmetric stretch	Symmetric stretch	Out-of-plane bending	In-plane deformation
		cm^{-1}	cm^{-1}	cm^{-1}	cm^{-1}
NF_3	[a]	1, 031	907	642	497
$N(CH_3)_3$	[b]	1, 036	827	423	365
PF_3	[c]	892	860	487	344
$P(CH_3)_3$	[d]	708	653	305	263
AsF_3	[e]	707	644	341	274
$As(CH_3)_3$	[d]	583	568	239	223
$O=CF_2$	[f]	1, 249	965	626	584
$O=C(CH_3)_2$	[g]	1, 202	896		547
$F_2C=CH_2$	[h]	1, 302	926	611	550
$(CH_3)_2C=CH_2$	[i]	986	800	391	378
BF_3	[j]	1, 446	888	691	480
$B(CH_3)_3$		1, 309	675	336	320

[a] E. L. Pace and Louis Pierce, J. Chem. Phys. **23**, 1248 (1955).
[b] K. W. F. Kohlrausch, Monatsh. **68**, 349 (1936).
[c] M. K. Wilson and S. R. Polo, J. Chem. Phys. **20**, 1716 (1952).
[d] E. J. Rosenbaum, D. J. Rubin, and C. R. Sandberg, J. Chem. Phys. **8**, 366 (1940).
[e] J. B. Howard and E. B. Wilson, Jr., J. Chem. Phys. **2**, 630 (1934).
[f] A. H. Nielsen, T. G. Burke, P. J. H. Woltz, and E. A. Jones, J. Chem. Phys. **20**, 596 (1952).
[g] D. Price, J. Chem. Phys. **9**, 725 (1941).
[h] D. C. Smith, J. R. Nielsen, and H. H. Claassen, J. Chem. Phys. **18**, 326 (1950).
[i] J. E. Kilpatrick and K. S. Pitzer, J. Research NBS **38**, 191 (1947) RP1768.
[j] D. M. Gage and E. F. Barker, J. Chem. Phys. **7**, 455 (1939); D. M. Yost, D. DeVault, T. F. Anderson, and E. N. Lassetre, J. Chem. Phys. **6**, 424 (1938).

The skeletal force constants were calculated by treating the methyl groups as point masses [10]. The B—C stretching force constant f_{BC}, which depends on the asymmetric stretching frequency only, is found to be 4.03×10^5 dynes/cm as compared with Siebert's value of 3.64×10^5 dynes/cm. The self-consistency of the point-mass methyl treatment can be demonstrated by comparing the calculated value of $(\nu_3^2+\nu_4^2)$ with the experimentally determined value. Using Siebert's assignment, these numbers are 1.57×10^6 and 1.42×10^6 cm^{-2}, respectively. The modified assignment proposed here gives 1.62×10^6 and 1.82×10^6, respectively.

The methyl stretching and deformation modes are assigned in the usual way. Assuming a structure of C_s symmetry, the bands at 855, 906, and 1,149 cm^{-1} are assigned to a′ methyl rocking modes, and 968, 983, and 1,162 cm^{-1} are assigned to a″ rocking modes. These bands are assigned in such a way that

where possible the a′ transitions are most intense in the Raman effect and a″ transitions are most intense in the infrared spectrum. Assuming a structure of C_{3h} symmetry, the methyl rocking modes are assigned as follows: a′-906, a″-968, e′-1,149, e″-864 cm^{-1}, although 968 and 864 cm^{-1} violate the selection rules. Raman lines at 394, 486, 755, and 1,060 cm^{-1} remain unexplained. The 1,060 cm^{-1} line might correspond to the impurity band observed near this frequency in the infrared spectrum. The lines at 486, 755, and 1,060 cm^{-1} might arise from a methyl torsion vibration of frequency 160 cm^{-1}: $320+160=480$, $906-160=746$, $906+160=1{,}066$. The shoulder at 345 cm^{-1} in the infrared spectrum might result from a splitting of the skeletal deformation vibrations, or it might represent a B^{10} isotopic molecule vibration. The weak shoulder at about 960 cm^{-1} in the infrared spectrum might be the P branch corresponding to 968 cm^{-1}, or it might be an upper stage band $968+\nu_1-\nu_1$. In the assignment for the C_{3h} structure, the combination transitions assumed for the weak bands at 1,300, 2,444, 2,472, and 3,729 cm^{-1} are in violation of selection rules, and the strong peaks at 983 and 1,162 cm^{-1} are assigned to combination transitions.

5. Entropy and Methyl Rotation Barrier

Using observed vibration frequencies, moments of inertia $I_A=I_B=112.92\times10^{-40}$ and $I_C=209.02\times10^{-40}$ g-cm,^{2} and a reduced methyl moment of inertia of 5.322×10^{-40} g-cm^2, the contribution to the entropy at 199.92° K from translation, over-all rotation, internal free rotation, and vibration is 69.31 cal deg^{-1} $mole^{-1}$ for the C_{3h} structure and 71.48 cal deg^{-1} $mole^{-1}$ for the C_s structure. The difference is largely due to the difference in symmetry number of 81 for C_{3h} and 27 for C_s. Recently Furukawa and Park [11] determined the entropy of trimethylborane calorimetrically and found $S_{199.92}=68.29$ cal deg^{-1} $mole^{-1}$. The difference of 0.34 cal deg^{-1} $mole^{-1}$ per rotor for C_{3h} and 1.06 cal deg^{-1} $mole^{-1}$ for C_s symmetry requires for agreement a sinusoidal barrier to free rotation of 750 cal/mole or 1,640 cal/mole for the C_{3h} and C_s structures, respectively.

6. Conclusion

In several respects the assignment for a trimethylborane structure of C_s symmetry is more satisfactory than the assignment for a C_{3h} structure. Furthermore, the higher methyl rotation barrier associated with the C_s structure would seem more acceptable upon comparison with similar molecules, and indeed French and Rasmussen [12] predicted a barrier of 1,720 cal/mole on empirical grounds. On the other hand, the nature of the barrier to rotation about a single bond and the role of methyl interactions in determining the barrier are not understood. Hence it is by no means clear that the use of standard methods for calculating the barrier is justified in the case of trimethylborane, or that the comparison of barriers between molecules is meaningful. Therefore, no conclusion is made regarding the correct structure of trimethylborane.

The author is grateful to A. R. Glasgow, Jr., and G. S. Ross, Sr., who prepared and purified the samples used and performed the cell filling operations; to G. T. Furukawa and R. P. Park for permitting the use of their thermodynamic data in advance of publication; to D. E. Mann for his helpful discussions and advice; and to W. H. Evans for checking the thermodynamic calculations.

7. References

[1] G. Goubeau and H. J. Becher, Z. anorg. u. allgem. Chem. **268,** 1 (1952).
[2] Hans Siebert, Z. anorg. u. allgem. Chem. **268,** 13 (1952).
[3] E. J. Levy, Dissertation, Univ. Delaware, Tech. Research Rept. MCC–1023–TR–118 (June 1955).
[4] G. S. Ross, C. A. Hewitt, D. Enagonio, and A. R. Glasgow, J. Am. Chem. Soc. (publication pending).
[5] J. V. Bell, J. Heisler, H. Tannenbaum, and J. Goldenson, Anal. Chem. **25,** 1720 (1953).
[6] H. A. Levy and L. O. Brockway, J. Am. Chem. Soc. **59,** 2085 (1937).
[7] N. Sheppard and D. M. Simpson, J. Chem. Phys. **23,** 582 (1955).
[8] P. L. Pickard, C. L. Dulaney, and G. W. Polly, Ultraviolet and infrared absorption spectra of organoboron compounds, Report No. CCC–1024–TR–96 (Univ. Oklahoma, February 1955).
[9] E. J. Blau and B. W. Mulligan (private communication).
[10] G. Herzberg, Infrared and Raman spectra of polyatomic molecules, p. 178 (D. Van Nostrand Co., Inc., New York, N. Y., 1945).
[11] G. T. Furukawa and R. P. Park (private communication).
[12] F. A. French and R. S. Rasmussen, J. Chem. Phys. **14,** 389 (1946).

Washington, June 15, 1955.

Journal of Research of the National Bureau of Standards Vol. 56, No. 6, June 1956 Research Paper 2685

Pyrolysis of Cellulose in a Vacuum[1,2]

S. L. Madorsky, V. E. Hart, and S. Straus

Samples of cotton, cotton hydrocellulose, and viscose rayon, both by themselves and impregnated with sodium carbonate or sodium chloride, were pyrolyzed at 250° to 397° C in a high vacuum. The volatile products were fractionated and the fractions analyzed in the mass spectrometer and by infrared absorption. The volatile fractions consisted mainly of CO, CO_2, water, and levoglucosan (tar). The residue consisted mainly of carbon (char). Impregnation of the cellulosic materials with salts caused a decrease in the yield of tar and an increase in the yields of CO, CO_2, H_2O, and char. Rates of thermal degradation of the same materials were investigated in the range 245° to 305° C by a loss-of-weight method, using a very sensitive tungsten spring balance enclosed in a vacuum. Plots of rates of loss of weight versus percentage of loss of weight, in the case of pure cellulosic materials, pass through maxima at about 13 to 23 percent loss of weight, then drop gradually to the carbonization end point. In the case of samples impregnated with sodium carbonate or sodium chloride, the initial rates of loss of weight are very high, but drop rapidly to the carbonization end point. The activation energies of thermal degradation of the pure cellulosic materials are much greater than those of the same materials impregnated with sodium carbonate or sodium chloride.

1. Introduction

An investigation of the thermal degradation or pyrolysis of cellulose in a vacuum was undertaken in connection with the problem of rendering cellulosic materials used in fabrics flame-resistant. Flaming of these materials takes place in two principal consecutive steps: (1) the cellulose first degrades under the influence of heat to form volatile and nonvolatile products; (2) the flammable constituents of the products ignite and the heat evolved promotes further decomposition of the cellulose. In rendering cellulosic materials resistant to flaming, the conditions of degradation are so altered as to increase the amount of the nonflammable products at the expense of the flammable products.

This paper deals with the first of the two steps enumerated above. The advantages of conducting pyrolysis in a vacuum, instead of in air or in an inert gas, are that the degradation products are prevented from reacting with oxygen (in the case of air) and that the volatile products are more quickly and completely removed from the hot zone, where they might otherwise undergo secondary reactions. In a vacuum the volatile products are more easily collected and fractionated for analysis.

Pyrolysis of cellulose at reduced pressures has been reported by several investigators [1, 2, 3, 4].[3] Their results indicate the formation of tar, char, H_2O, CO_2, and CO in various yields, depending on conditions of pyrolysis. In this investigation a vacuum of 10^{-3} to 10^{-5} mm Hg was maintained during pyrolysis, and a study was made of the nature and proportion of the various products and also of the rates of degradation of pure cellulosic materials with or without additives. A considerable amount of research has been conducted in recent years at the Bureau on the thermal degradation of vinyl, butadiene, and aromatic polymers; the methods and apparatus developed and used in this research have now been applied to the study of thermal degradation of cellulose. The method can be divided into two parts:

(1) Pyrolysis of a small sample in an evacuated apparatus, and subsequent investigation of the decomposition products.

(2) Determination of rates of thermal degradation at several temperatures, and calculation of the activation energies of the degradation reactions involved.

2. Materials Used

Three forms of cellulose were used: cotton cellulose, cotton hydrocellulose, and viscose rayon. The cotton, which was an Empire cotton obtained from the Southern Utilization Branch of the U. S. Department of Agriculture, was dewaxed by extraction with boiling alcohol. It was freed from pectic substances by immersion in boiling 1-percent sodium hydroxide in the absence of air for 2 hr, washed in distilled water, neutralized with dilute acetic acid, again washed in water, and dried in air at room temperature. The hydrocellulose was obtained by immersion of a portion of the purified cotton in 6 *N* HCl for approximately 15 hr. After washing with distilled water to remove the acid, the hydrocellulose was dried in air at room temperature. The viscose rayon was a commercial yarn, 900 denier, 100 filament. It was washed in warm dilute aqueous ammonia, rinsed in warm water, and dried in air at room temperature.[4]

In order to determine the amount of moisture and other volatiles adsorbed on the cellulosic materials, samples were "dried" to a constant weight in a vacuum at 100° C. It was found that this could be accomplished in about 60 min. Losses, in percentages of dry samples, were: 3.7, 4.1, and 8.6, for

[1] This work was performed as a part of the research project sponsored by the Office of Quartermaster General, Department of the Army.

[2] This paper was presented at the 128th National Meeting of the American Chemical Society in Minneapolis, Minn., September 12 to 16, 1955.

[3] Figures in brackets indicate the literature references at the end of this paper.

[4] The authors are indebted to Florence H. Forziati of the Textiles Section of the Bureau for supplying the purified cotton, hydrocellulose, and rayon.

cotton, hydrocellulose, and viscose rayon, respectively. In the actual pyrolysis experiments, the samples were dried in the above manner in the vacuum apparatus and the volatiles were pumped off prior to pyrolysis. The original weights of the samples were corrected for the above determined weight losses.

In some of the experiments, samples of cotton impregnated with NaCl or Na_2CO_3 and viscose rayon impregnated with Na_2CO_3 were used. The cellulose was impregnated with the salt in the following manner: A weighted amount of cellulose was placed in the container in which it was to be pyrolyzed. A weighed amount of salt was added to the same container. A small amount of water was then added and the water evaporated in an oven at about 80° C. Drying of the sample and additive was then completed in a vacuum in the same manner as for the nonimpregnated samples. All calculations of losses, yields, residues, etc., were made on the basis of dry celluloses.

3. Pyrolysis

3.1. Apparatus and Experimental Procedure

In order to obtain a detailed analysis of the volatile products of pyrolysis, these were separated into fractions. The following volatile and nonvolatile fractions were collected:

1. Residue.
2. Fraction V_{pyr}, volatile at the temperature of pyrolysis, but not at 25° C.
3. Fraction V_{25}, volatile at 25° C, but not at −80° C.
4. Fraction V_{-80}, volatile at −80° C, but not at −190° C.
5. Fraction V_{-190}, volatile at −190° C.[5]

[5] In previous work [5] on pyrolysis of polymers, fractions V_{pyr}, V_{25}, V_{-80}, and V_{-190} were designated as fractions II, IIIB, IIIA, and IV, respectively.

The pyrolysis apparatus is the same as that used in the thermal degradation of polytetrafluoroethylene [6], and is shown diagrammatically in figure 1.

In figure 1, A is a quartz tube, closed at one end and fitted into a larger quartz tube, B, also closed at one end. Tube B is attached to the vacuum system by means of a ground joint, C. A vacuum of about 10^{-3} mm of mercury could be obtained by means of a rotary oil pump, not shown in the figure, a liquid nitrogen-cooled trap, P, and a mercury-diffusion pump E. A cylindrical electric heater, not shown in the figure, could be moved in a fixed horizontal position so that tube A fitted approximately in the center of the heater muffle. The temperature was measured by means of a platinum versus platinum-10 percent rhodium thermocouple fixed permanently in the muffle of the heater, so that when the heater was moved in position for pyrolysis, the thermocouple came in contact with tube B approximately at a point where the sample was located in tube A near its closed end. The heater was so constructed that an essentially uniform temperature could be maintained over the entire specimen. The temperature could be maintained within ±0.5 deg C at pyrolysis temperatures.

After the cellulose specimen was placed in tube A and the tube inserted into tube B, the apparatus was evacuated overnight. When the heater, which had been kept at the desired temperature, but away from the apparatus overnight, was moved into position, tube A reached the desired temperature within a few minutes.

During pyrolysis the apparatus was cut off from the evacuation pump by means of stopcock D, while the mercury diffusion pump E remained in operation. The combined volatile fractions V_{25}, V_{-80}, and V_{-190} were confined between D and E. The mercury pump was rated to hold 25-mm back pressure, with a high vacuum on the inlet side; it was actually operated at a back pressure of not over

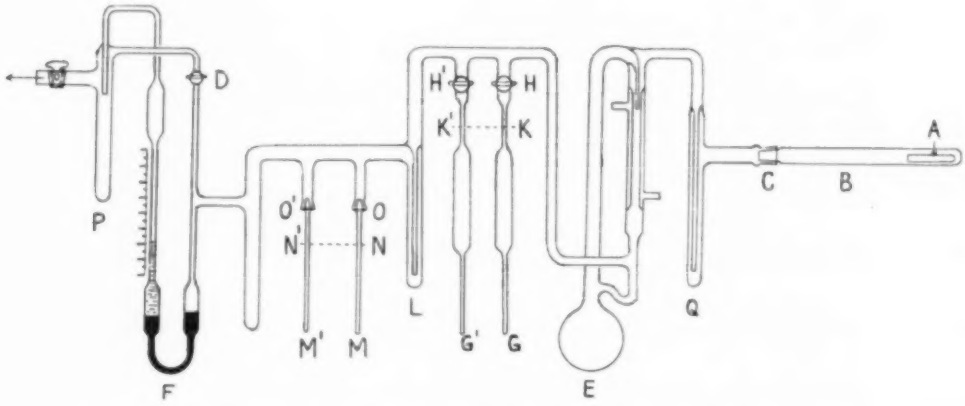

FIGURE 1. *Apparatus for the study of thermal degradation of cellulosic materials.*

A, Small quartz tube in which the sample is placed; B, large quartz tube; E, mercury diffusion pump; F, multiplying manometer; G, G′, tubes for collecting fraction V_{-190}; L, trap; M, M′, tubes for collecting fractions V_{25} and V_{-80}; P, liquid nitrogen-cooled trap.

6 mm. The pressure was measured in the calibrated space between this mercury pump and stopcock D by means of a multiplying manometer, F, containing a low-vapor-pressure silicone oil in the left arm of the manometer, above a mercury column.

A sample of the gaseous fraction V_{-190}, noncondensable at the temperature of liquid nitrogen, was collected for analysis at the end of an experiment in the following manner. Liquid nitrogen was placed around trap L. The condensable material, consisting of combined fractions V_{-80} and V_{25}, was drawn into L, and a sample of the remaining gaseous fraction V_{-190} was then taken for analysis in 60-ml tube G or G′ by sealing off the tube at K or K′. The weight of fraction V_{-190} was calculated from its volume, pressure, and composition.

After evacuating the excess fraction V_{-190}, the material that condensed in trap L was separated into two fractions, V_{-80} and V_{25}, with the aid of dry ice. These fractions were collected by means of liquid nitrogen in 3-mm tubes M and M′, which were attached to the vacuum system by means of ground joints O and O′. The tubes were sealed at N and N′, weighed, and the contents analyzed in the mass spectrometer.

Fraction V_{pyr}, volatile at the temperature of pyrolysis but not at room temperature, deposited during pyrolysis as a yellowish tarry material in the quartz tube B just outside the heater. It was dissolved in methanol, transferred into a weighing bottle, the solvent evaporated, and the tarry material was then weighed.

The nonvolatile residue remaining in tube A was weighed in a weighing bottle. The total recovery weight of the products volatilized in each pyrolysis experiment was within a few tenths of a milligram of the loss in weight of the original dry sample. All weighings were made on a semimicro balance.

3.2. Results of Pyrolysis

Results of pyrolysis experiments are shown in table 1. Experiments 2a to 2g, inclusive, were carried out in consecutive steps on the same specimen

TABLE 1. *Pyrolysis of cellulose in a vacuum*

Experiment	Temperature	Weight of sample	Duration		Volatilization		Volatile fractions, of total volatilized part, for step			
			For step	Cumulative	For step	Cumulative	V_{pyr} (Tar)	V_{25} (H_2O)	V_{-80} (CO_2)	V_{-190} (CO)
COTTON										
	°C	mg	min	min	%	%	%	%	%	%
1	250	49.1	300	300	2.7	2.7	26.3	53.9	12.0	7.8
2a	280	83.3	38	38	3.3	3.3	33.9	50.7	10.5	4.9
2b	280	83.3	58	96	7.0	10.3	55.9	36.1	6.0	2.0
2c	280	83.3	53	149	9.1	19.4	63.8	29.6	5.4	1.2
2d	280	83.3	100	249	15.9	35.3	----	----	----	----
2e	280	83.3	77	326	9.8	45.1	70.2	23.6	4.7	1.5
2f	280	83.3	180	506	16.7	61.8	----	----	----	----
2g	280	83.3	155	661	7.8	69.6	70.8	21.9	5.5	1.8
3	321	39.5	9	9	22.0	22.0	65.2	28.2	4.3	2.3
4	397	13.8	159	159	91.4	91.4	69.6	22.5	6.2	1.7
HYDROCELLULOSE										
5a	280	80.0	35	35	4.3	4.3	40.6	49.7	6.7	3.0
5b	280	80.0	86	121	8.1	12.4	59.0	32.3	6.9	1.8
5c	280	80.0	72	193	9.3	21.7	62.4	31.5	4.7	1.4
5d	280	80.0	130	323	17.3	39.0	----	----	----	----
5e	280	80.0	120	443	13.1	52.1	73.7	20.9	4.0	1.4
5f	280	80.0	185	628	13.5	65.6	76.7	18.0	3.7	1.6
VISCOSE RAYON										
6a	280	85.6	7	7	3.3	3.3	19.6	61.7	11.7	7.0
6b	280	85.6	19	26	3.7	7.0	24.4	59.1	10.5	6.0
6c	280	85.6	22	48	5.3	12.3	39.5	48.4	8.7	3.4
6d	280	85.6	24	72	6.2	18.5	51.8	37.9	7.8	2.5
6e	280	85.6	65	137	16.3	34.8	----	----	----	----
6f	280	85.6	32	169	6.2	41.0	52.6	37.1	8.1	2.2
7	295	12.5	57	57	45.3	45.3	48.2	40.8	7.8	3.2
COTTON IMPREGNATED WITH Na_2CO_3 (7%)										
8a	251	10.0	180	180	36.8	36.8	6.1	61.0	19.6	13.3
8b	291	10.0	30	[a] 210	14.6	51.4	15.3	54.6	22.7	7.4
COTTON IMPREGNATED WITH NaCl (8%)										
9	280	7.1	120	120	49.3	49.3	12.2	59.3	14.9	13.6

[a] Cotton impregnated with Na_2CO_3 degraded initially so fast that it was not convenient to start experiment at 291° C. Instead, the sample was first heated for 180 min at 251°, with a resulting loss of 36.8%; the residue was then heated for another 30 min at 291°, with a further loss of 14.6%. Total loss in weight was 51.4%.

of cotton. Similarly, experiments 5a to 5f, inclusive, were carried out on the same specimen of hydrocellulose, and experiments 6a to 6f on the same specimen of viscose rayon. These three series of experiments were carried out at 280° C. A sample of cotton impregnated with Na_2CO_3 (7%) [6] was pyrolyzed in two consecutive steps, at 251° and 291° C. A sample of cotton impregnated with NaCl (8%) was pyrolyzed in one step at 280° C. Fractions V_{25}, on mass-spectrometer analysis, were found to consist mainly of water mixed with a small amount of acetaldehyde, as is shown later. Fractions V_{-80} and V_{-190}, also on mass-spectrometer analysis, were found to consist of CO_2 and CO, respectively. According to table 1, cotton and hydrocellulose behaved similarly on pyrolysis, whereas viscose rayon yielded more H_2O, CO_2, and CO, and less tar, than the first two cellulosic materials. The addition of NaCl or Na_2CO_3 had the effect of increasing the yields of H_2O, CO_2, and CO, and decreasing the yield of tar.

In table 2 cumulative yields of fractions are shown for 280° C (except in the case of purified cotton impregnated with Na_2CO_3, where the initial rate of degradation was so fast that the first 37% volatilization was carried out at 251° C and an additional 14% at 291° C). The data shown in table 2 were calculated on the basis of the data in table 1, interpolating where necessary.

The temperature effect on yields of the various fractions is shown in table 3, where a comparison is made of results obtained at different temperatures, but for about the same extent of degradation. According to this table the temperature effect through a range of about 250° to 321° C is not pronounced.

[6] The weight of the Na_2CO_3 was 7 percent of that of the dry cotton.

TABLE 2. *Volatile fractions obtained in the pyrolysis of cellulose*

Sample	Temperature	Time	Volatilization	Cumulative volatiles in the fractions [a]			
				V_{pyr} (tar)	V_{25} (H_2O)	V_{-80} (CO_2)	V_{-190} (CO)
	°C	*min*	%	%	%	%	%
Cotton	280	661	70	65	27	6	2
Hydrocellulose	280	628	66	66	27	5	2
Viscose rayon	280	169	41	45	43	9	3
Cotton impregnated with Na_2CO_3 (7%) [b]	251	180	37	9	59	21	11
	291	30	14				
Cotton impregnated with NaCl (8%)	280	120	49	12	59	15	14

[a] In percentage of total volatiles.
[b] See footnote, table 1.

TABLE 3. *Effect of temperature on yield of fractions in the pyrolysis of cellulose*

Material	Experiment	Temperature	Volatilization, cumulative	Volatile fractions of total volatilized part			
				V_{pyr} (tar)	V_{25} (H_2O)	V_{-80} (CO_2)	V_{-190} (CO)
		°C	%	%	%	%	%
Cotton	1	250	2.7	26	54	12	8
	2a	280	3.3	34	51	10	5
	2a to 2e	280	19.4	64	30	5	1
	3	321	22.0	65	28	4	3
Viscose rayon	6a to 6f	280	41.0	53	37	8	2
	7	295	45.3	48	41	8	3

4. Analysis of Fractions

4.1. Mass Spectrometer Analysis

Mass-spectrometer analysis of fractions V_{-190} and V_{-80} showed them to consist of CO and CO_2, respectively. Similar analysis for fraction V_{25}, as shown in table 4, indicates that water is the main constituent. The only other constituent is acetaldehyde, which appears in amounts varying from 3 to 16 percent. The reason for this variation is not apparent from the present limited data.

TABLE 4. *Mass-spectrometer analysis of fraction* V_{25}

Component	Viscose rayon [a]		Cotton impregnated with NaCl (8%)	Cotton impregnated with Na_2CO_3 [a] (7%)	
	1	2		1	2
	Mole %	*Mole %*	*Mole %*	*Mole %*	*Mole %*
Water	84	92	97	97	91
Acetaldehyde	16	8	3	3	9

[a] Analyses 1 and 2, in the case of viscose rayon, were made of fractions V_{25} from experiments 6a and 7 (table 1); in the case of cotton impregnated with Na_2CO_3 (7%), analyses 1 and 2 were made of fractions V_{25} from experiments 8a and 8b, respectively (table 1).

Analysis of fraction V_{pyr} (tar) was performed by Bradt and Mohler in a 60° Nier mass spectrometer, using a method that they have developed [7]. The sample was heated in a vacuum-tube furnace that opened directly into the ionization chamber, and the temperature was increased step by step until there was no further evaporation. Mass spectra were recorded at each step. In addition to fraction V_{pyr}, these investigators also vaporized or pyrolyzed directly into the mass spectrometer filter paper, purified cotton, viscose rayon, cellobiose, and levoglucosan. There are no background patterns of pure compounds available for mass-spectrometer analysis of these substances, and the conclusions drawn on the basis of the mass spectra obtained must therefore be considered as tentative.[7]

Filter paper, cotton, and viscose rayon gave similar mass spectra. When heated above 100° C there was some evolution of H_2O, CO_2, and CO. At 240° and higher, a rather complicated mass spectrum extending to mass 144 appeared. Cellobiose appeared to degrade at 250° C, and the

[7] The authors are indebted to P. Bradt and F. L. Mohler of the Mass Spectrometry Section of the Bureau for performing these analyses and for interpreting the results.

spectrum showed small peaks, indicating masses heavier than 144. Its spectrum was much like those of the cellulosic materials.

Levoglucosan evaporated in a narrow temperature range at about 130° C. Its mass spectrum showed peaks corresponding to H_2O, CO_2, and CO. These peaks were rather small as compared with those that were obtained for the celluloses.

The mass spectra obtained for fraction V_{pyr} (tar) from cotton and viscose rayon were similar. At an evaporation temperature of about 130° C, these spectra were almost identical with that from levoglucosan. However, there was in the tar a compound that was less volatile than levoglucosan and that degraded at higher temperatures to give a spectrum more like the product obtained from direct pyrolysis of cellulose into the mass spectrometer. It may be significant that all the spectra, whether from cellulose, levoglucosan, or tar, contained peaks for masses 126 and 144. These masses correspond to that of levoglucosan or of the cellulose structural unit, molecular weight 162, with 2 and 1 molecules of water, respectively, split off.

4.2. Infrared Analysis of Fraction V_{pyr}

Samples of pure levoglucosan and of fraction V_{pyr} (tar) from cotton were dissolved in methanol. Thin films were deposited on rock salt by evaporating the solvent, and infrared absorption spectra of the resulting films were obtained. As shown in figure 2,[8] the only significant difference between the two spectra is the presence of an absorption band at 5.78 microns in the spectrum of fraction V_{pyr} (tar). This suggests that fraction V_{pyr} contained both levoglucosan and a compound that contains C=O groups.

[8] The authors are indebted to Florence H. Forziati and Robert M. Brownell of the Textiles Section of the Bureau, for performing these infrared absorption analyses and for interpreting the results.

4.3. Average Molecular Weight of Fraction V_{pyr}

The average molecular weight of fraction V_{pyr} (tar) from cotton was determined by a microfreezing-point lowering method from a solution in phenol. Four determinations were made on this fraction and four on pure levoglucosan as a control. The molecular freezing-point lowering for phenol is given in the literature as 7.3° C. Sufficient sample was used in each determination to give a freezing-point depression of approximately 3° C. The molecular weight of levoglucosan was found to be 166 ± 2 as compared with 162 theoretical. The average molecular weight of fraction V_{pyr} was found to be 152 ± 1.

5. Rates of Degration and Activation Energies

5.1. Rate Measurements in a Spring Balance

The rates of thermal degradation of cellulosic materials were determined by means of a very sensitive tungsten spring balance enclosed in a Pyrex housing, which could be evacuated to about 10^{-5} mm Hg. This apparatus and the method have been described previously [6] in connection with a study of the thermal degradation of a number of polymers. The method, briefly, consists in heating a sample of about 4 to 6 mg in a crucible suspended from the tungsten spring, and recording at regular intervals the loss in weight of the sample due to pyrolysis and evaporation, as indicated by a change in position of a crossline on a wire extension of the spring.

In preparing for a rate experiment the crucible containing the sample was suspended from the tungsten spring into a tube projecting down from the vacuum apparatus. The apparatus was pumped to a vacuum of approximately 10^{-6} mm Hg and left standing. In the meantime an electric furnace, kept in a position away from the projected tube, was heated overnight to the temperature required for the given experiment. In the morning the furnace was

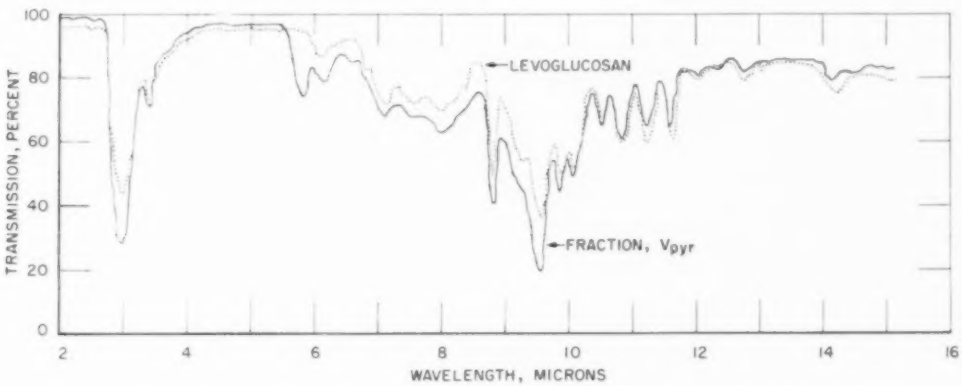

FIGURE 2. *Infrared absorption spectra of the tarry fraction V_{pyr} and of levoglucosan.*

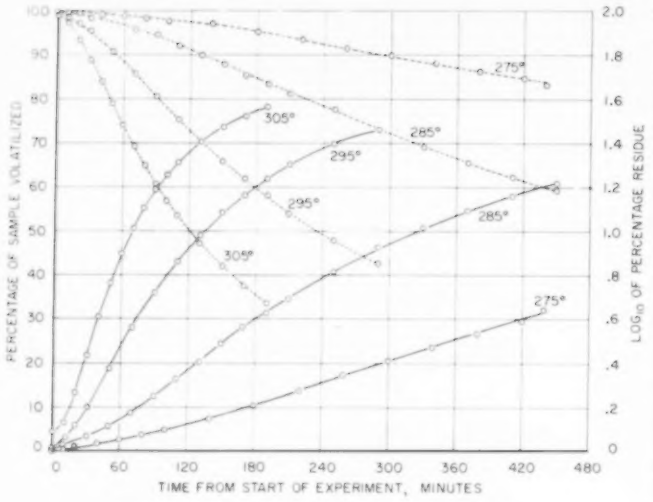

FIGURE 3. *Thermal degradation of cotton.*

———, percentage of sample volatilized versus time; ·····, $\log_{10}$ of percentage residue versus time.

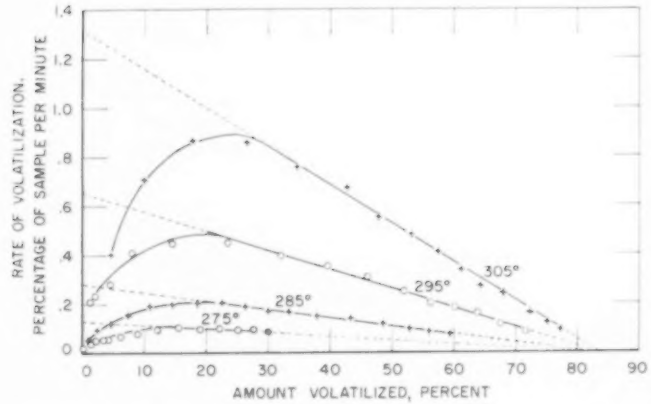

FIGURE 4. *Rates of volatilization of cotton, in percentage of sample per minute, as a function of percentage volatilization (K_1 rates).*

Dotted lines represent extrapolations of the rate curves.

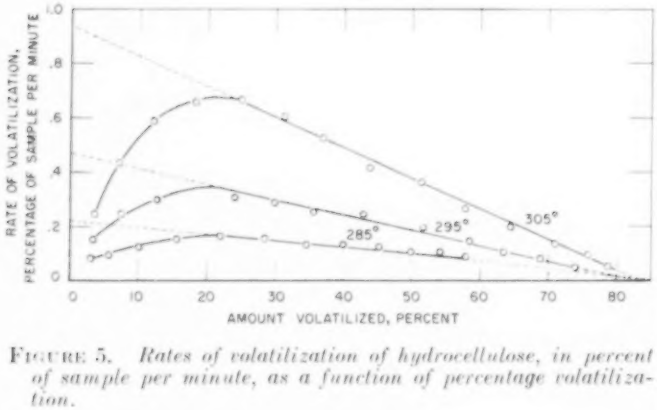

FIGURE 5. *Rates of volatilization of hydrocellulose, in percent of sample per minute, as a function of percentage volatilization.*

Dotted lines represent extrapolations of the rate curves.

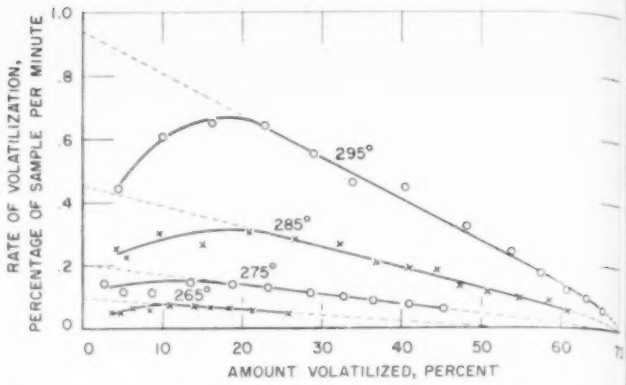

FIGURE 6. *Rates of volatilization of viscose rayon, in percent of sample per minute, as a function of percentage volatilization.*

Dotted lines represent extrapolations of the rate curves.

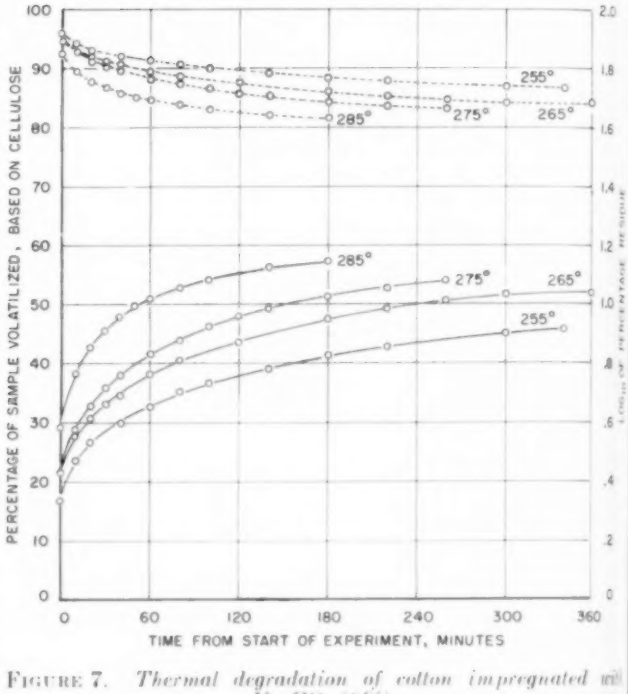

FIGURE 7. *Thermal degradation of cotton impregnated with Na_2CO_3 (9%).*

———, percentage of sample volatilized versus time; ·····, $\log_{10}$ of percentage residue versus time.

raised into position around the sample. It ordinarily took about 15 min for the crucible to reach the required temperature. Duration of the experiment was counted from the time this temperature was reached. The temperature was controlled by means of an electronic thermostat to within ±0.2 deg C.

The results of rate experiments on cotton are shown in figures 3 and 4. The rates, K_1, in percentage of the original dried cellulose per minute, are initially low and pass through maxima, beyond

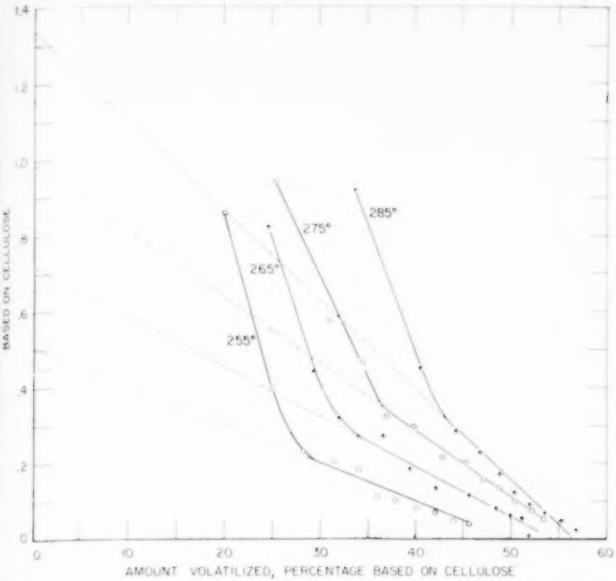

FIGURE 8. *Rates of volatilization of cotton impregnated with* Na_2CO_3 *(9%), in percentage of cellulosic residue per minute, as a function of percentage volatilization* (K_2 *rates).*

Dotted lines represent extrapolations of the rate curves.

which they follow straight lines. The points at which extrapolations of these lines intersect with the abscissas are defined as carbonization end points expressed in percentage of volatilization. The char yield, in percent of sample, for any particular temperature can be obtained by subtracting the carbonization end point from 100. By extrapolating the straight parts of the K_1 rate curves to the ordinate, the apparent initial rates were obtained. The importance of these apparent initial rates lies in the fact that the samples have the same composition only at zero degradation, and these rates can thus be used for the purpose of comparison or for calculating activation energies.

The curves obtained by plotting percentage of sample volatilized and logarithm of percentage residue against time for hydrocellulose and viscose rayon, were similar to the curves obtained for cotton, figure 2, and are not shown here. The K_1 rate of volatilization curves for hydrocellulose and viscose rayon are shown in figures 5 and 6, respectively. The apparent initial K_1 rates and the carbonization end points for hydrocellulose and viscose rayon were obtained by extrapolation, as in the case of cotton.

Results of rate experiments on cotton impregnated with Na_2CO_3 (9 %) are shown in figures 7 and 8. The thermal stability of the cotton was greatly reduced as a result of the admixture with sodium carbonate. This reduction in stability was particularly great for the initial stages of the degradation. In the 15-min interval during which the cotton was raised from room temperature to the desired temperature, about 18 to 30 percent of the cotton volatilized, depending upon the final temperature.

The rate curves for Na_2CO_3-impregnated cotton are shown in figure 8. In this case the rates were expressed in percentages of residues existing at the instant (excluding Na_2CO_3) instead of percentages of the original samples and are designated as K_2 rates. This was done for the reason that the K_2 plots are straight lines beyond 30 to 40 percent volatilization, while the K_1 plots are curved through their whole extent. Extrapolated initial rates are the same whether they are obtained from K_1 or K_2 rate curves.

The plots showing percentage volatilization versus time and logarithm of percentage residue versus time for viscose rayon impregnated with Na_2CO_3 (9%) and cotton impregnated with NaCl (9%) are not shown here. These plots were similar to the corresponding plots for cotton impregnated with Na_2CO_3 (9%), shown in figure 7. The K_2 rate curves for viscose rayon impregnated with Na_2CO_3 and cotton impregnated with NaCl are shown in figures 9 and 10, respectively. The straight parts of the K_2 plots in figures 9 and 10 were extrapolated to obtain the apparent initial rates and the carbonization end points. In all cases, the plots of logarithm of residue versus percentage volatilization (shown in figs. 3 and 7 as dotted lines), were not straight lines, indicating that the over-all degradation reaction is not of first order.

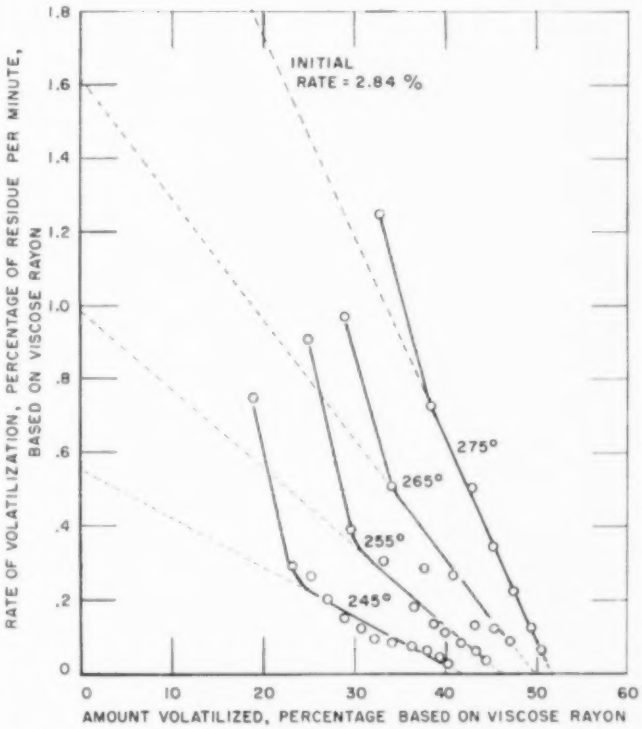

FIGURE 9. *Rates of volatilization of viscose rayon impregnated with* Na_2CO_3 *(9%), in percentage of cellulosic residue per minute, as a function of percentage volatilization.*

Dotted lines represent extrapolations of the rate curves.

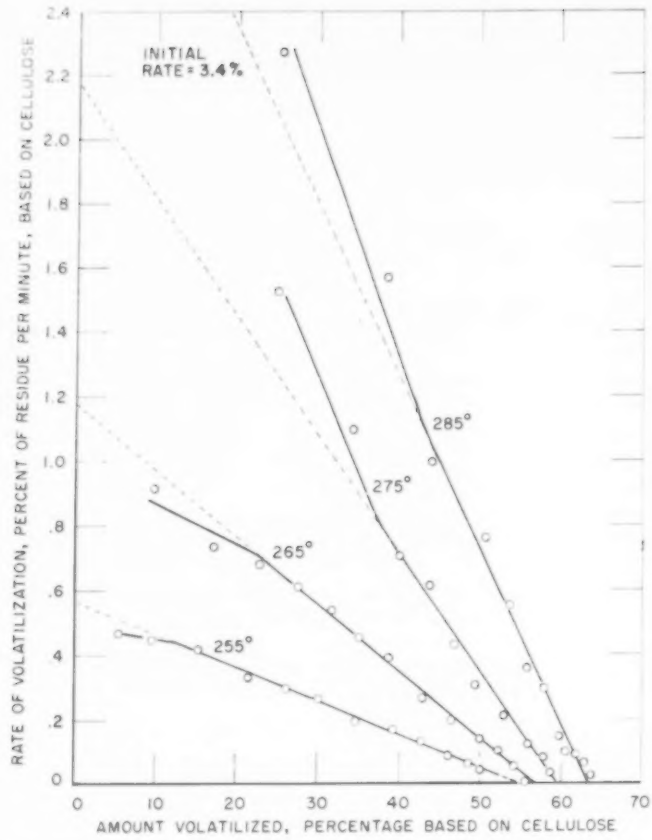

FIGURE 10. *Rates of volatilization of cotton impregnated with NaCl (9%), in percentage of cellulosic residue per minute, as a function of percentage volatilization.*

Dotted lines represent extrapolations of the rate curves.

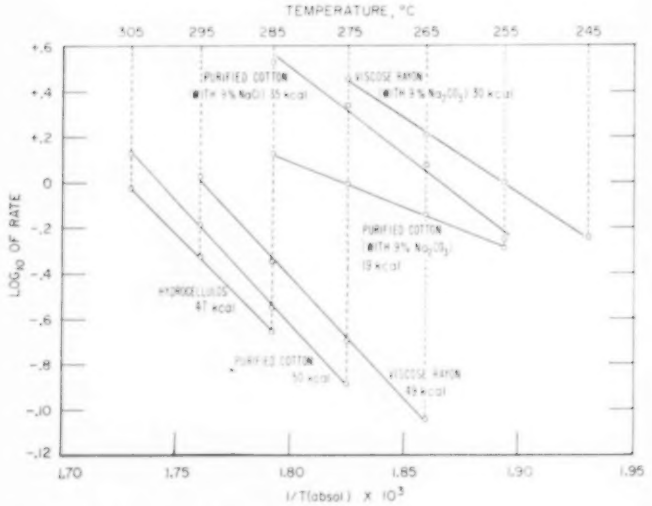

FIGURE 11. *Activation energy of thermal degradation of cellulosic materials, based on extrapolated initial rates.*

TABLE 5. *Rates of thermal degradation of cellulose samples*

Temperature	Heating duration	Loss of weight *	Apparent initial rate	Carbonization end point	Activation energy
		COTTON			
°C	min	%	%/min	%	kcal/mole
275	440	32	0.13	79	50
285	450	61	.28	81	
295	290	73	.65	82	
305	190	78	1.34	83	
		HYDROCELLULOSE			
285	460	60	0.22	82	47
295	460	76	.47	82	
305	290	80	.94	83	
		VISCOSE RAYON			
265	460	27	0.09	51	49
275	440	46	.20	64	
285	360	62	.45	69	
295	240	67	.94	71	
		COTTON IMPREGNATED WITH Na_2CO_3 (9%)			
255	340	46	0.51	49	19
265	360	52	.72	54	
275	260	54	.98	56	
285	180	57	1.34	57	
		VISCOSE RAYON IMPREGNATED WITH Na_2CO_3 (9%)			
245	300	41	0.55	42	30
255	220	45	.99	46	
265	140	48	1.61	50	
275	120	51	2.84	52	
		COTTON IMPREGNATED WITH NaCl (9%)			
255	420	51	0.56	55	35
265	340	56	1.18	57	
275	240	59	2.18	60	
285	240	64	3.40	64	

* Referred to dry cellulose.

Pertinent data on all the rate experiments by the loss-of-weight method in the tungsten-spring apparatus, are shown in table 5. The activation energies are shown in the last column of this table. These activation energies were obtained graphically, as shown in figure 11, by plotting the $\log_{10}$ of the apparent initial rate at any given temperature versus $1/T \times 10^3$, where T is the absolute temperature. The over-all activation energy, E, in kilocalories per mole, is the slope of the straight line, obtained from the formula

$$E = -\frac{d \log K}{d(1/T)} \times 4.57 \times 10^{-3}.$$

A comparison of initial rates for all the materials investigated is given in table 6 for 275° and 285° C, the two temperatures at which the most complete data were obtained. Table 7 gives a condensed summary of data showing the effect of additions of Na_2CO_3 and NaCl on the yield of flammable and nonflammable fractions in the pyrolysis of cellulosic materials in a vacuum.

TABLE 6. *Comparison of rates of thermal degradation of cellulose samples at 275° and 285° C*

Sample	Initial rates, in percent of sample per min, at—	
	275°	285°
Cotton	0.13	0.28
Hydrocellulose	[a].10	.22
Viscose rayon	.20	.45
Cotton impregnated with Na_2CO_3 (9%)	.98	1.34
Viscose rayon impregnated with Na_2CO_3 (9%)	2.84	[a]5.48
Cotton impregnated with NaCl (9%)	2.18	3.40

[a] Calculated on the basis of activation energy.

TABLE 7. *Flammable and nonflammable volatile products and char obtained in the vacuum pyrolysis of cellulose materials (temperature of pyrolysis, 280° C)*

Material	Flammable			Nonflammable			Char[a]
	Tar	CO	Total	H_2O	CO_2	Total	
	%	%	%	%	%	%	%
Cotton	52	2	54	21	5	26	20
Hydrocellulose	53	2	55	21	4	25	20
Viscose rayon	30	2	32	29	6	35	33
Cotton impregnated with Na_2CO_3[b]	5	6	11	33	12	45	44
Cotton impregnated with NaCl	7	9	16	37	9	46	38

[a] Since the carbonization end points were not determined experimentally at 280° C, the char values for this temperature were estimated from figures 4, 5, 6, 8, and 10.

[b] Residue from pyrolysis for 180 min at 251° was pyrolyzed further for 30 min at 291°. Volatilization in the second step was from 36.8% (volatilized in the first step) to 51.4%, i. e., 14.6% (see table 1).

5.2. Rates Calculated from Pyrolysis Data

The data obtained in the step pyrolysis experiments at 280° C, shown in table 1, for cotton, hydrocellulose, and viscose rayon, were used in calculating the rates of volatilization in terms of averages for each individual step. Because in the pyrolysis experiments the degradation products were collected, weighed, and analyzed, it was possible to calculate rates of volatilization for each fraction, as well as for the total volatiles. These rates are shown plotted against percentage volatilization at 280° C in figures 12, 13, 14, and 15, for fractions V_{pyr}, V_{25}, V_{-80}, and

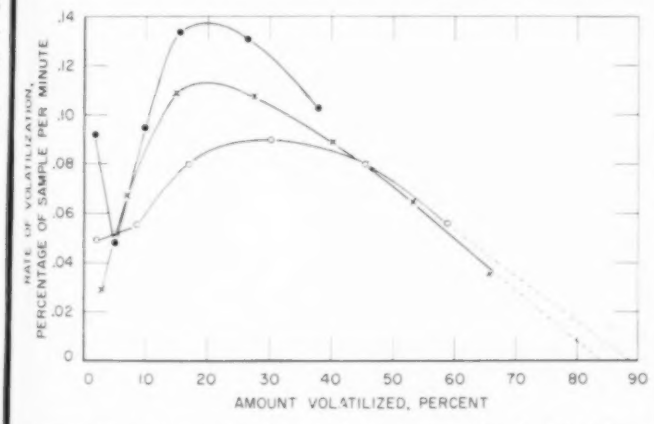

FIGURE 12. *Rates of volatilization at 280° C calculated from pyrolysis data.*

Rates of volatilization of the tarry fraction V_{pyr}, in percent of sample per minute, as a function of percentage volatilization for: ●, viscose rayon; ×, cotton; and ○, hydrocellulose.

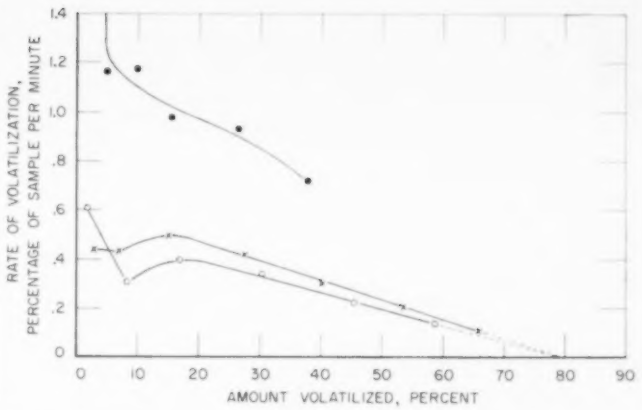

FIGURE 13. *Rates of volatilization at 280° C calculated from pyrolysis data.*

Rates of volatilization of fraction V_{25}, in percentage of sample per minute, as a function of percentage volatilization, for: ●, viscose rayon; ×, cotton; and ○, hydrocellulose.

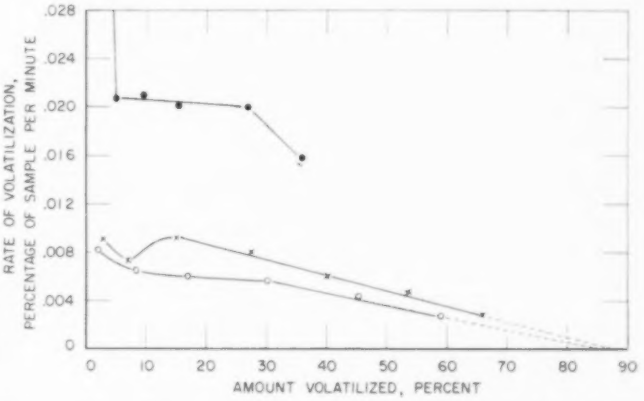

FIGURE 14. *Rates of volatilization at 280° C calculated from pyrolysis data.*

Rates of volatilization of fraction V_{-80}, in percentage of sample per minute, as a function of percentage volatilization, for: ●, viscose rayon; ×, cotton; and ○, hydrocellulose.

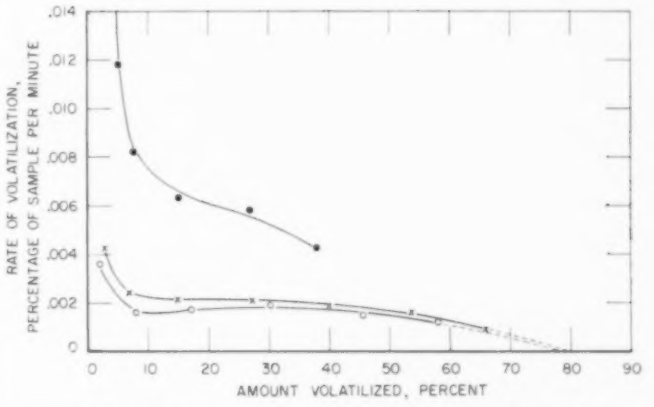

FIGURE 15. *Rates of volatilization at 280° C, calculated from pyrolysis data.*

Rates of volatilization of fraction V_{-180}, in percentage of sample per minute, as a function of percentage volatilization, for: ●, viscose rayon; ×, cotton; and ○, hydrocellulose.

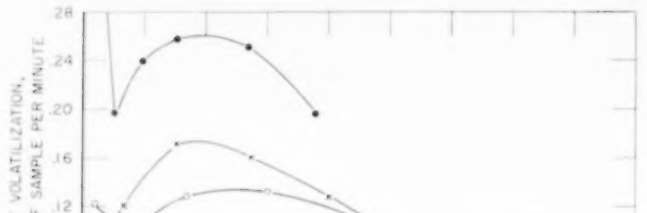

FIGURE 16. *Rates of volatilization at 280° C, calculated from pyrolysis data.*

Over-all rates of volatilization, in percentage of sample per minute, as a function of percentage volatilization, for: ●, viscose rayon; ×, cotton, and ○, hydrocellulose.

V_{-190}, respectively, and in figure 16 for the total volatiles. The rates shown in figure 16 do not differ much from the K_1 rates determined in the spring-balance apparatus and shown in figures 4, 5, and 6. Extrapolation of the rate curves for cotton and hydrocellulose in figures 12, 13, 14, 15, and 16 leads to similar carbonization end points as were found in the spring-balance rate experiments. In the case of viscose rayon, where pyrolysis at 280° C was carried only to 41 percent volatilization, the carbonization end point is not shown.

6. Discussion

Although the cotton used in this work had a lower crystallinity and higher degree of polymerization than the hydrocellulose, there is little difference in their behavior on pyrolysis, whether in regard to ratio of products or to rates of degradation. The crystalline forces seem to weaken at the pyrolysis temperature, and, therefore, have little effect on the results of pyrolysis. As to the effect of chain length, it was shown previously [8] in the case of a number of polymers that long chains break up on heating during the initial stage of thermal degradation, even before volatilization occurs. This tends to eliminate the effect of chain length on pyrolysis, except where polymers of very low degree of polymerization are involved. Viscose rayon has low crystallinity and low degree of polymerization, and the type of its crystalline structure is different from that of cotton and hydrocellulose. Results of pyrolysis of viscose rayon indicate a lower yield of tar, a higher yield of H_2O, CO_2, and CO, and a faster rate of degradation than is the case with cotton and hydrocellulose. Further work will be required to determine the causes of the differences observed.

The presence of Na_2CO_3 or NaCl in intimate contact with the cellulose has a profound effect on the results of pyrolysis of cellulose. The tar yield is drastically reduced whereas the yield of H_2O, CO_2, and CO is increased. Although the actual initial rates in the case of pure substances are low, rising to a maximum at about 15 to 20 percent volatilization, these rates in the presence of Na_2CO_3 and NaCl start extremely fast and do not show any maxima. The apparent initial rates are also much higher in the presence of the salts than is the case with the untreated substances.

As shown in table 7, the char yield is about the same for cotton and hydrocellulose. In the presence of salts, the char yield is about doubled. In the case of viscose rayon the char yield is about 1.5 times as much as in cotton or hydrocellulose.

In the pyrolysis of untreated celluloses, up to about 20 percent volatilization, the yield of tar rises gradually, whereas the reverse is true of the yields of H_2O, CO_2, and CO. Beyond about 20 percent volatilization the yields are stabilized and reach constant values. The data are insufficient to show whether the same is true with regard to the salt-impregnated celluloses.

Mass-spectrometer, infrared, and cryoscopic analysis of fraction V_{pyr}, all point to the conclusion that this fraction consists mainly of levoglucosan. However, there are definite indications that there is present in fraction V_{pyr}, in addition to levoglucosan, some small amount of other compound or compounds. These indications are: (1) a small part of fraction V_{pyr} is insoluble in H_2O, although all of it is soluble in methanol; (2) the infrared absorption spectrum of fraction V_{pyr} differs from that of levoglucosan in having an absorption band at 5.78 μ; (3) there are some differences in the mass spectra of fraction V_{pyr} and levoglucosan.

As shown in table 7, the yield of fraction V_{pyr} (tar) is 52 percent and 53 percent for cotton and hydrocellulose, respectively. This means that approximately 1 out of every 2 structural units in these celluloses vaporizes as a levoglucosan molecule. In viscose rayon, which yields 30 percent tar, approximately 1 out of every 3 structural units appears in the distillate as levoglucosan. The next largest volatile fraction is H_2O, which amounts to 21 percent for cotton and hydrocellulose, and 29 percent for viscose rayon. After discounting the hydrogen and oxygen that vaporize from cellulose as parts of levoglucosan, the highest possible theoretical yield of H_2O from the other cellulose structural units would be 27 percent from cotton and hydrocellulose and 37 percent from viscose rayon. The difference between the theoretical and actual yield of H_2O in the pyrolysis of the celluloses is accounted for by the formation of CO_2 and CO, and by the presence of H and O in the char. That the chars obtained at the carbonization end points at 280° C (20% for cotton or cellulose and 33% for viscose rayon, as given in table 7) contained volatile material was shown by experiments in which these chars were

heated in a quartz tube in a vacuum by means of a Meker burner to about 1,000° C. The loss in weight of the chars was roughly one-half for all the three celluloses.

The results of pyrolysis suggest the following possible mechanism for the thermal degradation of cellulose in a vacuum. A dehydration process takes place randomly along the chain. Another process, which takes place simultaneously, consists in thermal scissions of the polymer chain resulting in the formation of levoglucosan, H_2O, CO_2, and CO. The C—O bonds in the chain are less stable thermally than the C—C bonds. This was shown by the present authors in a series of experiments on the pyrolysis of polyethylene, and polyethylene oxide. The polyethylene oxide was found to have a lower thermal stability and a lower activation energy of thermal degradation than polyethylene. The various C—O bonds in the chain are indicated in the structural formula (1) of the polymer as k, l, m, and n.

Random scissions of bonds k, l, or n result in a more or less complete breakdown of a part of the chain, yielding H_2O, CO_2, CO, and C. A random scission of the C—O m bond may result in the formation of an oxygen linkage between carbons 1 and 6 by a process analogous to the formation of levoglucosan from phenyl-β-D-glucoside. McCloskey and Coleman [9] have shown in formula (2) that this reaction takes place in two steps.

Whether in the pyrolysis of cellulose this process takes place in one step [10], formula (3), or in two steps, is problematical. Pyrolysis is unlike hydrolysis in an aqueous alkaline medium and a close analogy between the two reactions is not justified. The formation of levoglucosan units in cellulose pyrolysis takes place when scission of the C—O m bonds occur one structural unit away from the ends formed through a random scission of a C—O m bond.

The presence of Na_2CO_3 and NaCl may have a catalytic effect on the dehydration and bond scissions taking place inside and outside the rings in the cellulose chain, resulting in increased yield of H_2O CO_2, and CO at the expense of levoglucosan, and also in an increased rate of degradation of the celluloses, particularly in the initial stages.

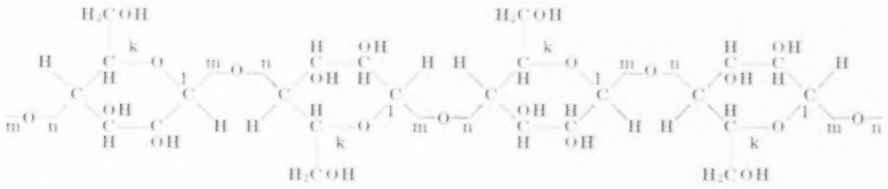

(1)

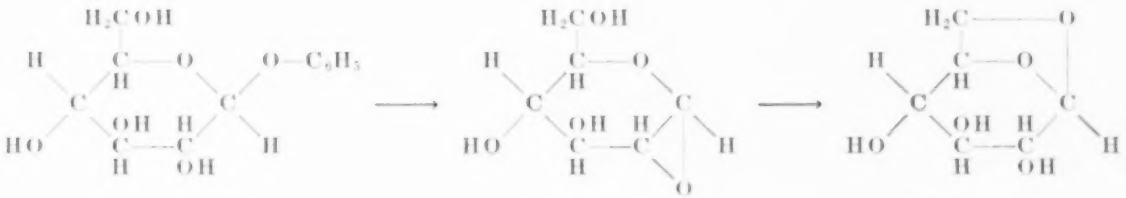

Phenyl-β-D-glucoside — 1,2-Anhydro sugar — Levoglucosan

(2)

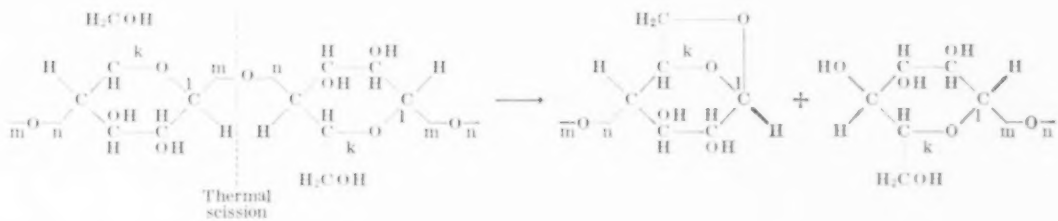

(3)

7. References

[1] J. Sarasin, Archiv. Sci. Phys. Nat. **IV,** 465 (1918).
[2] A. Pictet and J. Sarasin, Helv. Chim. Acta **1,** 87–96 (1918).
[3] H. J. P. Venn, J. Textile Inst. **15,** T414–T418 (1924).
[4] K. Tamaru, Bul. Chem. Soc. Japan **24,** 164–8 (1951).
[5] S. L. Madorsky, V. E. Hart, S. Straus, and V. A. Sedlak, J. Research NBS **51,** 327 (1953) RP2461.
[6] S. L. Madorsky, J. Polymer Sci. **9,** 133 (1952); **11,** 491 (1953).
[7] P. Bradt and F. L. Mohler, J. Research NBS **55,** 323 (1955) RP2637.
[8] S. L. Madorsky and S. Straus, J. Research NBS **53,** 361 (1954) RP2553.
[9] C. M. McCluskey and G. H. Coleman, J. Org. Chem. **10,** 184 (1945).
[10] W. G. Parks, R. M. Esteve, jr., M. H. Gollis, R. Guercia, and A. Petrarca, paper presented at the 127th Meeting of the American Chemical Society, Cincinnati, Ohio, March 29 to April 7, 1955.

Washington, March 12, 1956.

Journal of Research of the National Bureau of Standards Vol. 56, No. 6, June 1956 Research Paper 2686

Response Function of Thallium-Activated Sodium-Iodide Scintillation Counters*

Martin J. Berger and J. Doggett

Measurements of gamma rays with NaI(Tl) crystals yield pulse height distributions related to the true energy spectrum by an integral equation whose kernel (response function) is the probability that an incident photon of energy E will give rise to a pulse of size E'. The response function has been calculated by the Monte Carlo method for photons with energies from 0.279 to 4.45 Mev. Results are presented for cylindrical crystals ranging in size from 0.25 (radius) by 0.5 inch (length) to 2.5 by 9 inches. They are based on the analysis of 50,000 photon histories sampled with the use of the Standards Electronic Automatic Computer (SEAC). Analytical corrections were made for the escape of annihilation radiation and bremsstrahlung from the crystal.

1. Introduction

The response function of a NaI(Tl) crystal spectrometer relates the observed pulse height distribution to the true gamma-ray spectrum. The primary means of determining this function is, and presumably will remain, experimental. But a good theoretical understanding will contribute toward improving scintillation spectrometry.

While the theory of the diffusion of gamma radiation in an infinite medium is now well developed, the calculation of the response function is a boundary problem whose exact solution is beyond the scope of theory in its present state.

The subject of this article is a Monte Carlo calculation of the response function, i. e., an experiment carried out on paper. While this falls short of an analytical theory, it is relatively simple to do, and has important advantages compared to a physical experiment. One is not hampered by the limited availability of monoenergetic sources nor by accidental disturbing effects such as background radiation.

Exploratory Monte Carlo calculations of the response function have already been made by Campbell and Boyle [1] for energies $E \geq 6$ Mev, and by Foote and Koch [2] for $E \geq 4.45$ Mev. An approximate analytical calculation for $E \leq 1.3$ Mev was carried out by Maeder, Müller, and Wintersteiger.[3] These authors computed the effect of the first interaction of the incident photon in the crystal exactly and made an elaborate estimate of the effect of multiple interactions. This approximation limits the validity of their considerations to small crystals not much larger than one mean free path of the incident radiation.[4] They confined their attention mostly to cylindrical crystals whose radius equals their length. In view of the complexity of their "orders of scattering" calculation and of the approximations whose consequences cannot be easily surveyed, a direct recalculation of their results seemed of value. Moreover, one would also like to know more about the influence of the crystal shape on the response function.

Monte Carlo calculations have been made of the response functions of cylindrical crystals of diverse shapes ranging in size from small to very large for radiation incident with energies of 0.279, 0.661, 1.17, 1.33, 2.62, and 4.45 Mev.

The absorption and Compton scattering of photons in the crystals were calculated by random sampling, the computations being carried out on the SEAC. Approximate analytical corrections were applied to the Monte Carlo results to account for the escape of secondary bremsstrahlung and annihilation radiation from the crystals.[5] These corrections were quite small at 1.17 and 1.33 Mev, but appreciable at 2.62 and 4.45 Mev. Because of the approximate nature of the corrections, the most important and accurate parts of this work are those pertaining to the four lowest energies where the corrections were negligible. Most of the results are for collimated sources, while some sample calculations pertain to broad beams, point-isotropic sources, and off-axis collimated sources.

The main results of this investigation are: (1) The confirmation and expansion of the results of Maeder et al. for small crystals; (2) the extension to large crystals in which multiple interactions are important and to higher energies; (3) last but not least, the creation of a SEAC code by means of which response functions for source and crystal geometries peculiar to a given experimental situation can be readily computed with a modicum of effort.

*This work was supported by the United States Atomic Energy Commission.

[1] J. G. Campbell and A. J. F. Boyle, Australian J. Phys. **6**, 171 (1953).

[2] R. S. Foote and H. W. Koch, Rev. Sci. Instr. **25**, 746 (1954).

[3] D. Maeder, R. Müller, and V. Wintersteiger, Helv. Phys. Acta **27**, 3 (1954).

[4] Maeder et al. also attempted a calculation for an "infinitely large" crystal, i.e., for a semi-infinite scattering medium, by considering the first two interactions exactly, and estimating the effect of subsequent interactions. As we shall show in section 4.1, this procedure was inaccurate (except at low energies) so that it does not provide a good basis for extrapolating their results from small to large crystals.

[5] One of the reasons for this approximate procedure was the temporary non-availability of SEAC during the latter part of this investigation. It would have been better to carry through the entire calculation on the automatic computer. This is particularly easy for quanta resulting from the annihilation of positrons produced in a first interaction of the primary photon. The source distributions of these photons within the crystal can easily be calculated, and their subsequent history traced by means of the existing SEAC code. We hope to change the SEAC code in the future so that it can handle the escape of all secondary radiation, and to extend the calculations above 4.45 Mev. In the meantime, there was some merit in reporting the present results for 2.62 and 4.45 Mev, since calculations in this energy range have not been reported previously.

2. Method of Calculation

2.1 Formulation of the Problem

The response function can be expressed in the form

$$R(E,E'')=\int_0^E L(E,E')\,g(E',E'')\,dE' \qquad (1)$$

where $L(E,E')dE'$ is the probability that a photon of initial energy E will deliver to the crystal—as the result of one or more interactions—an amount of energy between E' and $E'+dE'$; and $g(E',E'')dE''$ is the probability that upon delivery of energy E' to the crystal, the light output as amplified by the attached photomultiplier will indicate an apparent energy (pulse height) between E'' and $E''+dE''$.

It is an experimental fact that

$$g(E',E'')=(2\pi\alpha E')^{-1/2}\exp\{-(E'-E'')^2/2\alpha E'\}. \qquad (2)$$

The value of the parameter α depends on the physical characteristics of the crystal-photomultiplier system. We shall consider this parameter as determined experimentally, and concentrate on the calculation of the loss function $L(E,E')$.

To clarify the physical picture, it is useful to break the loss function up into a number of component parts, writing

$$L(E,E')=Y(E)\{K(E,E')+p(E)\delta(E-E')\}. \qquad (3)$$

$Y(E)$ is the efficiency, i. e., the probability that a photon incident with energy E will have at least one interaction (scattering or absorption) in the crystal. For a collimated source

$$Y(E)=1-\exp[-\mu(E)L] \qquad (4)$$

where L is the length of the crystal, and $\mu(E)$ the narrow beam linear absorption coefficient.

$K(E,E')dE'$ is the probability that an interacting photon will emerge from the crystal after one or more Compton scatterings, leaving behind an amount of energy between E' and $E'+dE'$. The function $p(E)$ represents the probability that an interacting photon will be absorbed (possibly after a number of Compton scatterings), while the delta function $\delta(E-E')$ indicates that the entire energy E is delivered to the crystal in a photon history terminating in absorption. We note the normalization

$$\int_0^E dE'\,K(E,E')+p(E)=1. \qquad (5)$$

For a wide range of conditions the shape of the loss function depends largely on the ratio of the numbers of absorbed and emergent photons, and only rather insensitively on $K(E,E')$. In a rough approximation, the shape can therefore be characterized by $p(E)$, which—following Maeder—we shall call the photofraction. In experimental terms,

$$p(E)=\frac{\text{area under the "photopeak" of the pulse height distribution}}{\text{area under the entire pulse height distribution}}. \qquad (6)$$

Knowledge of the photofraction is useful in other connections. Thus if one wants to use a crystal for counting photons in the presence of a high background, it may be desirable to count only the large pulses resulting from complete photon absorption. The required "photoefficiency" of the crystal is $Y(E)\,p(E)$. Counting of photons in the "photopeak" only is particularly useful for disentangling complex spectra containing several lines.[6]

2.2. Random Sampling

For the calculation of the loss function, a direct stochastic analog method paralleling the physical processes in all respects, has been chosen. Scintillation crystals are very efficient detectors; hence the efficiency of an analog Monte Carlo calculation is also high, and the computational cost of statistical and analytical refinements would be out of proportion to the possible gain in efficiency.

The calculation proceeds along the following lines. We start a photon at a specified position on the crystal surface with specified energy and direction. The position of the first interaction is determined as if the photon moved in an infinite scattering medium; the distance traveled to the point of interaction is distributed exponentially, the mean of the distribution being the inverse of the total linear narrow beam absorption coefficient. If the interaction occurred outside the region occupied by the crystal, the photon is recorded as having had no interaction, and another photon history is begun. If the interaction is inside, we determine by random sampling whether it is an absorption or Compton scattering, the relative probabilities for these contingencies being proportional to the respective cross sections. In case of an absorption, the photon history is terminated, and another begun. In case of a scattering, the new energy and direction of the photon after the collision are sampled from the Klein-Nishina distribution, whereupon the location of the next interaction is sampled in the same manner as before. If this interaction occurs outside the crystal, the photon is considered to have escaped, and the energy left behind in the crystal is recorded. If the interaction was inside, we proceed as before, deciding whether it was an absorption or scattering, etc. The procedure is repeated until the photon has either left the crystal, or has reached an energy

[6] W. E. Kreger, Phys. Rev. **98**, 1554 (1954); see also footnote 3.

lower than 50 kev, in which case the photon is considered as absorbed. The bias introduced by this cutoff is negligible because of the steep rise of the photoelectric absorption cross section for NaI at energies below 50 kev.

The detailed equations for carrying out the sampling procedure have been presented elsewhere, together with an account of the numerical manipulation required to adapt the various cross sections to computation on a high-speed computer.[7]

The required absorption coefficients were obtained from the tabulation of G. White.[8]

2.3. Machine Computation

In the SEAC program, the calculation was set up for the simultaneous consideration of nine crystals of different sizes. For the sake of convenience, these sizes were chosen so that the crystals formed a nested sequence, each crystal containing completely the next smaller one. When a photon in the random sampling experiment escaped from a crystal, the history was continued for all crystals of larger size. This procedure resulted in great economy of computing time.[9] Beyond that, it increases the statistical efficiency of comparisons of the response functions of crystals of different shapes.

The output of a SEAC calculation consists of the following information for each of nine crystals:

a. The efficiency $Y(E)$. This information is in a sense redundant since it can also be easily obtained by a direct analytical calculation (eq (4)). But a comparison between analytical and Monte Carlo efficiencies provides a useful check that the computer operation was error-free.

b. The spectrum (in histogram form) of the energy packets supplied to the crystal by photons which eventually escape:

$$k_n(E)=\int_{\frac{n}{32}E}^{\frac{n+1}{32}E} K(E,E')dE' \qquad (n=0,1,\ldots 31).$$

c. The photofraction $p(E)$.

It was convenient to generate and process photon histories in groups of 1,000. For photons with an initial energy of 660 kev, this took about 35 to 40 min of SEAC time; for higher energies the running time was a little longer.

2.4. Escape of Secondary Radiation

In the Monte Carlo calculations it was assumed that the entire energy released in the successive scatterings or final absorption of the incident photons remained in the crystal. Actually this is the case only at low energies. At energies above the threshold for pair production, annihilation quanta may escape from the crystal; additional energy can be lost in the form of bremsstrahlung. In the energy region of interest (up to 4.45 Mev) the effect of bremsstrahlung was found to be minor compared to that of annihilation radiation. Not only is the latter greater quantitatively, but it also affects the shape of the response function in a more distinct fashion, giving rise to two additional peaks corresponding to the complete escape of 1 or 2 annihilation quanta subsequent to the absorption of a primary photon.

The appropriate corrections were made according to the approximate procedure outlined in the appendix. The photofraction $p(E)$ was corrected both for annihilation radiation and bremsstrahlung. In order to avoid excessive computation, the detailed shape of the response function was corrected only for annihilation radiation, and an adjustment for the effects of bremsstrahlung was made by a subsequent renormalization of the function $K(E,E')$.

2.5. Gaussian Broadening of the Response Function

It follows from eq (1), (2), (3), and (4) that the response function

$$\left.\begin{aligned} R(E,E'')=&\frac{Y,E)}{\sqrt{2\pi\alpha E}}\cdot \\ &\int_0^E K(E,E')\,\frac{1}{\sqrt{E'}}\exp\{-(E''\\ &-E')^2/2\alpha E'\}\,dE' \\ &+\frac{Y(E)p(E)}{\sqrt{2\pi\alpha E}}\exp\{-(E''-E)^2/2\alpha E\} \\ =&H(E,E'')+G(E,E'') \\ &\text{(tail)}\qquad\text{(photopeak)} \end{aligned}\right\} \quad (7)$$

For numerical applications the parameter α was chosen to be 0.00146 E(Mev), corresponding to a width at half-maximum $W=0.09\sqrt{E}$. This is a typical value in close agreement with experimental data of Foote and Koch (see footnote 2).

In the evaluation of $H(E,E'')$ one must take into account that $K(E,E')$ is available only in histogram form

$$k_n=\int_{\frac{n}{32}E}^{\frac{n+1}{32}E} K(E,E')\,dE', \qquad n=0,1,\ldots 31.$$

[7] M. Berger, J. Research NBS **56**, 343 (1956) RP2640.

[8] G. White (private communication).

[9] There is another obvious way of increasing the efficiency of the computation, namely, by treating the first interaction analytically, and sampling only subsequent interactions. This procedure avoids photon histories which result in no interaction at all, and thus contribute only information on the efficiency (which in any case can be determined analytically), but not the shape of the loss function. This procedure leads to complications when one tries to consider several crystals simultaneously, and it was decided that—on balance—the possible gain in efficiency was not sufficient to compensate for the increased amount of manipulation and computing time.

It is assumed that the k_n's have been corrected if necessary, for escape of secondary radiation. We consider them to form a row matrix $k(E)=(k_0k_1 \ldots k_{31})$. We similarly replace $H(E,E'')$ by a row matrix.

$$h(E)=(h_0h_1 \ldots h_{31}), \text{ where } h_n(E)=\int_{\frac{n}{32}E}^{\frac{n+1}{32}E} H(E,E')dE'.$$

The convolution of $K(E,E')$ with a Gaussian is replaced by a matrix multiplication:

$$h=Tk, \tag{8}$$

where the matrix element T_{nm} (a kind of transition probability) is given by

$$\left.\begin{aligned} T_{nm}=\int_0^1 dt \frac{1}{\sqrt{2\pi\alpha\frac{n+t}{32}}}\cdot \\ \int_{\frac{m}{32}E}^{\frac{m+1}{32}E} dE' \exp\left\{-\left(E'-\frac{n+t}{32}E\right)^2\Big/2\alpha\left(\frac{n+t}{32}\right)E\right\}. \end{aligned}\right\} \tag{9}$$

The exact location of a pulse within an interval of size $E/32$ is not known from the Monte Carlo calculation. We assume a uniform distribution, which is the reason for the average with respect to t in (9).

3. Results

3.1. Efficiency and Photofraction for Collimated Radiation [10]

Crystals of such sizes as are either readily available commercially, or are in use in this laboratory, were selected for computation. In table 1, the crystal efficiencies are listed for collimated radiation of various energies incident along the axis of the cylindrical crystals, computed according to eq (4). The figures in parentheses indicate the values that were obtained by the Monte Carlo calculations. The agreement is excellent.

In table 2, the photofraction $p(E)$ is given. This is the corrected value taking into account the escape of secondary radiation. The amount Δp which had to be subtracted from the raw Monte Carlo result p_0 in order to make the correction is indicated in parentheses. The indicated errors are standard deviations computed as follows. The standard deviation of p_0 is

$$\sigma_0=\left[\frac{p_0(1-p_0)}{YN}\right]^{1/2} \tag{10}$$

where N is the total number of photon histories contributing to the determination of p_0. (N is also shown in tables 1 and 2.) The correction Δp was assumed to have a standard deviation $(1/10)\Delta p$. This is a nominal figure representing an "educated guess." The total standard deviation is

$$\sigma=[\sigma_0^2+(1/10\Delta p)^2]^{1/2}. \tag{11}$$

[10] Collimated radiation means a narrow pencil of radiation incident along the crystal axis.

TABLE 1. *Crystal efficiency*

The values listed without parentheses were calculated according to eq (4); those in parentheses are the corresponding Monte Carlo results obtained through the analysis of the indicated number of photon histories.

Crystal No.	1	2	3	4	5	6	7	8	9	
Radius (in.)	2.5	2.5	2.5	0.875	0.75	0.75	0.75	0.5	0.25	No. of histories N
Length (in.)	9.0	8.0	4.0	2.0	2.0	1.5	1.0	1.0	0.5	
	Efficiency $Y(E)$									
Energy E (Mev)										
0.279	1.000 (1.000)	1.000 (1.000)	0.998 (.999)	0.958 (.957)	0.958 (.957)	0.908 (.903)	0.796 (.798)	0.796 (.798)	0.548 (.546)	6,000
.661	0.998 (.998)	0.996 (.996)	.936 (.938)	.747 (.748)	.747 (.748)	.643 (.644)	.497 (.497)	.497 (.497)	.290 (.295)	10,000
1.17	.988 (.987)	.981 (.979)	.861 (.859)	.627 (.635)	.627 (.635)	.522 (.529)	.389 (.395)	.389 (.395)	.218 (.223)	5,000
1.33	.984 (.986)	.975 (.977)	.841 (.833)	.602 (.599)	.602 (.599)	.499 (.495)	.369 (.363)	.369 (.363)	.206 (.191)	5,000
2.62	.958 (.964)	.940 (.946)	.755 (.760)	.504 (.507)	.504 (.507)	.410 (.409)	.296 (.292)	.296 (.292)	.161 (.164)	6,000
4.45	.950 (.947)	.930 (.927)	.735 (.741)	.486 (.484)	.486 (.484)	.393 (.398)	.283 (.282)	.283 (.282)	.153 (.153)	5,000

TABLE 2. *Photofraction $p(E)$*

The values listed without parentheses pertain to photofractions corrected for the escape of annihilation radiation and bremsstrahlung. The corresponding figures in parentheses indicate the correction Δp that had to be subtracted from the raw Monte Carlo values $p_0(E)$. The indicated standard deviations were computed according to eq (11).

Crystal No.	1	2	3	4	5	6	7	8	9	No. of histories N
Radius (in.)	2.5	2.5	2.5	0.875	0.75	0.75	0.75	0.5	0.25	
Length (in.)	9.0	8.0	4.0	2.0	2.0	1.5	1.0	1.0	0.5	
	Photofraction $p(E)$									
Energy E (Mev)										
0.279	0.973 ±.002	0.973 ±.002	0.971 ±.002	0.915 ±.004	0.900 ±.004	0.882 ±.004	0.843 ±.005	0.814 ±.006	0.711 ±.008	6,000
.661	.887 ±.003	.884 ±.003	.821 ±.004	.542 ±.005	.508 ±.006	.481 ±.006	.442 ±.007	.377 ±.007	.243 ±.008	10,000
1.17	.778 ±.006 (.002)	.775 ±.006 (.002)	.682 ±.007 (.002)	.368 ±.008 (.003)	.343 ±.008 (.003)	.315 ±.009 (.005)	.282 ±.010 (.005)	.235 ±.010 (.005)	.140 ±.011 (.003)	5,000
1.33	.767 ±.006 (.003)	.758 ±.006 (.004)	.667 ±.007 (.005)	.351 ±.009 (.009)	.325 ±.009 (.009)	.303 ±.009 (.010)	.272 ±.010 (.013)	.224 ±.010 (.013)	.120 ±.011 (.011)	5,000
2.62	.653 ±.008 (.051)	.643 ±.009 (.056)	.531 ±.010 (.069)	.243 ±.014 (.117)	.226 ±.015 (.122)	.201 ±.016 (.128)	.175 ±.017 (.135)	.144 ±.017 (.131)	.0950 ±.018 (.130)	6,000
4.45	.621 ±.015 (.139)	.608 ±.015 (.141)	.491 ±.020 (.184)	.169 ±.033 (.319)	.157 ±.033 (.319)	.132 ±.035 (.332)	.119 ±.036 (.331)	.0826 ±.037 (.347)	.0880 ±.039 (.349)	5,000

3.2. An Empirical Formula for the Photofraction

It has already been noted by Maeder et al., that for small crystals at an energy of 0.511 Mev the photofraction is a smooth function of $\sqrt{LR}$ where L is the crystal length and R the radius. The results of table 2 show that this also holds true for large crystals and in the entire energy range from 0.279 to 4.45 Mev.

Moreover, the dependence of the photofraction on the crystal size can be accurately represented by a simple empirical formula, under conditions where the correction due to the escape of secondary radiation is absent or small (i. e., at 0.279, 0.661, and 1.17 Mev for all the crystals, and at 1.33 for all but the smallest crystal considered.)[11]

The formula is:

$$p(\sqrt{LR},E)=A(E)-B(E)e^{-C(E)\sqrt{LR}} \qquad (12)$$

where L and R are the length and radius of the crystal. With the parameters A, B, and C listed in table 3, formula (12) represents the values of $p(E)$ given in table 2 with an accuracy that is 1 to 2 percent in most cases, occasionally 3 to 4 percent, and in the worst cases 5 to 7 percent. These deviations are presumably due to the fact that $p(E)$ depends on L and R in a more complicated way than through $\sqrt{LR}$.

[11] At higher energies a simple expression of the type (12) does not appear to work well. In any case the high-energy results are not precise enough to make fitting by a formula worthwhile.

TABLE 3. *Parameters of the empirical formula, eq (12), for the photofraction*

E	A(E)	B(E)	C(E)
Mev			*cm*$^{-1}$
0.279	0.973	0.514	0.658
.661	.940	.841	.219
1.17	.980	.934	.124
1.33	.985	.942	.120

Formula (12) also predicts the correct number albedo for a semi-infinite medium. When $L\to\infty$ and $R\to\infty$

$$p(\infty,E)=A(E)=1-\text{number albedo.} \qquad (13)$$

When we extrapolate in the other direction ($L\to 0$ and $R\to 0$)

$$p(0,E)=A(E)-B(E)=\mu_{PH}/\mu \qquad (14)$$

where μ_{PH}/μ is the ratio of the photoelectric to the total attenuation coefficient. Thus, of the three parameters A, B, and C, two are fixed by (13) and (14), and only C, a quantity with the dimensions of an attenuation coefficient, is adjustable. This makes it rather remarkable that a simple formula like (12) works.

3.3. Shape of the Response Function for Collimated Radiation

The response functions for all the crystals listed in tables 1 and 2 (except No. 2) are shown in figures 1,a and 1,b for incident energies of 0.279, 0.661, 1.17, 1.33, 2.62, and 4.45 Mev. For the sake of clarity of presentation we have plotted only the response function exclusive of the photopeak, i. e., the function $H(E,E')$ as defined in eq (7). The photopeaks are indicated by arrows.

The Gaussian broadening has been calculated according to the prescription given in section 2.5. It should be mentioned that the shape of the response function is rather insensitive to the magnitude of α. The results are presented in histogram form, the range between the energy of incidence E, and zero energy being covered by 32 intervals of equal size.

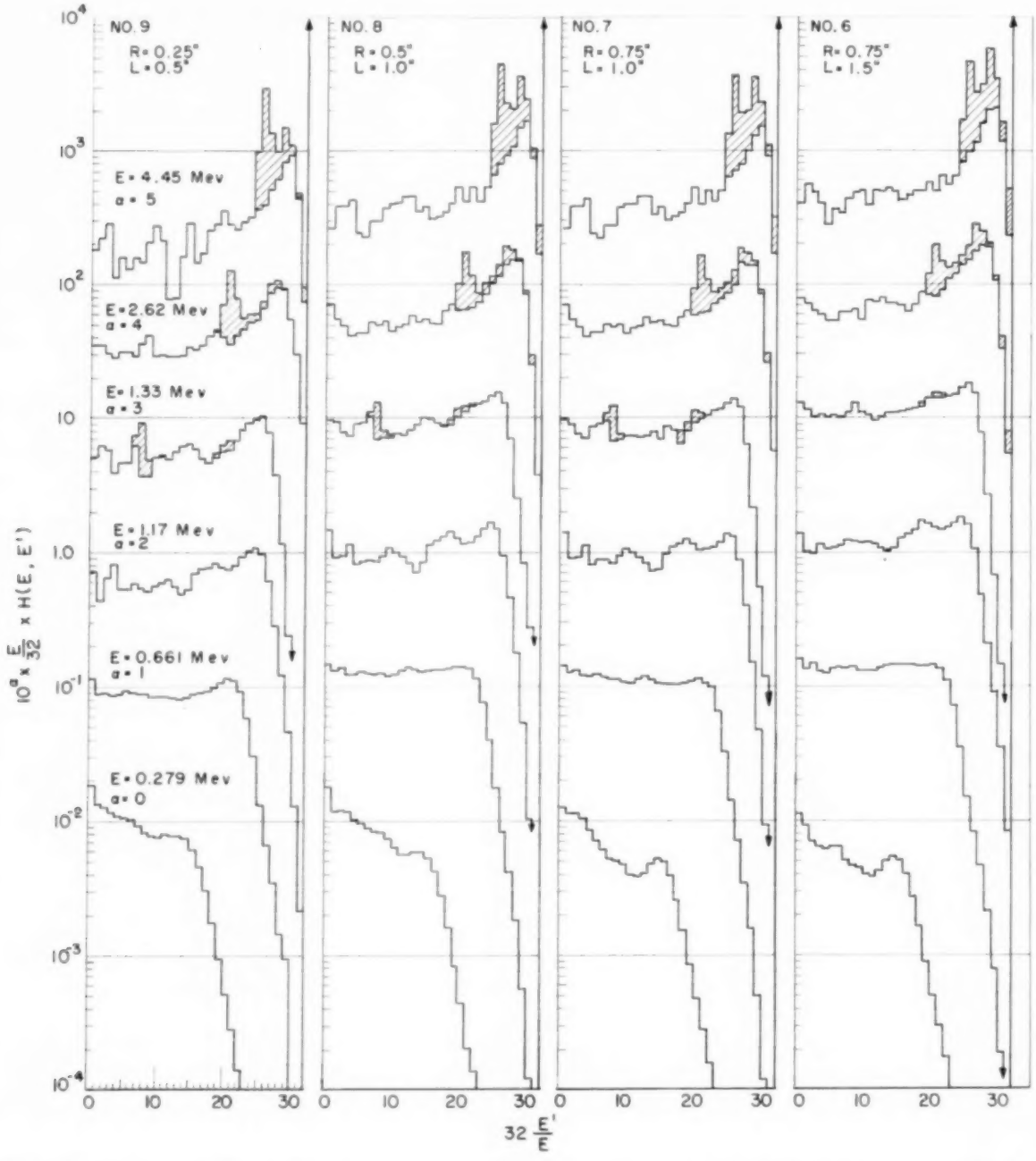

FIGURE 1. *Response functions of* NaI(Tl) *scintillation crystals for collimated radiation incident along the crystal axis.*

a, Crystals No. 9, 8, 7, and 6.

Only the "Compton tails" of the spectra are shown; the photopeaks are merely indicated by arrows. All curves are normalized so as to correspond to one incident photon the area under them being $Y(E)$ [1-$p(E)$]. The curves for different energies have been shifted apart through multiplication by indicated scale factors 10^a. The shaded areas represent the pulses which have been shifted from the photopeak because of the escape of annihilation radiation.

The histograms are normalized absolutely so that they correspond to one photon incident on a crystal. The area under each histogram is thus $Y(E)[1-p(E)]$.[12] In order to supply the missing photopeak, one need merely add a Gaussian with the desired standard deviation (cf. eq (7)) and multiplied by a weight factor $Y(E)p(E)$; $Y(E)$ and $p(E)$ can be found in tables 1 and 2.

The shaded parts of the histograms indicate the contribution to the scintillation spectrum due to the escape of secondary radiation. In other words, they represent pulses which would have ended up in the photopeak if the absorptions had not been spurious. It can be seen that at sufficiently high source energies the response functions have two peaks at energies mc^2 and 2 mc^2 below the incident energy E, which are associated with the escape of 1 or 2 annihilation quanta.

It can be seen that the shapes of the response functions for various crystal sizes, and even for different energies, are on the whole rather similar.

[12] To separate the histograms for different energies, the ordinates were multiplied by indicated scale factors 10^{α}.

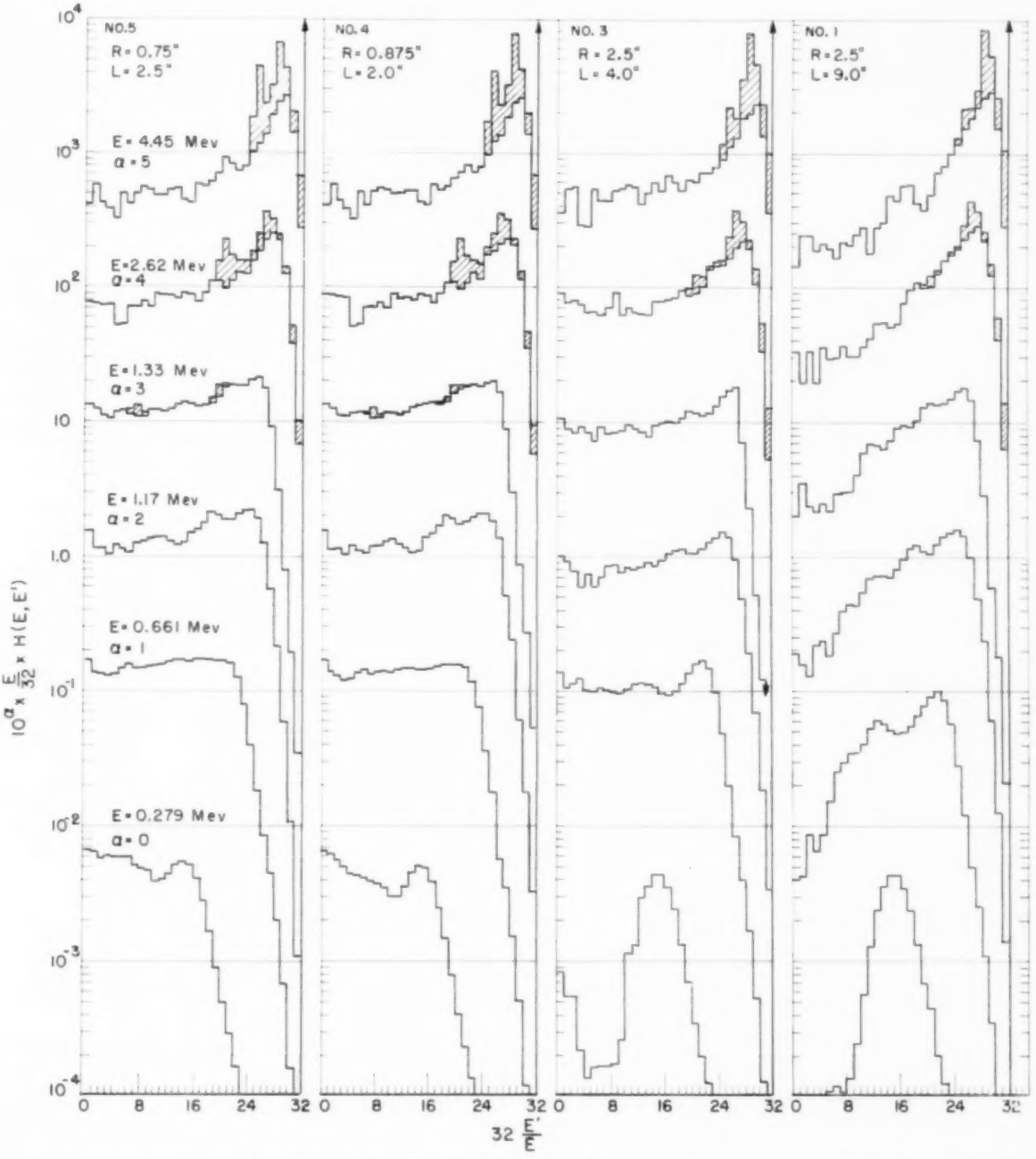

FIGURE 1. *Response functions of* NaI(Tl) *scintillation crystals for collimated radiation incident along the crystal axis*—Cont.

b, Crystals No. 5, 4, 3, and 1.

The statistical fluctuations of the Monte Carlo calculations, as evidenced by the irregularities of the histograms, are much worse for high than for low incident energies. It is noticeable that quite similar local irregularities occur for histograms pertaining to the same energy but different crystals. This phenomenon is due to the use of the same groups of photon histories for all the crystals.

3.4. Other Source Geometries

Monte Carlo calculations of the response function for any desired source geometry can easily be accomplished through the proper choice of the initial conditions, photon positions and directions, in the random sampling process. Sample results of such calculations for 0.661 Mev radiation are presented in figures 2, 3, and 4.

a. Broad-Beam Radiation

In figure 2 the ratio p_{BB}/p is plotted against r/R, where p_{BB} is the photofraction for a broad cylindrical beam with cross-sectional radius r, p is the photofraction for a collimated source, and R is the crystal radius. Three curves are shown, for crystals No. 3, large; No. 6, medium-sized; and No. 9, small.

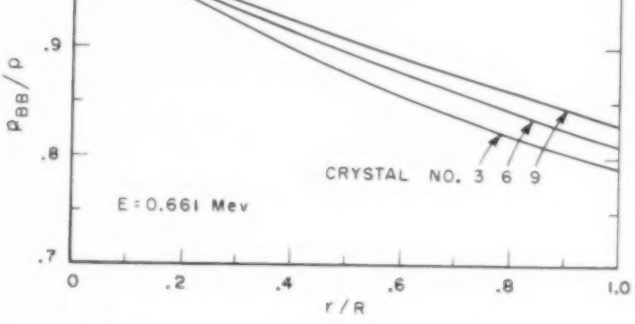

FIGURE 2. *Comparison of the photofractions for broad beams, and for collimated radiation incident along the crystal axis.*

The ratio p_{BB}/p is plotted as a function of r/R, where r is the radius of the broad beam, and R that of the crystal. The source energy is 0.661 Mev.

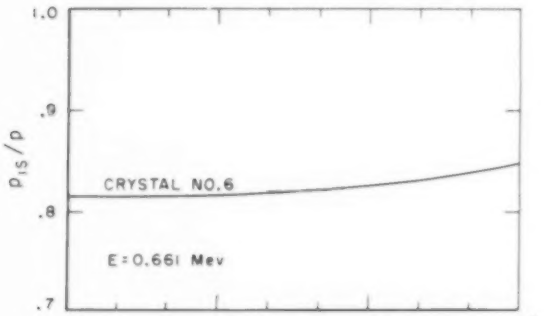

FIGURE 3. *Comparison of the photofractions for point-isotropic sources, and for collimated radiation incident along the crystal axis.*

The ratio p_{IS}/p is plotted as a function of $\tan^{-1}(D/R)$, where D is the distance from the crystal to the point source (located on the crystal axis), and R is the crystal radius.

b. Point-Isotropic Source

In figure 3, the ratio p_{IS}/p is plotted against $\tan^{-1} R/D$ where p_{IS} is the photofraction for a point-isotropic source located at a distance D from the crystal on the cylinder axis. The curve pertains to crystal No. 6. The end-point of this curve, for $\tan^{-1}R/D=0°$, was obtained from the corresponding broad-beam result.

c. Off-Axis Collimated Beam

In figure 4, the shape of the response function is shown for collimated pencils of radiation incident at various distances s from the crystal axis, for crystals No. 4 and No. 1. The normalization and other details are the same as in figure 1; the photofractions are also shown.

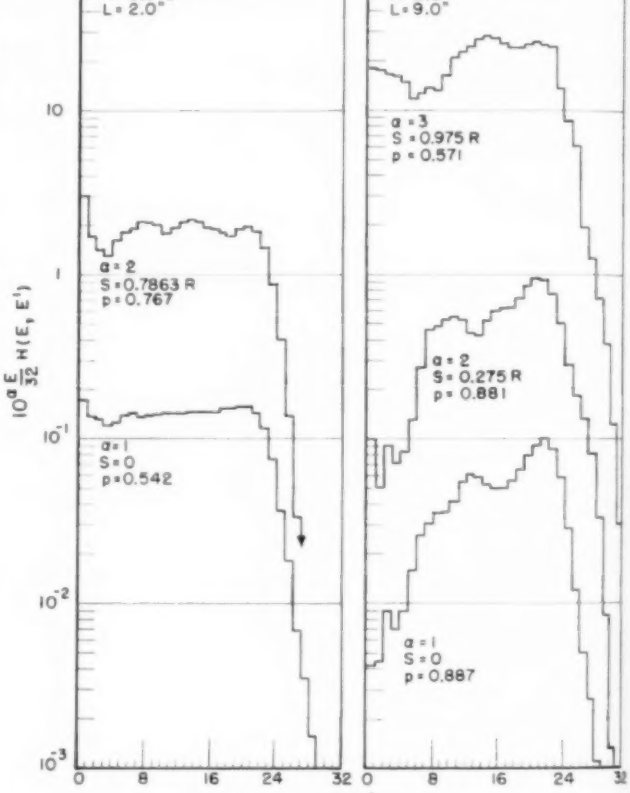

FIGURE 4. *Response function of NaI(Tl) scintillation crystals for collimated radiation incident offcenter at a distance s from the crystal axis.*

The curves are normalized so as to correspond to one incident photon, the area under them being $Y(E)[1-p(E)]$. The curves for different values of s have been shifted apart through multiplication by indicated scale factors 10^{α}. Only the "Compton tails" of the spectra are shown; the photopeaks are indicated by arrows, and the values of the photofractions are shown beside the corresponding curves.

4. Discussion

4.1. Comparison With Other Calculations

Our results for the value of the photofraction for collimated radiation incident on *small* crystals are in good agreement with those obtained by Maeder et al. For example, at an energy of 0.661 Mev one finds:

	Crystal number					
	9	8	7	6	5	4
p(Maeder)	0.246	0.368	0.418	0.471	0.507	0.546
p(table 2)	.243	.377	.442	.481	.508	.542

At 0.279 Mev and 1.17 Mev the agreement is almost as good (with the exception of a 15 percent discrepancy for the smallest crystal (No. 9) at 1.17 Mev).

No other results comparable to our photofractions for large crystals No. 1, 2, and 3 exist. Maeder et al. did, however, attempt to compute the photofraction for the limiting case of an infinitely large crystal (i. e., a semi-infinite medium), calculating the first two interactions of the incident photon exactly, and estimating the effect of the subsequent interactions. We have calculated the photofraction for this case by extrapolation based on the empirical formula (12) and arrive at the following comparison:

Infinitely large crystal	Energy (Mev)		
	0.279	0.661	1.17
p(Monte Carlo)	0.975	0.940	0.980
p(Maeder)	.975	.876	.802

The "orders of scattering" approach, in the limit of very large crystals, agrees with the more exact calculation only at 0.279 Mev, where multiple interactions are unlikely because of the large gamma-ray absorption cross section, but leads to a significant underestimate of the photofraction at higher energies.

Our albedo values $1-p$ are in good agreement with the results of a calculation by Hayward and Hubbell.[13] Note that the albedo is greater at 0.661 Mev than at 0.279 or 1.17 Mev. There is also experimental evidence for the occurrence of this maximum at an intermediate energy.[14]

The pictures of the response function given by Maeder et al. are similar in appearance to ours, but not detailed enough for an accurate comparison in regard to shape.

4.2. Comparison With Experimental Results

For small crystals a detailed comparison with experiments has been made by Maeder et al., which can equally well be applied to our results. It indicates fair agreement between theory and experiment, but there is a consistent tendency for the experimental photofractions to be somewhat lower than the theoretical values. This discrepancy may be reduced in part if one takes into account energy losses due to electron escape from the crystal.[15]

Measurements of Foote and Koch (see footnote 2) indicate for collimated radiation incident on a large crystal ($R=2.5$ in., $L=4$ in.) photofractions $p=0.8$ at 0.661 Mev, and 0.64 for cobalt-60 radiation, while the corresponding theoretical values are $p=0.821$, and 0.675 respectively.[16]

Further results for a large crystal ($R=2$ in., $L=4$ in.) have recently been reported by Kreger (see footnote 6). His incident radiation was a broad beam with cross-sectional radius $r=0.25\ R$. Hence the comparison must be made for the broad-beam photofraction p_{BB}. We have so far only calculated this correction at an energy of 0.661 Mev, but estimate that with an error of only a few percent the same fractional correction can also be applied at the other energies of Kreger's experiment.

	Energy (Mev)				
	0.279	0.661	1.17	1.32	2.62
p (Kreger)	0.93	0.725	0.57	0.54	0.47
p (present results)	(.90)	.74	(.60)	(.58)	(.50)

The agreement is seen to be quite good at 0.661 Mev, where the exact value of the correction is known, and fairly good elsewhere.

Summing up the entire experimental evidence, both for small and large crystals, we can state the experimental photofraction is invariably below the theoretical values, by a smaller or greater amount. One is led to the conclusion that in the experiments there is always background radiation present (such as back-scattered radiation from the radiation source, and from the material surrounding the detector) which would be counted in the tail end of the pulse-height spectrum and would thus tend to depress the value of the photofraction.

The authors thank Dr. Evans Hayward for several stimulating and enlightening discussions, and Miss Mary Orr for her assistance with the hand computations.

5. Appendix: Escape of Secondary Radiation

5.1. Effect on the Photofraction

To estimate the effect of the escape of secondary radiation on the value of the photofraction p, we must determine the probability that an absorption is

[13] E. Hayward and J. Hubbell, Phys. Rev. **93**, 955 (1954).
[14] H. W. Koch (private communication).
[15] K. Lidén and N. Starfelt, Arkiv Fysik **7**, 428 (1954).
[16] The photofraction for cobalt-60 radiation, $\bar{p}=\dfrac{Y(1.17)p(1.17)+Y(1.33)p(1.33)}{Y(1.17)+Y(1.33)}$.

"spurious" i. e., that it results in, or is preceded by, the escape of at least one secondary photon from the crystal (with an energy greater than 50 kev).[17]

We shall ignore the displacement of charged particles in the crystal.[18] Bremsstrahlung and annihilation quanta are thus assumed to be emitted at the point of absorption of the primary photon. Moreover, the emission is assumed to be isotropic. First, attention is concentrated on the spurious absorptions which occur in the first interaction of the incident photon (i. e., prior to any Compton scatterings), and return later to the relatively unimportant spurious absorptions resulting from other interactions. Secondary radiation is therefore considered as originating from an exponentially distributed line source on the axis of the crystal (on the assumption that the incident radiation is collimated).

The following notation will be used for the various attenuation coefficients: μ_{PH} = photoelectric absorption coefficient, μ_P = pair production absorption coefficient, μ_C = Compton scattering attenuation coefficient; $\mu=\mu_{PH}+\mu_P+\mu_C$ = total attenuation coefficient.

Annihilation Radiation. If an absorption of a primary photon of energy E results in pair formation and subsequent annihilation of the positron, the probability that at least one of the two annihilation quanta will escape from a cylindrical crystal (with radius R and length L) is given, approximately, by the following expression:

$$p_0=\frac{\mu(E)}{1-\exp\,[-\mu(E)L]}\int_0^L dx e^{-\mu(E)x}\int_0^1 d\,\cos\theta\{1-(1-e^{-s_1\mu'})\,(1-e^{-s_2\mu'})p_1^*p_2^*\} \quad (15)$$

where $\mu'=\mu(mc^2)$, and s_1 and s_2 are the distances traveled in the crystal by the two annihilation quanta (emitted in opposite directions).

$$\left.\begin{array}{llll}
\text{If } 0\le x\le L/2 & & & \\
\cos\theta_1\le\cos\theta\le 1 & s_1=x/\cos\theta & s_2=(L-x)/\cos\theta & \\
\cos\theta_2\le\cos\theta\le\cos\theta_1 & s_1=x/\cos\theta & s_2=R/\sin\theta & \\
0\le\cos\theta\le\cos\theta_2 & s_1=R/\sin\theta & s_2=R/\sin\theta & \\
\text{If } L/2\le x\le L & & & \\
\cos\theta_2\le\cos\theta\le 1 & s_1=x/\cos\theta & s_2=(L-x)/\cos\theta & \\
\cos\theta_1\le\cos\theta\le\cos\theta_2 & s_1=R/\sin\theta & s_2=(L-x)/\cos\theta & \\
0\le\cos\theta\le\cos\theta_1 & s_1=R/\sin\theta & s_2=R/\sin\theta &
\end{array}\right\} \quad (16)$$

where

$$\cos\theta_1=\left[1+\left(\frac{R}{L-x}\right)^2\right]^{-1/2},\ \cos\theta_2=\left[1+\left(\frac{R}{x}\right)^2\right]^{-1/2}.$$

[17] The limit of 50 kev was selected because the same low-energy cutoff was also used in the main Monte Carlo calculation.

[18] The ranges for 0.3, 1.0, and 4.0 Mev electrons in NaI are approximately 0.02, 0.17, and 0.861 cm, respectively. Hence only at the highest energy (4.45 Mev) and for the two smallest of the crystals considered (No. 8 and 9) could the neglect of electron displacement lead to a significant overestimate of the photofraction.

p_1^* and p_2^* are photofractions for the two annihilation quanta, which—we believe—can be accurately approximated by the photofraction p for an energy of 0.511 Mev, as obtained by interpolation from table 2.

Bremsstrahlung. The probability of escape of a bremsstrahlung quantum of energy E' can be expressed by a formula similar to (15):

$$P_1(E')=\frac{\mu(E)}{1-\exp\,[-\mu(E)L]}\int_0^L dx e^{-\mu(E)x}\,\frac{1}{2}\int_{-1}^1 d\,\cos\theta\,\{e^{-s\mu(E')}+[1-e^{-s\mu(E')}][1-p^*(E)]\} \quad (17)$$

where we again set $p^*(E)=p(E)$, and the path length s is defined as follows:

$$\left.\begin{array}{lll}
\cos\theta_2<\cos\theta\le 1; & s=\dfrac{x}{\cos\theta} & \\
-\cos\theta_1<\cos\theta\le\cos\theta_2; & s=\dfrac{R}{\sin\theta} & \\
-1\le\cos\theta\le-\cos\theta_1; & s=\dfrac{x-L}{\cos\theta} &
\end{array}\right\} \quad (18)$$

($\cos\theta_1$ and $\cos\theta_2$ have the same meaning as above). Let $\phi(E,E')dE'$ denote the probability, per unit path length, for an electron or positron of energy E to produce a photon in the energy interval $(E', E'+dE')$,[19] and let dE/ds be the average energy loss per unit path length of an electron or positron due to ionizing collisions.[20] The probability of an escape of a bremsstrahlung quantum produced by an electron or positron of energy E in the course of slowing down is

$$P_2(E)=\frac{1}{R(E)}\int_{\hat{E}}^E dE'\int_{\hat{E}}^{E'} dE''\left[\phi(E',E'')\Big/-\frac{dE}{ds}(E')\right]P_1(E''), \quad (19)$$

where $R(E)$ is the electron or positron range, and $\hat{E}=50$ kev is the cutoff.

Let $\psi(k)dk$ be the probability that one of the members of the pair has acquired initially a fraction between k and $k+dk$ of the total available kinetic energy.[20] The probability of the escape of at least one photon in the form of bremsstahlung emitted by a pair of total energy E while slowing down is

$$P_3(E)=\int_0^1 dk\psi(k)[P_2(kE)+P_2(E-kE)-P_2(kE)P_2(E-kE)]. \quad (20)$$

[19] H. Bethe and W. Heitler, Proc. Roy. Soc. [A] **146**, 83 (1934).

[20] H. Bethe, Handbuch der Physik, **24**, 519 (1933).

The above formula assumes that each member of the pair can emit at most one photon with energy greater than 50 kev in the course of slowing down. We believe that the effects of plural photon production can be safely neglected in the energy range of interest here.

Combined Effect. The probability that the absorption of a primary photon of energy E in a first interaction will be spurious due to the combined effects of bremsstrahlung and annihilation radiation is

$$P_4(E)=\frac{\mu_{\mathrm{PH}}}{\mu_{\mathrm{PH}}+\mu_{\mathrm{P}}}P_2(E)+\frac{\mu_{\mathrm{P}}}{\mu_{\mathrm{PH}}+\mu_{\mathrm{P}}}[P_3(E-2mc^2)+P_0-P_3(E-2mc^2)P_0]. \tag{21}$$

In evaluating this formula we found that the neglect of bremsstrahlung (i. e., setting P_2 and $P_3=0$) would lower P_4 by only a few percent (a maximum of $\sim 11\%$ for crystal No. 9 at 4.45 Mev). The probability, per incident photon, of a spurious absorption in the first interaction is

$$P_5(E)=[Y(E)/\mu(E)]\,[\mu_{\mathrm{PH}}(E)+\mu_{\mathrm{P}}(E)]P_4(E). \tag{22}$$

Next we must determine a corresponding probability of spurious absorption in a second interaction. One contribution to this probability is similar in origin to (21), and can be written:

$$P_6(E)=[Y(E)/\mu(E)]\int_{\hat{E}}^{E}dE'\,\frac{\mu_{\mathrm{PH}}(E')+\mu_{\mathrm{P}}(E')}{\mu(E')}\,k(E,E')Q(E')P_4^*(E'), \tag{23}$$

where $k(E,E')$ is the Klein-Nishina differential coefficient for Compton scattering with energy change from E to E'; Q is the probability that the scattered incident photon will not escape from the crystal without further interaction [21]; and $P_4^*(E)$ is the probability that a given absorption event is spurious, and is analogous to $P_4(E)$, but should take into account the fact that the source of secondary radiation is no longer concentrated on the crystal axis. We have ignored this circumstance, because the evaluation of an exact expression for $P_4^*(E)$ would be exceedingly complicated, and have set $P_4^*(E)=P_4(E)$. It is hoped that this will introduce only a minor error, for the following reasons: For small crystals, such a geometrical error might be serious, but a second interaction is quite rare; for large crystals, in which multiple interactions are more common, the geometrical error is much less significant. In any case, the contribution of P_6 to the change in the photofraction will be small, so that a rough-and-ready treatment is in order.

There is also the possibility that an absorption taking place in a second interaction is spurious because it was preceded by the escape of a bremsstrahlung quantum from a Compton recoil electron. The probability for this to happen is

$$P_7(E)=[Y(E)/\mu(E)]\int_{\hat{E}}^{E}dE'\,\frac{\mu_{\mathrm{PH}}(E')+\mu_{\mathrm{P}}(E')}{\mu(E')}\,k(E,E')Q(E')P_1(E-E'). \tag{24}$$

Thus a spurious interaction will occur with probability

$$P_8(E)=P_6(E)+P_7(E)-P_6(E)P_7(E) \tag{25}$$

per incident photon in a second interaction; and with probability

$$P_9(E)=P_5(E)+P_8(E)-P_5(E)P_8(E) \tag{26}$$

in a first or second interaction. At the highest energy and for the largest crystal considered, the value of P_8 was only 15 percent of P_5, and generally it was much smaller. Subsequent interactions will lower the photon energy further and make spurious absorptions even more unlikely. Hence we felt justified in ending our calculations with the effects of the second interaction. The change in the photofraction is thus

$$\Delta p=-P_9(E)Y(E). \tag{27}$$

5.2. Effect on the Shape of the Response Function

In considering the detailed shape of the response function we have calculated only the effects of annihilation radiation from a first interaction. Other escaping secondary radiation was taken into account only insofar as it shifted pulses from the photopeak into tail of the response function (i. e., by an appropriate renormalization of $K(E,E')$).

None, or one, or both of the annihilation quanta resulting from a pair production can escape from the crystal without further interaction. The probabilities for these contingencies can be obtained by replacing the integrand in the inner integral in (15) by the expressions

$$\left.\begin{aligned}&\text{(a) (no escape)} &&: (1-e^{-\pi_1\mu'})(1-e^{-\pi_2\mu'})\\ &\text{(b) (one escape)} &&: e^{-\pi_1\mu'}(1-e^{-\pi_2\mu'})+e^{-\pi_2\mu'}(1-e^{-\pi_1\mu'})\\ &\text{(c) (two escapes)} &&: e^{-\pi_1\mu'}e^{-\pi_2\mu'}.\end{aligned}\right\} \tag{28}$$

[21] An expression for Q has been given by Maeder et al. (footnote 3, eq 44, 45, 46); their H_0 is our YQ.

In case (a) the energy E' left in the crystal is the sum of three terms; two of them are each distributed as

$$L(mc^2)/Y(E)=K(mc^2,E')+p(mc^2)\delta(E'-mc^2) \quad (29)$$

the third contribution is a constant amount of energy $E-2mc^2$.

In case (b), E' is the sum of two terms, one distributed according to (29), the other a constant equal to $E-2mc^2$. In case (c) $E'=E-2mc^2$. The correction of the response function was performed by shifting the appropriate number of pulses from the photopeak to the "tail" of the pulse height spectrum, distributing them according to the distribution functions described above weighted according to (28).

WASHINGTON, November 4, 1955.

INDEX TO VOLUME 56

January to June 1956—Research Papers 2641 to 2686

A

Page

Abscissas and weights for Gaussian quadratures of high order, RP2645 35
Acetylene-d_2, vibrational constants of, RP2675 279
Achhammer, B. G., M. R. Harvey, J. E. Steward, Index of refraction and particle size as factors in the infrared spectrophotometry of polyvinyl chloride, RP2670 225
Acquista, N., E. K. Plyler, Infrared measurements from 50 to 100 microns, RP2660 149
Advances in the design and application of the radiofrequency permeameter, RP2673 261
Air, surge voltage breakdown of, in a nonuniform field, RP2669 201
Alkaline earth oxides at 21° C, isothermal compressibilities, RP2666 187
Allen, H. C., Jr., L. R. Blaine, E. K. Plyler, Vibrational constants of acetylene-d_2, RP2675 279
Alloys, zinc-base, polarographic determination of lead and cadmium in, RP2679 301
Alpha and beta brasses, relationship between crystal orientation and stress-corrosion cracking, RP2662 159
Ambler, E., R. P. Hudson, An examination of the helium vapor pressure scale of temperature, using a magnetic thermometer, RP2654 99
Antenna, vertical, radiation from, over a curved stratified ground, RP2671 237
Arifrod, B. M., Dielectric relaxation for a three-dimensional rotator in a crystalline field: theory for a general six-site model, RP2651 ..... 8, 1

B

Barium oxide-boric oxide-silica system, surface tension of molten glasses in, RP2661 155
Barium titanate, preparation of barium titanyl oxalate tetrahydrate for conversion to, RP2677 289
Barium titanyl oxalate tetrahydrate, preparation for conversion to barium titanate of high purity, RP2677 289
Bates, R. G., V. E. Bower, E. R. Smith, Calcium hydroxide as a highly alkaline *p*H standard, RP2680 305
Berger, M. J., J. Doggett, Reflection and transmission of gamma radiation by barriers: semianalytic Monte Carlo calculation, RP2653 89
—, *J. Doggett,* Response function of thallium-activated sodium-iodide scintillation counters, RP2686 355
—, Penetration of gamma radiation from a plane monodirectional oblique source, RP2656 111
Binary alkaline-earth borate glasses, thermal expansion, RP2650 73
Blaine, L. R., H. C. Allen, Jr., E. K. Plyler, Vibrational constants of acetylene-d_2, RP2675 279
Bower, V. E., R. G. Bates, E. R. Smith, Calcium hydroxide as a highly alkaline *p*H standard, RP2680 305
Bradley, J. C., L. Haar, A. S. Friedman, Ideal gas thermodynamic functions of the isotopic hydrogen cyanides, RP2668 197
Brasses, alpha and beta, crystal orientation and stress-corrosion cracking, RP2662 159
Breakdown of air in a nonuniform field, surge voltage, RP2669 201

C

Calcium hydroxide as a highly alkaline *p*H standard, RP2680 305
Calculation of thermodynamic functions for polyatomic molecules, RP2655 105
Calorimeter for measuring the power in a high-energy X-ray beam, RP2642 9
Carlson, E. T., Hydrogarnet formation in the system lime-alumina-silica-water, RP2683 327
Cellulose, pyrolysis in a vacuum, RP2685 343
Cements and related materials, behavior under hydrostatic pressures up to 10,000 atmospheres, RP2646 39
Characteristics of an image-forming system, RP2672 245
Clabaugh, W. S., E. M. Swiggard, R. Gilchrist, Preparation of barium titanyl oxalate tetrahydrate for conversion to barium titanate of high purity, RP2677 289
Compressibilities, isothermal, of alkaline earth oxides, RP2666 187
Computer for calculating the water content of gases, RP2674 269
Cones, H. N., J. H. Park, Surge voltage breakdown of air in a nonuniform field, RP2669 201
Constant, dielectric, of water, RP2641 1
Constants, vibrational, of acetylene-d_2, RP2675 279
Crystal orientation and stress-corrosion cracking in alpha and beta brasses, RP2662 159
Cyanide, isotopic hydrogen, ideal gas thermodynamic functions, RP2668 197

D

Davis, P., P. Rabinowitz, Abscissas and weights for Gaussian quadratures of high order, RP2645 35
Descriptions and analyses of the third and fourth spectra of zirconium, Zr III and Zr IV, RP2663 167
Dicalcium ferrite and hexacalcium dialumino ferrite, heats of formation, RP2681 313
Dielectric constant of water from 0° to 100° C, RP2641 1
Dielectric relaxation for a three-dimensional rotator in a crystalline field: theory for a general six-site model, RP2651 81
Diniak, A. W., E. R. Weaver, A new computer for calculating the water content of gases, RP2674 269
Doggett, J., M. J. Berger, Reflection and transmission of gamma radiation by barriers: semianalytic Monte Carlo calculation, RP2653 89
—, —, Response function of thallium-activated sodium-iodide scintillation counters, RP2686 355
Domen, S., J. McElhinney, B. Zendle, A calorimeter for measuring the power in a high-energy X-ray beam, RP2642 9

E

Page

Electrical resistivity in vitreous ternary lead silicates, RP2658 135
Electrical resistivity of vitreous ternary lithium-sodium silicates, RP2665 183
Electrolytic separations of lead and cadmium in zinc-base alloys, RP2679 301
Enfield, A. W., A. L. Rasmussen, A. Hess, Advances in the design and application of the radiofrequency permeameter, RP2673 261
Entropy, residual, of linear polymers, RP2648 55

F

Ferrite, hexacalcium dialumino and dicalcium, heats of formation, RP2681 313
Formulas for inverse osculatory interpolation, RP2647 51
Frequency conversion with positive nonlinear resistors, RP2664 179
Friedman, A. S., J. C. Bradley, L. Harr, ideal gas thermodynamic functions of the isotopic hydrogen cyanides, RP2668 197
Fundamental factors controlling electrical resistivity in vitreous ternary lead silicates, RP2658 135
Furukawa, G. T., M. L. Reilly, Heat capacity of polyisobutylene from 0° to 380° K, RP2676 285

G

Gamma radiation, penetration of, from a plane monodirectional oblique source, RP2656 111
Gamma radiation, reflection and transmission by barriers, semianalytic Monte Carlo calculation, RP2653 89
Gaseous atmospheres, thermal decomposition of polytetrafluoroethylene in, RP2644 27
Gases, water content, computer for calculating, RP2674 269
Gaussian quadratures of high order, abscissas and weights, RP2645 35
Gilchrist, R., W. S. Clabaugh, E. M. Swiggard, Preparation of barium titanyl oxalate tetrahydrate for conversion to barium titanate of high purity, RP2677 289
Glasses, binary alkaline-earth borate, thermal expansion, RP2650 73
Glasses, molten, surface tension of, in the system barium oxide-boric oxide-silica, RP2661 155
Goldberg, K., A matrix with real characteristic roots, RP2652 87

H

Haar, L., J. C. Bradley, A. S. Friedman, Ideal gas thermodynamic functions of the isotopic hydrogen cyanides, RP2668 197
Haas, P. H., R. D. Harrington, R. C. Powell, A re-entrant cavity for measurement of complex permeability in the very-high-frequency region, RP 2657 129
Half-wave potential measurements, polarographic, RP2659 143
Harrington, R. D., R. C. Powell, P. H. Haas, A re-entrant cavity for measurement of complex permeability in the very-high-frequency region, RP2657 129
Harrison, W. N., S. W. Strauss, D. G. Moore, L. E. Richards, Fundamental factors controlling electrical resistivity in vitreous tenary lead silicates, RP2658 135
Hart, V. E., Molecular weights of thermally degraded polymethyl methacrylate, RP2649 67
—, *S. L. Madorsky, S. Straus,* Pyrolysis of cellulose in a vacuum, RP2685 343
Harvey, M. R., J. E. Stewart, R. G. Achhammer, Index of refraction and particle size as factors in the infrared spectrophotometry of polyvinyl chloride, RP2670 225
Heat capacity of polyisobutylene from 0° to 380° K, RP2676 285
Heats of formation of hexacalcium dialumino ferrite and dicalcium ferrite, RP2681 313
Helium vapor pressure scale of temperture, an examination using a magnetic thermometer, RP2654 99
Hess, A., A. L. Rasmussen, A. W. Enfield, Advances in the design and application of the radiofrequency permeameter, RP2673 261
Hexacalcium dialumino ferrite and dicalcium ferrite, heats of formation, RP2681 313
Hoffman, R., E. S. Newman, Heats of formation of hexacalcium dialumino ferrite and dicalcium ferrite, RP2681 313
Hudson, R. P., E. Ambler, An examination of the helium vapor pressure scale of temperature using a magnetic thermometer, RP2654 99
Hunt, C. M., C. E. Weir, R. L. Blaine, Behavior of cements and related materials under hydrostatic pressures up to 10,000 atmospheres, RP2646 39
Hydrogarnet formation in the system lime-alumina-silica-water, RP2683 327
Hydrogen cyanides, isotopic, ideal gas thermodynamic functions, RP2668 197
Hydrostatic pressures, behavior of cements and related materials under, RP2646 39
Hydrothermal reactions in the lime-alumina-silica-water system, RP2683 327

I

Ideal gas thermodynamic functions of the isotopic hydrogen cyanides, RP2668 197
Image-forming system, characteristics of, RP2672 245
Improved synthesis of sodium D-glucuronate-6-C^{14} and of D-glucose-6-C^{14}, RP2667 191
Index of refraction and particle size as factors in the infrared spectrophotometry of polyvinyl chloride, RP2670 225
Infrared absorption spectrum of trimethylborane, RP2684 337
Infrared measurements from 50 to 125 microns, RP2660 149
Infrared spectrophotometry of polyvinyl chloride, index of refraction and particle size as factors, RP2670 225
Inverse osculatory interpolation, formulas, RP2647 51
Ions, trivalent and tetravalent, pyrochlore compounds containing double oxides of, RP2643 17

Page

Isbell, H. S., R. Schaffer, Improved synthesis of sodium D-glucuronate-6-C^{14} and of D-glucose-6-C^{14}, RP2667 191
Isothermal compressibilities of alkaline earth oxides at 21° C, RP2666 187
Isotopic hydrogen cyanides, ideal gas thermodynamic functions, RP2668 197

K

Kiess, C. C., New descriptions and analyses of the third and fourth spectra of zirconium, Zr III and Zr IV, RP2663 167
Koch, H. W., J. M. Wyckoff, Response of a sodium-iodide scintillation spectrometer to 10- to 20-million-electron-volt electrons and X-rays, RP2682 319

L

Lead and cadmium in zinc-base alloys, polarographic determination, using electrolytic separations at controlled potential, RP2679 301
Lead silicates, vitreous ternary, electrical resistivity, RP2658 135
Lime-alumina-silica-water system, hydrogarnet formation, RP2683 327
Linear polymers, residual entropy, RP2648 55
Lithium-sodium silicates, vitreous ternary, electrical resistivity, RP2665 183
Logan, H. L., Relationship between crystal orientation and stress-corrosion cracking in alpha and beta brasses, RP2662 159

M

Madorsky, S. L., V. E. Hart, S. Straus, Pyrolysis of cellulose in a vacuum, RP2685 343
Magnetic thermometer, use of, in examination of helium vapor pressure scale of temperature, RP2654 99
Magnetic toroids, permeability, measurement, RP2657 129
Malmberg, C. G., A. A. Maryott, Dielectric constant of water from 0° to 100° C, RP2641 1
Maryott, A. A., C. G. Malmberg, Dielectric constant of water from 0° to 100° C, RP2641 1
Matrix with real characteristic roots, RP2652 87
McCamy, C. S., A five-band recording spectroradiometer, RP2678 293
McElhinney, J., P. Zendle, S. Domen, A calorimeter for measuring the power in a high-energy X-ray beam, RP2642 9
Michaelsen, J. D., L. A. Wall, Thermal decomposition of polytetrafluoroethylene in various gaseous atmospheres, RP2644 27
Molecular weights of thermally degraded polymethyl methacrylate, RP2649 67
Molecules, polyatomic, calculation of thermodynamic functions for, RP2655 105
Monte Carlo calculation, semianalytic, reflection and transmission of gamma radiation by barriers, RP2653 89
Moore, D. G., S. W. Strauss, W. N. Harrison, L. E. Richards, Fundamental factors controlling electrical resistivity in vitreous ternary lead silicates, RP2658 135

N

Newman, E. S., R. Hoffman, Heats of formation of hexacalcium dialumino ferrite and dicalcium ferrite, RP2681 313
Numerical analysis, matrix with real characteristic roots, RP2652 87

O

Optical image-forming system, characteristics of, RP2672 245
Osculatory interpolation, inverse, formulas for, RP2647 51
Oxides, alkaline-earth, isothermal compressibilities, RP2666 187
Oxides, double, of trivalent and tetravalent ions, pyrochlore-type compounds containing, RP2643 17

P

Page, C. H., Frequency conversion with positive nonlinear resistors, RP2664 179
Park, J. H., H. N. Cones, Surge voltage breakdown of air in a nonuniform field, RP2669 201
Particle size and index of refraction as factors in infrared spectrophotometry of polyvinyl chloride, RP2670 225
Penetration of gamma radiation from a plane monodirectional oblique source, RP2656 111
Permeability, complex, in the very-high-frequency region, a re-entrant cavity for measurement, RP2657 129
Permeameter, radiofrequency, advances in design and application, RP2673 261
pH standard, calcium hydroxide as a, RP2680 305
Plyler, E. K., H. C. Allen, Jr., L. E. Blaine, Vibrational constants of acetylene-d_2 279
—, *N. Acquista,* Infrared measurements from 50 to 125 microns, RP2660 149
Polarographic determination of lead and cadmium in zinc-base alloys, using electrolytic separations at controlled potential, RP2679 301
Polarographic half-wave potential measurements, some factors affecting the precision, RP2659 143
Polyatomic molecules, calculation of thermodynamic functions for, RP2655 105
Polyisobutylene, heat capacity from 0° to 380° K, RP2676 285
Polymers, linear, residual entropy, RP2648 55
Polymethyl methacrylate, thermally degraded, molecular weights, RP2649 67
Polytetrafluoroethylene, thermal decomposition in various gaseous atmospheres, RP2644 27
Polyvinyl chloride, index of refraction and particle size as factors in the infrared spectrophotometry, RP2670 225
Positive nonlinear resistors, frequency conversion with, RP2664 179
Potential measurements, polarographic half-wave, RP2659 143
Powell, R. C., P. D. Harrington, P. H. Haas, A re-entrant cavity for measurement of complex permeability in the very-high-frequency region, RP2657 129
Pyrochlore-type compounds containing double oxides of trivalent and tetravalent ions, RP2643 17
Pyrolysis of cellulose in a vacuum, RP2685 343

R

Page

Fabinowitz, P., P. Davis, Abscissas and weights for Gaussian quadratures of high order, RP2645 35
Radiation from a vertical antenna over a curved stratified ground, RP2671 237
Radiation, gamma, reflection and transmission by barriers, semianalytic Monte Carlo calculation, RP2653 89
Radiation, gamma, penetration from a plane monodirectional oblique source, RP2656 111
Radiofrequency permeameter, advances in the design and application of, RP2673 261
Radio wave propagation, radiation from a vertical antenna over a curved stratified ground, RP2671 237
Rasmussen, A. L., A. W. Enfield, A. Hess, Advances in the design and application of the radiofrequency permeameter, RP2673 261
Recording spectroradiometer, five-band, RP2678 293
Re-entrant cavity for measurement of complex permeability in the very-high-frequency region, RP2657 129
Reflection and transmission of gamma radiation by barriers: semianalytic Monte Carlo calculation, RP2653 89
Reilly, M. L., G. T. Furukawa, Heat capacity of polyisobutylene from 0° to 380° K, RP2676 285
Relationship between crystal orientation and stress-corrosion cracking in alpha and beta brasses, RP2662 159
Relaxation, dielectric, for a three-dimensional rotator in a crystalline field, theory for a general six-site model, RP2651 81
Residual entropy of linear polymers, RP2648 55
Resistors, positive nonlinear, frequency conversion with, RP2664 179
Resistivity, electrical, in vitreous ternary lead silicates, RP2658 135
Resistivity, electrical, of vitreous ternary lithium-sodium silicates, RP2665 183
Response function of thallium-activated sodium-iodide scintillation counters, RP2686 333
Response of a sodium-iodide scintillation spectrometer to 10- to 20-million-electron-volt electrons and X-rays, RP2682 319
Richards, L. E., S. W. Strauss, D. G. Moore, W. N. Harrison, Fundamental factors controlling electrical resistivity in vitreous ternary lead silicates, RP2658 135
Roth, R. S., Pyrochlore-type compounds containing double oxides of trivalent and tetravalent ions, RP2643 17

S

Salzer, H. E., Formulas for inverse osculatory interpolation, RP2647 51
Schaffer, R., H. S. Isbell, Improved synthesis of sodium D-glucuronate-6-C^{14} and of D-glucose-6-C^{14}, RP2667 191
Shack, P. V., Characteristics of an image-forming system, RP2672 245
Shermer, H. F., Surface tension of molten glasses in the system barium oxide-boric oxide-silica, RP2661 155
—, Thermal expansion of binary alkaline-earth borate glasses, RP2650 73
Silicates, vitreous ternary lead, electrical resistivity, RP2658 135
Silicates, vitreous ternary lithium-sodium, electrical resistivity, RP2665 183
Sodium D-glucuronate-6-C^{14} and D-glucose-6-C^{14}, improved synthesis, RP2667 191
Sodium-iodide scintillation counters, thallium-activated, response function, RP2686 333
Sodium-iodide scintillation spectrometer, response to 10- to 20-million-electron-volt electrons and X-rays, RP2682 319
Smith, E. R., F. G. Bates, V. E. Bower, Calcium hydroxide as a highly alkaline pH standard, RP2680 305
Smith, S. W., J. K. Taylor, Polarographic determination of lead and cadmium in zinc-base alloys, using electrolytic separations at controlled potential, RP2679 301
—, —, Some factors affecting the precision of polarographic half-wave potential measurements, RP2659 143
Spectra measurements, infrared, RP2660 149
Spectra, third and fourth, of zirconium, description and analyses, RP2663 167
Spectrometer, sodium-iodide scintillation, response to 10- to 20-million-electron-volt electrons and X-rays, RP2682 319
Spectrophotometry, infrared, of polyvinyl chloride, index of refraction and particle size, RP2670 225
Spectroradiometer, recording, five-band, RP2678 293
Spectrum, infrared absorption, of trimethylborane, RP2684 337
Standard, pH, calcium hydroxide as a highly alkaline, RP2680 305
Stewart, J. E., Infrared absorption spectrum of trimethylborane, RP2684 337
—, *M. R. Harvey, R. G. Achhammer,* Index of refraction and particle size as factors in the infrared spectrophotometry of polyvinyl chloride, RP2670 225
Straus, S., S. L. Madorsky, V. E. Hart, Pyrolysis of cellulose in a vacuum, RP2685 343
Strauss, S. W., Electrical resistivity of vitreous ternary lithium-sodium silicates, RP2665 183
—, *D. G. Moore, W. N. Harrison, L. E. Richards,* Fundamental factors controlling electrical resistivity in vitreous ternary lead silicates, RP2658 135
Stress-corrosion cracking and crystal orientation in alpha and beta brasses, RP2662 159
Surface tension of molten glasses in the system barium oxide-boric oxide-silica, RP2661 155
Surge voltage breakdown of air in a nonuniform field, RP2669 201
Sweggard, E. M., W. S. Clabaugh, R. Gilchrist, Preparation of barium titanyl oxalate tetrahydrate for conversion to barium titanate of high purity, RP2677 289
Synthesis of sodium D-glucuronate-6-C^{14} and D-glucose-6-C^{14}, RP2667 191

T

Taylor, J. K., S. W. Smith, Polarographic determination of lead and cadmium in zinc-base alloys, using electrolytic separations at controlled potential, RP2679 301
—, —, Some factors affecting the precision of polarographic half-wave potential measurements, RP2659 143
Temperature scale, helium vapor pressure, examination of, RP2654 99
Temperley, H. N. V., Residual entropy of linear polymers, RP2648 55
Thallium-activated sodium-iodide scintillation counters, response function of, RP2686 333

Page

Thermal decomposition of polytetrafluoroethylene in various gaseous atmospheres, RP2644 27
Thermal expansion of binary alkaline-earth borate glasses, RP2650 73
Thermally degraded polymethyl methacrylate, molecular weights, RP2649 67
Thermodynamic functions, calculation of, for polyatomic molecules, RP2655 105
Thermodynamic functions, ideal gas, of isotopic hydrogen cyanides, RP2668 197
Trimethylborane, infrared absorption spectrum of, RP2684 337
Trivalent and tetravalent ions, pyrochlore-type compounds containing double oxides of, RP2643 17

V

Vapor pressure scale of temperature, helium, RP2654 99
Vibrational constants of acetylene-d_2, RP2675 279
Vitreous ternary lead silicates, electrical resistivity, RP2658 135
Vitreous ternary lithium-sodium silicates, electrical resistivity, RP2665 183

W

Wait, J. R., Radiation from a vertical antenna over a curved stratified ground, RP2671 237
Wall, L. A., J. D. Michaelsen, Thermal decomposition of polytetrafluoroethylene in various gaseous atmospheres, RP2644 27
Water content of gases, computer for calculating, RP2674 269

Page

Water, dielectric constants of, RP2641 1
Weaver, E. R., A. W. Diniak, A new computer for calculating the water content of gases, RP2674 269
Weir, C. E., Isothermal compressibilities of alkaline earth oxides at 21° C, RP2666 187
—, *C. M. Hunt, R. L. Blaine*, Behavior of cements and related materials under hydrostatic pressures up to 10,000 atmospheres, RP2646 39
Woolley, H. W., Calculation of thermodynamic functions for polyatomic molecules, RP2655 105
Wyckoff, J. M., H. W. Koch, Response of a sodium-iodide scintillation spectrometer to 10- to 20-million-electron-volt electrons and X-rays, RP2682 319

X

X-ray beam, high-energy, a calorimeter for measuring the power, RP2642 9

Z

Zeudle, B., J. McElhinney, S. Domen, A calorimeter for measuring the power in a high-energy X-ray beam, RP2642 9
Zinc base alloys, polarographic determination of lead and cadmium in, RP2679 301
Zirconium, new descriptions and analyses of the third and fourth spectra, Zr III and Zr IV, RP2663 167

U. S. GOVERNMENT PRINTING OFFICE: 1956

Recent Publications of the National Bureau of Standards

Journal of Research of the National Bureau of Standards, volume **56**, No. 4, April 1956 (RP2663 to RP2671, incl.). Annual subscription $4.00.

Technical News Bulletin, volume **40**, No. 4, April 1956. 10 cents. Annual subscription $1.00.

Basic Radio Propagation Predictions for July 1956. Three months in advance. CRPL 140. Issued April 1956. 10 cents. Annual subscription $1.00.

Research Papers

Journal of Research, volume 56, number 4, April 1956. Single copies of the Journal vary in price. Single copies of Research Papers appearing in the Journal are not available for sale. The Superintendent of Documents, U. S. Government Printing Office, Washington 25, D. C., will reprint 100 or more copies of a Research Paper. Request for the purchase price should be mailed promptly to that office.

RP2663. New descriptions and analyses of the third and fourth spectra of zirconium, Zr III and Zr IV. C. C. Kiess.

RP2664. Frequency conversion with positive nonlinear resistors. Chester H. Page.

RP2665. Electrical resistivity of vitreous ternary lithium sodium silicates. Simon W. Strauss.

RP2666. Isothermal compressibilities of alkaline earth oxides at 21° C. C. E. Weir.

RP2667. Improved synthesis of sodium D-glucuronate-6-C^{14} and of D-glucose-6-C^{14}. R. Schaffer and H. S. Isbell.

RP2668. Ideal gas thermodynamic functions of the isotopic hydrogen cyanides. Joe C. Bradley, Lester Haar, and Abraham S. Friedman.

RP2669. Surge voltage breakdown of air in a nonuniform field. J. H. Park and H. N. Cones.

RP2670. Index of refraction and particle size as factors in the infrared spectrophotometry of polyvinyl chloride. Mary Reiney Harvey, James E. Stewart, and Bernard G. Achhammer.

RP2671. Radiation from a vertical antenna over a curved stratified ground. James R. Wait.

Publications in Other Journals

Alignment of cerium-141 and neodymium-147 nuclei. E. Ambler, R. P. Hudson, and G. M. Temmer. Phys. Rev. (57 E. 55th St., New York 22, N. Y.) **97**, No. 5, 1212–1221 (Mar. 1955).

Alignment of three odd-a rare-earth nuclei. E. Ambler, R. P. Hudson, and G. M. Temmer. Phys. Rev. (57 E. 55th St., New York 22, N. Y.) **101**, No. 1, 196–200 (Jan. 1956).

Transmission of positrons and electrons. H. H. Seliger. Phys. Rev. (57 E. 55th St., New York 22, N. Y.) **100**, No. 4, 1029–1037 (Nov. 1955).

Theoretical electromotive forces for cells containing a single solid or molten chloride electrolyte. Walter J. Hamer, Marjorie S. Malmberg, and Bernard Rubin. J. Electrochem. Soc. (Mount Royal and Guilford Aves., Baltimore 2, Md.) **103**, No. 1, 8–16 (Jan. 1956).

On asymptotic series for functions occurring in the theory of diffraction of waves by wedges. F. Oberhettinger. J. Math. and Phys. (Eric Reissner, Mass. Inst. of Technology, Cambridge 39, Mass.) **34**, No. 4, 245–255 (Jan. 1956).

American dental association specifications for dental materials. George C. Paffenbarger and W. T. Sweeney. J. Am. Dental Assoc. (222 E. Superior St., Chicago 11, Ill.) 11–76 (Mar. 1955).

Partially replicated Latin squares. W. J. Youden and J. S. Hunter. Biometrics (The Biometrics Society, 52 Hillhouse Ave., New Haven, Conn.) **11**, 399–405 (1955).

Solar H_α filaments and geomagnetic disturbances. Hope I. Leighton and Donald E. Billings. J. Atm. and Terrest. Phys. (Butterworth-Springer Ltd., 436 Strand, London WC2, Eng., or Academic Press Inc., 125 E. 23d St., New York 10, N. Y.) **7**, 349–350 (June 1955).

Extension of the Sen-White paper on atmospheric oscillations. Marvin L. White. J. Geophys. Res. (The Johns Hopkins Press, Baltimore 18, Md.) **60**, 531–532 (1955).

Sulfinic acid derivatives as accelerators in the polymerization of methyl methacrylate. G. M. Brauer and F. R. Burns. J. Polymer Sci. (250 5th Ave., New York 1, N. Y.) **19**, No. 92, 311–321 (Feb. 1956).

Temperature dependence of mechanical shear degradation. P. Goodman and A. B. Bestul. J. Polymer Sci. (250 5th Ave., New York 1, N. Y.) **18**, No. 88, 235–244 (Oct. 1955).

Characteristic energy losses of electrons in solids. L. Marton, Lewis B. Leder, and H. Mendlowitz. Advances in Electronics and Electron Phys. (Academic Press Inc., 125 E. 23d St., New York 10, N. Y.) **7** (1955).

Analysis of the (0,1) and (1,2) bands of the $^2\Delta$—$^2\Pi$ system of CH. Norman H. Kiess and Herbert P. Broida. Astrophys. J. (Univ. of Chicago Press, 5750 Ellis Ave., Chicago 37, Ill.) **123**, No. 1, 166–169 (Jan. 1956).

Aurora and airglow. C. T. Elvey and Franklin E. Roach. Sci. Am. (Circulation Mgr., Scientific American, 24 W. 40th St., New York 18, N. Y.) (Sept. 1955).

The ionosphere. T. N. Gautier. Sci. Am. (Circulation Mgr., Scientific American, 24 W. 40th St., New York 18, N. Y.) (Sept. 1955).

A subroutine for computations with rational numbers, Peter Henrici. J. Assoc. Computing Machinery (2 E. 63d St., New York 21, N. Y.) **3**, No. 1, 6–9 (Jan. 1956).

The height of the nightglow by the van Rhijn method. F. E. Roach and A. B. Meinel. Astrophys. J. (Univ. of Chicago Press, 5750 Ellis Ave., Chicago 37, Ill.) **122**, No. 3, 530–553 (Nov. 1955).

Thermal and gravitational excitation of atmospheric oscillations. Hari K. Sen and Marvin L. White. J. Geophys. Res. (The Johns Hopkins Press, Baltimore 18, Md.) **60**, No. 4, 483–495 (Dec. 1955).

Nightglow heights: a reinterpretation of old data. F. E. Roach and A. B. Meinel. Astrophys. J. (Univ. of Chicago Press, 5750 Ellis Ave., Chicago 37, Ill.) **3**, 554–557 (Nov. 1955).

Sweep-frequency pulse-transmission measurements over a 2400-km path. Peter G. Sulzer. J. Geophys. Res. (The Johns Hopkins Press, Baltimore 18, Md.) **60**, No. 4, 411–420 (Dec. 1955).

Some results of a sweep-frequency propagation experiment over an 1150-km east-west path. Bernard Wieder. J. Geophys. Res. (The Johns Hopkins Press, Baltimore 18, Md.) **60**, No. 4, 395–409 (Dec. 1955).

Publications for which a price is indicated are available only from the Superintendent of Documents, U. S. Government Printing Office, Washington 25, D. C. (foreign postage, one-third additional). Reprints from outside journals are not available from the National Bureau of Standards but can often be obtained from the publishers.

UNITED STATES
GOVERNMENT PRINTING OFFICE
DIVISION OF PUBLIC DOCUMENTS
WASHINGTON 25, D. C.

OFFICIAL BUSINESS

PENALTY FOR PRIVATE USE TO AVOID PAYMENT OF POSTAGE, $300 (GPO)

Journal of Research of the National Bureau of Standards Vol. 56, No. 6 June 1956

Contents

	Page
Calcium hydroxide as a highly alkaline *p*H standard. Roger G. Bates, Vincent E. Bower, and Edgar R. Smith. RP2680	305
Heats of formation of hexacalcium dialumino ferrite and dicalcium ferrite. E. S. Newman and Roald Hoffman. RP2681	313
Response of a sodium-iodide scintillation spectrometer to 10- to 20-million-electron-volt electrons and X-rays. H. W. Koch and J. M. Wyckoff. RP2682	319
Hydrogarnet formation in the system lime-alumina-silica-water. Elmer T. Carlson. RP2683	327
Infrared absorption spectrum of trimethylborane. James E. Stewart. RP2684	337
Pyrolysis of cellulose in a vacuum. S. L. Madorsky, V. E. Hart, and S. Straus. RP2685	343
Response function of thallium-activated sodium-iodide scintillation counters. Martin J. Berger and J. Doggett. RP2686	355
Index to volume 56 (January to June 1956, Research Papers RP2641 to RP2686).	367

Single copies of the above Research Papers are not available for sale, but the Superintendent of Documents, U. S. Government Printing Office, Washington 25, D. C., will reprint 100 or more copies, and request for the purchase price should be mailed promptly to that Office.

[A list of recent NBS publications is given on page 3 of the cover.]

5935

For sale by the Superintendent of Documents, U. S. Government Printing Office, Washington 25, D. C. Price 60c (Single copy). Subscription price: $4.00 a year; $1.25 additional for foreign mailing. Single copies vary in price.

UNITED STATES GOVERNMENT PRINTING OFFICE, WASHINGTON : 1956